DIPLOMARBEIT

Titel der Diplomarbeit

The position of the HOXA3 gene in a gene network relevant to diabetic microangiopathy

angestrebter akademischer Grad

Magister der Naturwissenschaften (Mag. rer.nat.)

Verfasser:	Andreas Thader
Matrikel-Nummer:	9825603
Studienrichtung (lt. Studienblatt):	A 441
Betreuer:	Dr. Nikolaus Wick (Medizinische Universität Wien) Univ.-Prof. Dr. Thomas Decker (Universität Wien)

Wien, am 8. September 2008

Index

Danksagung

Ich möchte mich herzlichst bei Herrn Dr. Nikolaus Wick und Herrn Prof. Stefan Thurner für die Aufnahme in die wissenschaftliche Arbeitsgruppe bedanken. Mein weiterer Dank gilt dem Vorstand des Institutes für klinische Pathologie, Herrn Prof. Dr. Dontscho Kerjaschki, für die Bereitstellung des Arbeitsplatzes.

Es ist mir ein großes Anliegen mich bei meinem Betreuer Herrn Dr. Nikolaus Wick für seine tatkräftige und vor allem freundliche Unterstützung während der gesamten Dauer meiner Diplomarbeit zu bedanken. Dankbar bin ich auch den Projektmitgliedern Aurea, Dejan, Dani, Hanni, und Elisabeth für die konstruktive und freundschaftliche Zusammenarbeit. Frau Romana Kalt danke ich für ihre ständige Hilfsbereitschaft und wertvollen Ratschläge bei im Labor auftretenden Problemen. Bedanken möchte ich mich auch bei den Mitgliedern der einzelnen Arbeitsgruppen des Institutes für klinische Pathologie, die mir im Laufe meiner Diplomarbeit mit Rat und Tat zur Seite gestanden haben.

Ganz besonders möchte ich meinen Eltern Leopoldine und Erwin Thader sowie meiner Lebenspartnerin und Freundin Mag. Nicole Jezek für die ständige Unterstützung und den fortwährenden Glauben an mich danken.

1 Abstract

Diabetic microangiopathy, a hyperglycaemia-induced damage of blood capillaries of long-term diabetic patients is characterized by thickening of the capillary basement membrane. Diabetic microvascular complications generally affect the eyes (retinopathy), kidneys (nephropathy) and nerves (neuropathy). A gene set consisting of 125 genes, identified by gene expression profiling comparing (i) blood vascular endothelial cells (BECs) derived from tissue samples of diabetic and non-diabetic patients and (ii) BECs cultured *in vitro* under diabetic conditions, as well as by literature search was hypothesized to control these complications. The 125 candidate genes were the basis of a gene network that was assumed to be of functional relevance for diabetic microangiopathy by demonstration of the functional links between the genes involved. One of the identified candidate genes was HOXA3, a member of the family of homeobox genes encoding homeodomain transcription factors. Quantitative real time PCR of cDNA samples derived from total RNA of immortalized human umbilical vein endothelial cells (iHUVECs) transiently transfected with pIRES2-EGFP carrying the coding sequence of HOXA3 was executed, in order to study the effects of HOXA3 overexpression on the candidate gene set. Thereby, transient expression of HOXA3 was found to result in elevated expression of genes encoding proteins that act in adipocytes or are involved in reorganization of the actin cytoskeleton. In a final gene network comprising 37 genes and relevant to diabetic microangiopathy, expression of HOXA3 was positively regulated by CFL1 encoding cofilin 1 and downregulated by CASP3 coding for caspase 3. CFL1 a member of the family of actin depolymerising factor (ADF)/cofilins is known to contribute to cytoskeletal dynamics in nonmuscle cells whereas CASP3 encodes an effector caspase that mediates apoptosis of β-cells of the pancreas. Furthermore, it was found that HOXA3 may also have an activating effect on its own expression.

The number of functional links to other genes involved determined the position of a gene within our network. Genes occupying a central position were thought to be key players in the occurrence of microvascular complications since they had a higher number of functional links than genes placed in a peripheral position. In our gene network assumed to be of relevance for diabetic microangiopathy, HOXA3 occupied a peripheral position.

2 Zusammenfassung

Unter diabetischer Mikroangiopathie versteht man den durch Hyperglykämie verursachten Schaden an Blutkapillaren von Patienten, die über einen längeren Zeitraum unter erhöhtem Blutglukosespiegel stehen. Eine Verdickung der kapillären Basalmembran ist charakteristisch für das Auftreten dieser mikrovaskulären Komplikationen, die im Allgemeinen in den Kapillaren der Augen (Retinopathie) und der Nieren (Nephropathie) sowie in den Nerven (Neuropathie) zu finden sind. Basierend auf sowohl vergleichender Analyse der Genexpression in Blutgefäßendothelzellen (BECs) von Diabetikern und gesunden Menschen, sowie in BECs, die *in vitro* unter diabetischen Bedingungen kultiviert wurden, sowie durch Literatursuche konnten 125 Kandidatengene identifiziert werden, von denen man annahm, das Auftreten diabetischer Mikroangiopathie zu kontrollieren. Diese 125 Gene sollten die Grundlage für ein Gennetzwerk bilden, mit dessen Hilfe die genregulatorischen Interaktionen dargestellt werden konnten, welche für das Eintreten von diabetischen mikrovaskulären Komplikationen verantwortlich sind. Unter den identifizierten Kandidatengenen befand sich HOXA3, ein Mitglied der Familie von Homöoboxgenen, die für Transkriptionsfaktoren mit einer Homöodomäne kodieren. Um die Auswirkung der Überexpression des HOXA3 Gens auf die Expression der Kandidatengene zu untersuchen, wurden immortalisierte BECs einer humanen Nabelschnurvene (iHUVECs) transient mit dem Expressionsvektor pIRES2-EGFP, der die kodierende Sequenz von HOXA3 enthielt, transfiziert. Nach Isolation der gesamten RNA und reverser Transkription, wurde die resultierende cDNA Probe einer quantitativen real time PCR unterzogen. Durch die quantitative real time PCR konnte gezeigt werden, dass infolge einer Überexpression des HOXA3-Gens die Expression solcher Gene stark erhöht wurde, welche entweder in Adipozyten aktiv sind oder eine Rolle bei der Reorganisation des Aktinzytoskeletts spielen.

In dem von uns gestalteten, 37 Gene umfassenden Netzwerk, wurde die Expression von HOXA3 zum einen durch CFL1 positiv reguliert und zum anderen durch CASP3 inhibiert. CFL1 kodiert für Cofilin 1, ein Aktin bindendes Protein, das zur zytoskelettalen Dynamik in Nicht-Muskelzellen beiträgt, während das Genprodukt von CASP3, eine Effektorkaspase, den programmierten Zelltod von β-Zellen des Pankreas herbeiführt.

Die Position eines jeden Gens innerhalb des Netzwerks wurde durch die Zahl seiner direkten funktionellen Verknüpfungen mit anderen Genen bestimmt. Dabei waren jene Gene mit den meisten direkten funktionellen Verknüpfungen im Zentrum angeordnet, und ihnen wurde deshalb auch eine zentrale Rolle bei der Entstehung von diabetischen mikrovaskulären

Komplikationen beigemessen. Das HOXA3 Gen besetzte gemäß der Anzahl seiner direkten funktionellen Verknüpfungen eine periphere Position innerhalb des 37 Gene umfassenden Netzwerks.

3 Introduction

3.1 Diabetes mellitus and diabetic microangiopathy

3.1.1 Diabetes mellitus

Diabetes mellitus is a metabolic disorder existing in different forms, all of which are characterized by hyperglycaemia. In fact, diabetes mellitus is diagnosed in patients with fasting plasma glucose levels above 126 mg/dl (7.0mmol/l) or casual plasma glucose levels above 200mg/dl (11.1mmol/l).

Mechanisms contributing to the occurrence of hyperglycaemia are known to be failures in either action or secretion or both of the glucose-lowering pancreatic hormone insulin. A permanent state of hyperglycaemia causes various dysfunctions and defects of organs including the eyes (retinopathy), kidneys (nephropathy), nerves (neuropathy) and heart (cardiomyopathy). Clinical symptoms associated with the occurrence of hyperglycaemia are known to be polyuria, polydipsia and weight loss. In some cases, polyphagia, impaired vision and susceptibility to certain infections may be indicators of hyperglycaemia.

Patients suffering from diabetes mellitus bear an increased risk for atherosclerotic cardiovascular, peripheral arterial and cerebrovascular disease.

Several forms of diabetes mellitus are known, the three major types are type 1 diabetes, type 2 diabetes and gestational diabetes.

Type 1 diabetes, also referred to as insulin-dependent diabetes or juvenile-onset diabetes, is an autoimmune disease and occurs as the result of absolute insulin deficiency due to autoimmune destruction of insulin-producing pancreatic β-cells. Although type 1 diabetes can appear at any age, persons usually affected are children and adolescents. People with this form of diabetes require insulin for survival and therefore have to take insulin by injection up to several times a day. Type 1 diabetes accounts for 5-10 % of all patients suffering from diabetes. Markers identified for the autoimmune destruction of the β-cells of the pancreas are several autoantibodies targeted to islet cells, to insulin, to glutamic acid decarboxylase (GAD_{65}) and to tyrosine phosphatases IA-2 and IA-2β. Diabetic ketoacidosis (DKA), defined as a state characterized by hyperglycaemia, accumulated ketone bodies in the blood as well as increased acidity of the blood, is a life-threatening condition that can occur as a result of insulin deficiency. Diabetic ketoacidosis is commonly found in people with type 1 diabetes, although it can also happen to patients suffering from type 2 diabetes. Although the causes of

type 1 diabetes are widely unknown, it is believed that genetic predispositions and environmental factors may play a decisive role in the development of the disease. Another rare form of type 1 diabetes, referred to as idiopathic diabetes, is commonly found in people of African or Asian descent. In contrast to autoimmune mediated type 1 diabetes described above, this form is not characterized by autoimmune destruction of the β-cells of the pancreas, but rather by a lack of ß-cell autoimmunity markers.

The most prevalent form of diabetes is **type 2 diabetes** that accounts for 90-95% of all diabetes cases. Type 2 diabetes is also referred to as non-insulin dependent diabetes or adult-onset diabetes and occurs as the result of insulin resistance and relative insulin deficiency. In contrast to type 1 diabetes, there is no autoimmune destruction of pancreatic β-cells found in patients with type 2 diabetes. In many cases, type 2 diabetes remains unnoticed for years due to a gradual emergence of hyperglycaemia. Risk factors identified for type 2 diabetes include obesity, low physical activity and advanced age. Furthermore, the occurrence of type 2 diabetes is often linked to genetic predisposition. Unlike people suffering from type 1 diabetes, patients with type 2 diabetes often do not depend on insulin treatment for survival.

Glucose intolerance that arises or is first noticed during pregnancy is also known as **gestational diabetes mellitus (GDM)**. Several factors including obesity, a family history of diabetes, abnormal glucose metabolism before pregnancy and being a member of an ethnic group with a high incidence of diabetes are known to increase the risk for women of developing this form of diabetes. In the majority of cases, women affected by GDM are older than 25 years indicating the influence of age on the development of GDM (American Diabetes Association, 2007).

On the long term the result of all types of diabetes may be macrovascular and microvascular complications. In this thesis, only microangiopathic damage is dealt with.

3.1.2 Diabetic microangiopathy

Diabetic microangiopathy is a glucose-induced damage of blood capillaries of long-term diabetic patients. It is characterized by thickening of the capillary basement membrane. These diabetic microvascular complications are found in the eye (retinopathy) and in the kidney (nephropathy), and they are also involved in neuropathy. Besides direct damage to parenchymal cells, capillary damage is the most important mediator of organ dysfunction. Hyperglycaemia considered as the primary initiating factor for all types of diabetic microvascular disease seems to be responsible for several mechanisms characteristic for the

occurrence of diabetic microangiopathy. These mechanisms include structural, functional and biochemical changes. Structural changes in the form of thickening of the capillary basement membrane can result in occlusive angiopathy, tissue hypoxia and damage. Functional changes include increases in organ blood flow and vascular permeability, as well as abnormalities in blood viscosity, platelet and endothelial function (K Dahl-Jørgensen, 1998). Finally, four biochemical mechanisms are known to contribute to microvascular complications in diabetes, all of them induced by hyperglycaemia (Brownlee, 2001; Schalkwijk and Stehouwer, 2005).

Increased polyol pathway flux is one biochemical mechanism typical for the occurrence of diabetic vascular diseases. In the beginning of this pathway, the enzyme aldose reductase catalyzes the NADPH-dependent reduction of glucose to sorbitol. Under non-diabetic conditions, metabolism of glucose by the polyol pathway occurs at very low rates due to a low affinity of the enzyme aldose reductase for glucose. However, hyperglycaemia leads to increased conversion of intracellular glucose to sorbitol accompanied by an increase in oxidation of NADPH to $NADP^+$. Another enzyme of the polyol pathway, sorbitol dehydrogenase catalyzes the oxidation of sorbitol to fructose with simultaneous reduction of NAD^+ to NADH. Although there are many hypotheses about the damaging effects the products of the polyol pathway may have on cells, the role of this pathway in diabetic microvascular complications is not completely understood yet (Brownlee, 2001). The most plausible mechanism by which increased polyol pathway flux damages cells is based on the assumption that NADPH-dependent reduction of glucose to sorbitol depletes NADPH which in turn is essential for regeneration of reduced glutathione (GSH). The consequence of this NADPH consumption is oxidative stress (Lee and Chung, 1999).

Another biochemical mechanism induced by hyperglycaemia and critical for microvascular complications in diabetes is the **increased intracellular formation of advanced glycation end products (AGEs)**. Non-enzymatic glycation of proteins, defined as the condensation reaction of a sugar aldehyde or ketone with a free amino goup by nucleophilic addition, leads to formation of a Schiff base which rearranges to the Amadori product. In the final step, the irreversible advanced glycation end product (AGE) is formed (Brownlee et al., 1990).

Originally, non-enzymatic glycation reactions involving extracellular proteins and glucose were considered to be decisive for the production of AGEs. However, dicarbonyl precursors derived from glucose and generated intracellularly have been shown to form AGEs much faster suggesting that intracellular hyperglycaemia plays the central role in the formation of intracellular as well as extracellular AGEs. The highly reactive dicarbonyl compounds are known to be glyoxal, methylglyoxal and 3-deoxyglucosone which are formed from glycolytic

intermediates and react with extracellular and intracellular proteins to form AGEs (Wells-Knecht et al., 1995; Degenhardt et al., 1998). Methylglyoxal arising from glyceraldehyde-3-phosphate is thought to be the main AGE-precursor in endothelial cells and therefore plays a critical role in the development of vascular complications in diabetes mellitus (Bourajjaj et al., 2003).

Production of intracellular AGE precursors results in intracellular as well as extracellular alterations (Figure 1).

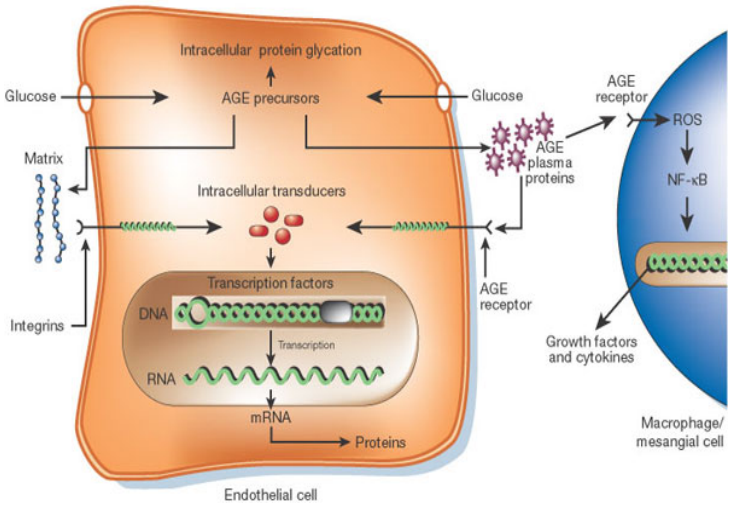

Figure 1. Mechanisms induced by production of intracellular AGE precursors alter gene expression in endothelial cells, mesangial cells and macrophages. Modifications of several proteins including intracellular, extracellular matrix and plasma proteins by intracellular AGE precursors are the basis of these alterations (Brownlee, 2001).

AGE formation on extracellular matrix proteins has been shown to influence interactions of these proteins with their respective receptors (integrins) on cells and other matrix components (Brownlee, 2001). Matrix proteins known to be targets of AGE formation are type I and type IV collagen as well as laminin. Type IV collagen and laminin are major components of the basement membrane and necessary for the maintenance of its normal structure and function. Therefore, AGE formation on these proteins impairs matrix-matrix as well as cell-matrix interactions (Tanaka et al., 1988; Tsilibary et al., 1988; Charonis et al., 1990). Another mechanism induced by binding of AGE modified plasma proteins to AGE receptors leads to altered gene expression in endothelial cells, mesangial cells and macrophages. AGE binding proteins identified on these cells and targeted by AGE modified plasma proteins are RAGE, galectin-3, the macrophage scavenger receptor type II, OST-48 and 80K-H (Neeper et al., 1992; Vlassara et al., 1995; Smedsrod et al., 1997; Li et al., 1996). Binding to RAGE has been found to generate reactive oxygen species (ROS) resulting in the activation of the transcription factor NF-κB and $p21^{Ras}$ (Yan et al., 1994; Lander et al., 1997). In mesangial cells and macrophages, AGE signalling leads to expression of various cytokines and growth factors such as IL-1, TNF-α and TGF-β (Schalkwijk and Stehouwer, 2005). Binding of AGE-

modified proteins to their receptors on endothelial cells induces expression of pro-coagulatory and pro-inflammatory molecules known to be thrombomodulin, tissue factor and the vascular cell adhesion molecule VCAM-1 (Schmidt et al., 1995; Brownlee, 2001). Furthermore, it has been found that AGE signalling in endothelial cells may induce VEGF and therefore seems to contribute to diabetes induced hyperpermiability of the capillary wall (Lu et al., 1995).

The third mechanism contributing to diabetic microvascular diseases leads to **activation of protein kinase C (PKC)**. Hyperglycaemia leads to increased formation of the activator of PKC, the lipid second messenger diacylglycerol (DAG). The PKC family includes at least eleven isoforms. Although DAG has been found to activate almost all of them, its primary targets are the β- and δ-isoforms. Hyperglycaemia-induced *de novo* synthesis of DAG is achieved by reduction of the glycolytic intermediate dihydroxyacetone phosphate to glycerol-3-phosphate followed by acylation reactions (Koya and King, 1998).

Activation of PKC affects the expression of numerous genes resulting in various structural and functional changes typical for microvascular complications in diabetes. Abnormalities in blood flow are the result of inhibition of eNOS (Kuboki et al., 2000) and activation of ET-1, both mediated by PKC (Glogowski et al., 1999). PKC activation has been found to induce VEGF leading to vascular permeability and angiogenesis (Williams et al., 1997). Capillary occlusion is the consequence of PKC mediated induction of TGF-β, fibronectin and collagen (Koya et al., 1997). PKC activation has been shown to cause vascular occlusion by activation of PAI-1 resulting in inhibition of fibrinolysis (Feener et al., 1996). Further genes found to be induced as a result of PKC activation are NFκB (Pieper et al., 1997) and NAD(P)H oxidases. The former activates expression of pro-inflammatory genes and the latter induces ROS leading to multiple effects.

The fourth biochemical pathway found to be relevant to diabetic microvascular complications is the **hexosamine pathway**. In this pathway, the enzyme glutamine:fructose-6-phosphate amidotransferase (GFAT) catalyzes the conversion of the glycolytic intermediate fructose-6-phosphate to glucosamine-6-phosphate which is subsequently converted into UDP-N-acetylglucosamine (UDPGlcNAc). UDPGlcNAc is required for O-linked glycosylation of proteins catalyzed by the enzyme O-GlcNAc transferase (OGT). Hyperglycaemia-induced increased flux through the hexosamine pathway has been found to result in increased expression of TGF-β1 (Kolm-Litty et al., 1998) and PAI-1 (Du et al., 2000). The mechanism responsible for elevated expression of TGF-β1 and PAI-1 is suggested to increase covalent modification of serine and threonine residues of transcription factors such as Sp1 by N-

acetylglucosamine. Furthermore, inhibition of eNOS activity has been shown to occur by O-acetylglucosaminylation at the Akt site of the protein (Du et al., 2001).

The four biochemical pathways described above have in common that they are activated by hyperglycaemia-induced oxidative stress (Figure 2). It has been found that hyperglycaemia leads to overproduction of superoxide O_2^- by the mitochondrial electron transport chain (Du et al., 2000). This is the result of hyperglycaemia-induced increased amounts of electron donors NADH and $FADH_2$ from the TCA cycle. According to these elevated levels of electron donors, the electron flow through the mitochondrial electron transport chain generates a high proton gradient across the inner mitochondrial membrane. The consequence of the increased mitochondrial membrane potential is a prolonged half-life of superoxide-producing ubisemiquinone of the mitochondrial electron transport chain (Brownlee, 2001). The overproduction of superoxide has been found to result in activation of the enzyme PARP which in turn inhibits the glycolytic enzyme GAPDH by poly-ADP-ribosylation (Du et al., 2003).

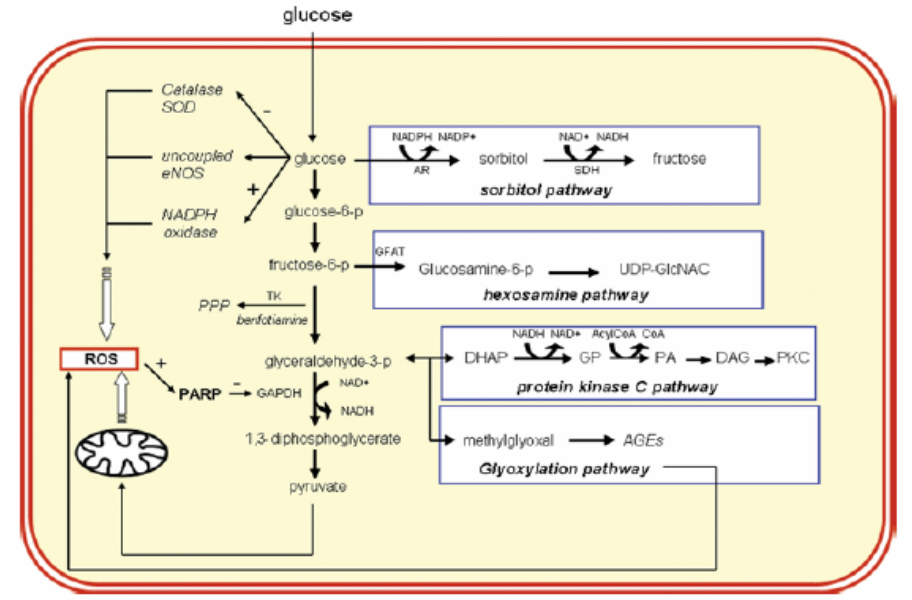

Figure 2. Hyperglycaemia-induced oxidative stress activates four biochemical pathways that are known to contribute to vascular complications in diabetes. Overproduction of superoxide activates the enzyme PARP which in turn inhibits the glycolytic enzyme GAPDH by poly-ADP-ribosylation resulting in accumulation of upstream glycolytic metabolites and activation of the four biochemical pathways (Schalkwijk and Stehouwer, 2005).

3.1.3 Identification of a gene network relevant to diabetic microangiopathy

In contrast to the biochemical mechanisms, there is only little knowledge about the genetic factors contributing to the development of diabetic microangiopathy. Therefore, the aim of diabetic research is the development of genetic markers for diabetic microangiopathy by finding genes that are associated with the occurrence of microvascular complications in diabetes (K Dahl-Jørgensen, 1998).
A cooperation project between the Institute for Pathology and the Complex Systems Research Group, both from the Medical University of Vienna, has been initiated, in order to identify a functionally relevant gene network critical for diabetic microangiopathy.

3.1.4 Preexisting data

The basis for this network is a set of 125 candidate genes that has been found by gene expression profiling comparing (i) BECs derived from tissue samples of diabetic and non-diabetic patients and (ii) BECs cultured *in vitro* under diabetic conditions, as well as by literature search.
The aim of identifying a gene network critical for diabetic microangiopathy is to display the functional links between the candidate genes representing upregulating and downregulating effects as well as autoregulatory mechanisms.
In order to examine the role of a candidate gene within a supposed gene network the gene has to be transiently expressed in an appropriate cell line. Total RNA isolated from cells overexpressing a certain gene is converted to cDNA by reverse transcription and applied to TaqMan Low Density Arrays spotted with primers and probes for all candidate genes. Subsequent quantitative real time PCR enables quantitative detection of PCR products after numerous PCR reactions carried out simultaneously according to the number of candidate genes. Finally, the upregulating and downregulating effects of a certain transiently expressed gene within the candidate gene set on the rest of this set can be measured. According to overexpression data, special computer software developed by the Complex Systems Research Group is used to create a gene network by reverse engineering. More precisely, a mathematical algorithm capable of reconstructing a network comprising a defined number of candidate genes is built. In order to identify the functional links between candidate genes within an assumed network, the expression of these genes is perturbed in the form of overexpression experiments. Gene expression dynamics or changes in expression level with

respect to time (dX/dt) of candidate genes within a network resulting from transient expression of one candidate gene are described as follows:

$dX/dt = f(A, X)$

In this formular X comprises all candidate genes within the network (X_1, X_2, X_3…..X_n) and the adjacency matrix A represents the functional links between the candidate genes.
In case of a steady state meaning a state of unaltered gene expression dX/dt can be set equal to zero.

3.2 The HOX gene family

3.2.1 General features of HOX genes

Homeobox (HOX) genes encode transcription factors, all of them possessing a so called homeodomain that has a DNA binding function. More precisely, the homeodomain is responsible for binding to specific sequences within the promoter region resulting in transcriptional regulation of the corresponding target genes (Levine and Hoey, 1988).
A total of 39 HOX genes organized in four clusters named A, B, C and D are found in mammals, whereas each cluster is located on a different chromosome. Another feature of HOX genes is the existence of 13 paralogue groups. Therefore each cluster is numbered from 1 to 13. Still, no one contains a full set of HOX genes (Claudia Kappen et al., 1989; Scott, 1992). Genes of the same group, referred to as *trans*-paralogues, are equally numbered and show a high degree of sequence. They are located on different chromosomes but occupy the same relative position. *Cis*-paralogues are adjacent on the same chromosome, i.e. within the same cluster (Greer et al., 2000). In the evolution of HOX genes, two steps occurred, resulting in the formation of the existing paralogue groups. In the first step, a primordial homeobox gene cluster complex was amplified in *cis*, whereas the second involved *trans*-duplication (Claudia Kappen et al., 1989).

3.2.2 Function of HOX genes

HOX genes were initially discovered in *Drosophila melanogaster* where they are known to act in anterior-posterior axis patterning during embryogenesis (Lewis, 1978; Ingham, 1988).

Further studies carried out with mammalian species have revealed that HOX genes also have an important function in adult cells in addition to their roles during embryonic development. Genes regulated by HOX transcription factors are critical for a number of cellular processes (Figure 3). These are organogenesis, cellular differentiation, cell adhesion and migration, cell cycle and apoptosis (Ulijaszek et al., 1998).

The individual paralogues of HOX genes can have complementary, overlapping or completely different functions. As already mentioned *trans*-paralogues show a high degree of sequence homology, and sometimes have a functional overlap, whereas *cis*-paralogues differ more in terms of sequence and function. In some cases, *trans*-paralogues, such as HOXA3 and HOXD3 have been shown to carry out identical functions. Embryonic HOXA3 null mice, which are homozygous for the HOXA3 null mutation and therefore do not express any HOXA3 protein, experience perinatal lethality that can be rescued by the introduction of HOXD3 into the HOXA3 locus. HOXA3 introduced into the HOXD3 locus by homologous recombination, has in turn rescued mice homozygous for HOXD3 null mutation, thereby preventing skeletal defects of atlas and axis. Interestingly, introduction of HOXA3 into the HOXD3 locus does not compensate the effects of homozygous HOXA3 null mutation on embryonic development. These data suggest that HOXA3 and HOXD3 can exhibit functional equivalence under certain circumstances only, although they do not have identical functions under normal conditions. However, the difference in biological functions between *trans*-paralogues, such as HOXA3 and HOXD3 does not seem to be a matter of different qualities of the respective genes. Otherwise, HOXA3 introduced into the HOXD3 locus would rescue embryonic mice, homozygous for HOXA3 null mutation. It is more plausible that their differential roles are the result of differences in their expression levels due to *cis*-acting sequences, controlling the expression of the respective loci (Greer et al., 2000; T Svingen and KF Tonissen, 2006)

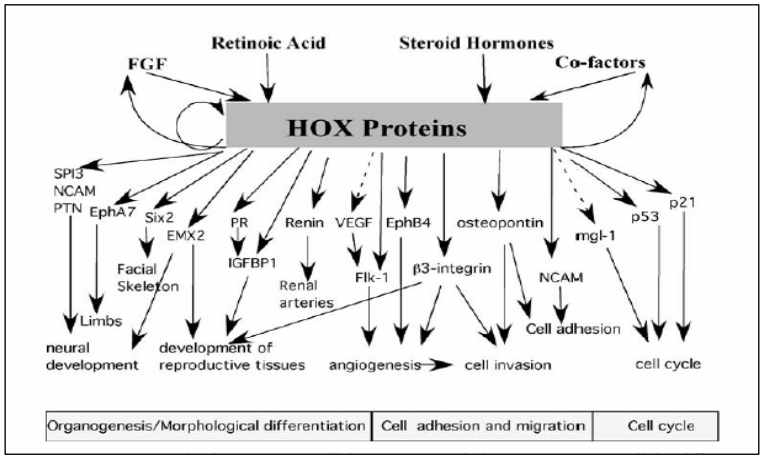

Figure 3. Mammalian target genes of transcription factors encoded by HOX genes and their respective roles in cellular processes. Genes regulated by HOX transcription factors are critical for a number of cellular processes including organo-genesis, cellular differentiation, cell adhesion and migration, cell cycle and apoptosis (T Svingen and KF Tonissen, 2006).

3.2.3 The homeodomain

As mentioned above, highly conserved 60 amino acid motif, the homeodomain, is found in transcription factors that are encoded by homeobox genes. Recognizing specific sequences within the promoter region of its target genes, this protein domain has a DNA binding function enabling transcriptional regulation. The homeodomain is encoded by a 180 base pair nucleotide sequence, referred to as the homeobox that is distinctive for homeobox genes (Levine and Hoey, 1988; McGinnis and Krumlauf, 1992).

Three alpha helices forming a helix turn helix motif as well as the N-terminal arm are composing the homeodomain (Kuziora and McGinnis, 1989). A high number of homeodomain proteins are known to bind specifically to a TAAT core sequence. Interaction with DNA is mediated by amino acid residues in the N-terminal arm and third helix. Thereby the N-terminal arm interacts with DNA in the minor groove, whereas the third helix contacts the major groove (Figure 4). X-ray crystallography and nuclear magnetic resonance spectroscopy have been used to come to this conclusion. Basic residues 3 and 5, both located on the N-terminal arm have been found to contact the nucleotides A_2 and T_1 respectively of the TAAT core sequence. On the third helix, a hydrophobic residue numbered 47 and a conserved asparagine (Asn) at position 51 have been identified to interact with T_4 and A_3 respectively of the DNA recognition sequence (Desplan et. al., 1988; Qian et al., 1989; Kissinger et al., 1990; Otting et al., 1990).

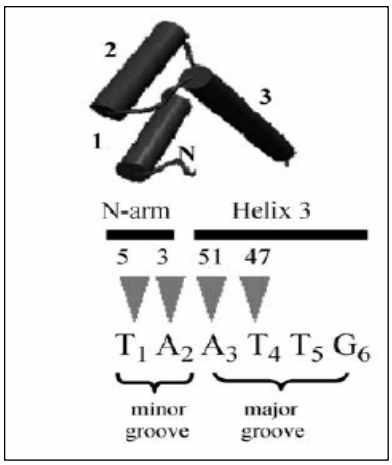

Figure 4. Structure of the homeodomain. The homeodomain is composed of an N-terminal arm and three alpha helices that form a helix turn helix motif. Amino acid residues in the N-terminal arm and in helix 3 mediate interaction with DNA in the minor and the major groove respectively. Numbers of amino acid residues interacting with theTAAT core sequence are shown (T Svingen and KF Tonissen, 2006).

3.2.4 HOXA3

A certain member of the HOX gene family, HOXA3 has been found to be of great importance for the development of thymus, thyroid and parathyroid in embryonic mice. Mice homozygous for HOXA3 mutation are characterized by the absence of thymus and parathyroids, as well as by thyroid hypoplasia. Embryonic HOXA3 is expressed in neural

crest derived mesenchymal cells of the pharyngeal arches and in the pharyngeal endoderm. These regions are known to give rise to thymus, thyroid and parathyroid explaining the strong influence of HOXA3 on the development of these structures. According to further studies, the transcription factors HOXA3 and PAX1 are necessary for the development of thymic epithelial cells which interact with thymocytes, in order to promote thymocyte maturation into T-cells. Mice heterozygous for HOXA3 and homozygous for PAX1 mutation have defects in thymic epithelial cell development. Decreased MHC class II expression and impaired capability to promote thymocyte development are typical for thymic epithelial cells of these mutants (Manley and Capecchi, 1995; Manley and Capecchi, 1998; Dong-ming Su and Manley, 2000).

Further studies have revealed that HOXA3 expression leads to cell migration in endothelial and epithelial cells. The consequence is an activity promoting both, angiogenesis and wound closure. Constitutive expression of HOXA3 in an immortalized human dermal microvascular endothelial cell line HMEC-1 has shown that HOXA3 causes upregulation of genes involved in cell-cell and cell-extracellular matrix (ECM) interactions. These genes, such as uPAR and MMP-14 are important for an increase of the angiogenic potential of endothelial cells by degradation of ECM-constituents. HOXA3 has been found to be upregulated in wounded tissues of mice, where it promotes angiogenesis in order to initiate wound repair. Interestingly, further studies have revealed a lack of HOXA3 in wounds of diabetic mice. However, transfer of HOXA3 expression plasmids into the wounded diabetic tissue has resulted in upregulation of uPAR and MMP-14, leading to accelerated wound closure. These data suggest a therapeutic value of HOXA3 for diabetic patients *via* its activity in endothelial cells (Kimberly et al., 2005).

HOXA3 also seems to play a role in diabetic microangiopathy, a process characterized by thickening of the capillary basement membrane of patients suffering from diabetes mellitus. A candidate gene set containing 125 genes, including HOXA3 has emerged to be of relevance to diabetic microangiopathy. This gene set has been identified by gene expression profiling comparing (i) BECs derived from tissue samples of diabetic and non-diabetic patients and (ii) BECs cultured *in vitro* under diabetic conditions, as well as by literature search. HOXA3 has been found to be upregulated under diabetic conditions (Nikolaus Wick et al., unpublished data). Furthermore, HOXA3 constitutively expressed in HMEC-1 leads to upregulation of collagen, type VI, alpha 1 (Kimberly et al., 2005). Thickening of the capillary basement membrane during diabetic microangiopathy is characterized by increases in type IV and type

VI collagen (Williamson JR, Tilton RG et al., 1988), suggesting a possible significance of HOXA3 for this process.

One aim of this diploma thesis is to report the role of transcription factor HOXA3 in diabetic microangiopathy by examining its effects upon transient expression in immortalized human umbilical vein endothelial cells (iHUVECs) on the genes within the candidate set. Another aim is to identify the position of the HOXA3 gene in a gene network that is assumed to be of relevance to diabetic microangiopathy.

4 Materials and methods

4.1 Buffers and solutions

4.1.1 Buffers and solutions for molecular biological methods

LB (Luria Broth) medium

10 g Bacto-tryptone (DIFCO, USA, cat. no. 211705)

5 g Bacto-yeast extract (DIFCO, cat. no. 212750)

10 g NaCl

1N NaOH was added until pH was adjusted to 7.5.

Water was then added to a final volume of 1000 ml. Finally, medium was autoclaved and cooled down to 50-55°C.

LB (Luria Broth) agar plates

700 ml LB medium (see above)

10.5 g agar (DIFCO, cat. no. 281230)

The mixture was autoclaved and cooled down to 50-55°C.

Antibiotics (30 µg/ml ampicillin, chloramphenicol or kanamycin) were added at a ratio of 1:1000 (700 µl) to yield a final concentration of 30 µg/µl. Afterwards, 20-30 ml volumes of medium were transferred into Petri dishes and the plates were stored at 4°C.

TENS lysis buffer (Plasmid preparation method "Genevieve")

0.5 ml 1M TRIS-HCl pH 8 (10mM)

100 µl 0.5M EDTA (1mM)

5 ml 1N NaOH (0.1N)

1.15 ml 20%SDS

43.25 ml Distilled water

4.1.2 Buffers and solutions for cell biology methods

Molecular weights

Tris: 121.14 g; Glycine: 75.07 g; EDTA: 380.2 g; DTT: 154.25 g;

1 x PBS (Washing buffer)

0.20 g KCl

0.20 g KH_2PO_4

1.15 g Na_2HPO_4

8.00 g NaCl

Distilled water was added to a final volume of 1000 ml. HCl was used to adjust pH 7.4.

0.1% Triton X-100

50 µl Triton X-100

Addition of 1 x PBS to a final volume of 50 ml

4.1.3 Buffers and solutions for SDS-PAGE/Western blot

1M Tris-HCl pH 6.8/8.8

121.14 g Tris base

1000 ml of double distilled water

Addition of HCl until pH 6.8/8.8 was adjusted

Laemmli Buffer

6.25 ml of 1M Tris-HCl, pH 6.8 (62.5 mM)

2.35 g SDS (2.35%)

0.038 g EDTA (1 mM)

10 ml Glycerol (10%)

0.001 g Bromphenol blue

1.543 g DTT (100 mM)

Water was added to a volume of 1000 ml. Laemmli Buffer containg DTT was aliquoted and stored at -20°C.

12% Acrylamid gel

3.3 ml Distilled water

4.0 ml 30% Acrylamid BIS (29:1, BioRad)

2.5 ml Tris-HCl, pH 8.8

0.1 ml 10% SDS

0.1 ml 10% APS

4.0 µl TEMED (N,N,N',N'-Tetramethylethylenediamine)

Stacking gel

3.4 ml Distilled water

830 µl 30% Acrylamid BIS (29:1, BioRad)

630 µl Tris-HCl, pH 6.8

50 µl 10% SDS

50 µl 10% APS

5 µl TEMED (N,N,N',N'-Tetramethylethylenediamine)

10 x Electrophoresis buffer for SDS-PAGE

360.325 g Glycin (192 mM)

75.7125 g Tris (25 mM)

25 g SDS (0.25%)

Distilled water was added to a volume of 2500 ml. For electrophoresis 10 x electrophoresis buffer was diluted 10 fold.

Transfer buffer for Western blot

36.034 g Glycine (192 mM)

7.571 g Tris (25 mM)

500 ml Methanol (20%)

Distilled water was added to a volume of 2500 ml and pH was adjusted to 8.5.

Ponceau S Red

0.1 % Ponceau S Rot in distilled water

5 % Acetic Acid

10 x TBS (Tris Buffered Saline)

24.5 g Tris

80.0 g NaCl

Distilled water was added to a volume of 1000 ml and pH was adjusted to 7.6

1 x TBS with Tween (TBST)

900 ml Distilled water

1 ml Tween-20

100 ml 10 x TBS

Blocking buffer (5% milk powder in TBST)

5 ml 10 x TBS

45 ml distilled water

2.5 g nonfat dry milk (5%)

50 µl Tween-20

Antibody dilution buffer (2.5% milk powder in TBST)

2 ml 10 x TBS

18 ml distilled water

0.5 g nonfat dry milk (2.5%)

20 µl Tween-20

4.2 Cloning vectors

Two cloning vectors (Figure 5) were used for cloning the coding sequence of the HOXA3 gene:

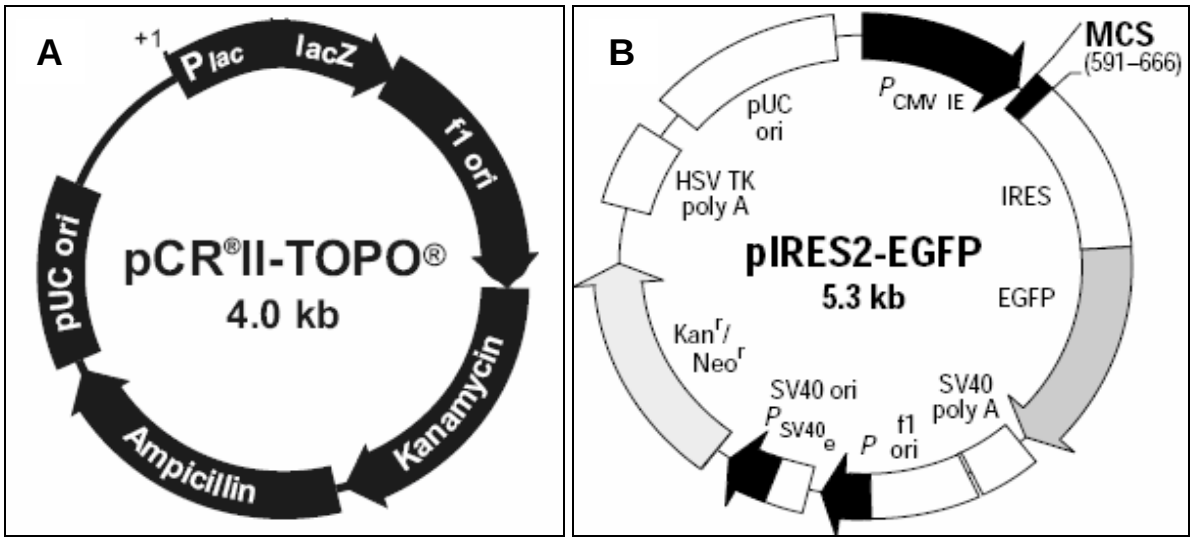

Figure 5. Cloning vectors used for cloning the coding sequence of the HOXA3 gene were pCR® II TOPO® (5a) and pIRES2-EGFP (5b).

After PCR, the coding sequence of the HOXA3 gene was subcloned into the **pCR® II TOPO® vector** (Figure 5a) that was purchased from Invitrogen. Topoisomerase I isolated from *Vaccinia* virus is covalently attached to the plasmid vector. After recognizing the specific sequence CCCTT on one strand, the enzyme binds to duplex DNA where it cleaves the phosphodiester backbone after the last thymidine (T) of the recognition sequence (Shuman, 1991). Topoisomerase I activity on both strands of the pCR® II TOPO® vector generates single 3`-thymidine (T) overhangs. PCR products generated by Taq polymerase possess single deoxyadenosines (A) at their 3`ends enabling insertion into pCR® II TOPO®.
DNA-cleavage by topoisomerase I results in covalent attachment of the enzyme to the 3`phosphate of the cleaved strand of the plasmid vector, as mentioned above. Release of topoisomerase I is achieved by nucleophilic attack of the 5`hydroxyl of the broken strand. Therefore, PCR products require 5`hydroxyl instead of 5`phosphates for successful ligation into the vector (Shuman, 1994).
The pCR® II TOPO® vector has a molecular size of 4.0 kb and contains two antibiotic resistance marker genes that provide resistance to kanamycin and ampicillin. Furthermore, a pUC origin of replication confering propagation in *E.coli* and an f1 origin for synthesis of single stranded DNA are located on the plasmid vector.

The multiple cloning site resides within the sequence of the lacZα gene that is connected to the lac promoter. Cloning a DNA sequence into the multiple cloning site leads to interruption of the lacZ sequence resulting in a loss of function of the lacZα gene to produce the protein beta galactosidase. The fact that beta galactosidase turns its substrate X-gal into a blue dye is used to select for cells that contain plasmid vectors with an interrupted multiple cloning site. In case of successful cloning of a coding sequence into pCR® II TOPO®, transformed cells remain white in presence of X-gal due to interruption of the lacZα gene. Blue stained cells possess a functional lacZα gene that turns X-gal into a blue dye. IPTG inactivates the lac repressor resulting in activation of the lac operon. Therefore, addition of IPTG is necessary in order to enable the blue/white selection method.

The coding sequence of the HOXA3 gene was cloned into the expression vector **pIRES2-EGFP** (Figure 5b) purchased from Clontech Laboratories, Inc., in order to study transient overexpression of HOXA3 in immortalized human umbilical vein endothelial cells (iHUVECs). The characteristic of pIRES2-EGFP is the presence of the internal ribosomal entry site (IRES) of the encephalomyocarditis virus (ECMV). On the expression vector, the internal ribosomal entry site is located between the multiple cloning site and the coding region of the enhanced green fluorescent protein (EGFP). This construction enables translation of the gene that is cloned into the multiple cloning site and the EGFP gene from a single bicistronic mRNA. The multiple cloning site itself is located between the immediate early promoter of cytomegalovirus ($P_{CMV\ IE}$) and the IRES sequence

Expression of the EGFP gene indicates successful transfection into iHUVECs and other eukaryotic cells with pIRES2-EGFP carrying the gene of interest. However, it is important to note that synthesis of the EGFP protein does not require cloning of a gene into the multiple cloning site of the expression vector. Therefore, pIRES2-EGFP may be used for control transfection. Processing of the bicistronic mRNA is directed by SV40 polyadenylation signals located downstream of the EGFP gene. Furthermore, pIRES2-EGFP contains an SV40 origin conferring replication in eukaryotic cells expressing the SV40T antigen.

Another feature of pIRES2-EGFP is the presence of both, a pUC origin of replication enabling propagation in *E.coli* and an f1 origin for synthesis of single stranded DNA. Antibiotic resistance genes confer resistance to kanamycin and neomycin (BD Biosciences Clontech).

4.3 Molecular biology methods

Bacterial cultures

DH10B TonA cultures transformed with plasmid pCMV-Sport6 carrying the HOXA3 gene were purchased as glycerol stock from Invitrogen (cat. no. 3905733). Before starting a PCR, overnight cultures had to be grown by combining 1.0 µl aliquots of the glycerol stock with 4 ml of LB-medium. In order to select for cells containing the pCMV-Sport6 plasmid the antibioticum ampicillin (100 mg/ml) was added at a ratio of 1:1000 to the mixture (final concentration of Ampicillin:100 µg/ml).

Plasmid DNA isolation (plasmid "miniprep")

Plasmid miniprep was done for 1.5 ml of each bacterial over night culture. After a quick spin in the Eppendorf Microcentrifuge at 10,000 rpm and following disposal of the supernatant the remaining cell pellet was dissolved in 300 µl of TENS and 150 µl of 3M potassium acetate to cause cell lysis. Then, the lysate was centrifuged for 2 min. at 13,000 rpm (17,900 x g) and the supernatant was transferred into a fresh tube. After adding 900 µl of 96% ethanol the resulting mixture was put on -80°C for 30 min. Afterwards the solution was centrifuged for 20 min. at 4°C and the supernatant was removed. The remaining cell pellet was washed with 900 µl of 70% ethanol and the resulting solution was centrifuged again for 2 min. at 13,000 rpm. After removing the ethanol the pellet was air dried and dissolved in 50 µl DNase free water.

Restriction digestion of pCMV-Sport6

After elution of plasmid DNA in 50 µl DNase free water a restriction digest of an aliquot of 5.0 µl and subsequent gel electrophoresis on 1 % agarose gel containing ethidium bromide were executed in order to control the success of pCMV-Sport6 isolation and to check whether the plasmids carried the right insert. The restriction endonucleases NheI (recognition sequence: GCTAGC) and StuI (recognition sequence: AGGCCT) were used to cut the insert out of pCMV-Sport6. All reagents used for digestion were purchased from New England BioLabs Inc.

The composition of the 20 µl reaction mix was as follows:

- 5.0 µl…….DNA
- 0.5 µl…….RNase
- 1.0 µl…….StuI
- 1.0 µl…….NheI
- 0.2 µl…….BSA (at a ratio of 1:100 to the total volume)
- 2.0 µl…….10 x buffer (NEBuffer 2; at a ratio of 1:10 to the total volume)
- 10.3 µl…….Water (aqua dest.)

The reaction mix was incubated for 1-2 hours at 37°C. Before the samples were applied to the gel, 5.0 µl of loading dye were added.

PCR of HOXA3

Primers for the PCR reaction (also from Invitrogen) were designed with the aid of the OligoPerfect™ Designer program provided by Invitrogen. Primers were designed corresponding to the start and the end of the coding sequence of the HOXA3 gene to ensure that only the coding sequence was amplified during the PCR reaction. Restriction enzyme sites were added to the 5`ends of both, forward and reverse primer. Forward primer contained a restriction site for XhoI (CTCGAG) and an additional 5`CAGT extension leading to a primer sequence as follows: 5`-CAGTCTCGAGATGCAAAAAGCGACCTACTA-3`, whereas reverse primer possessed a restriction site for SalI (GTCGAC) and an additional 5`CAGT extension yielding the primer sequence 5`-CAGTGTCGACTCACAGGTGGGTGAGCTTG-3`. Primers diluted 1:10 in distilled water were added to the PCR reaction mix. Primer extension was catalyzed by Taq Polymerase purchased from Pharmacia. PCR was meant to deliver products containing the recognition sequence for XhoI (CTCGAG) on their 5` ends and the recognition sequence for SalI (GTCGAC) on their 3`ends. The whole 50 µl PCR reaction mix was composed of as follows:

- 0.5 µl…….DNA
- 2.0 µl…….dNTPs
- 3.0 µl…….Rapid load
- 5.0 µl…….PCR 10 x buffer (Pharmacia)
- 2.0 µl…….Primer (from 1:10 dilution)
- 0.5 µl…….Taq polymerase (5000 U/ml; Pharmacia)
- 37.0 µl…….Water (aqua dest.)

The PCR program was as follows:

95°C	5 min.	
76°C	2 min. (Addition of Taq polymerase)	
95°C	1 min.	40 cycles
60°C	1 min.	
72°C	90 sec.	
72°C	10 min.	
4°C	forever	

PCR was performed by GeneAmp PCR System 9600 for 40 cycles. The expected 1.3 kb PCR product was visualized by electrophoresis on 1% agarose gels containing ethidium bromide.

Extraction of the PCR products from the agarose gel and purification

Extraction and purification of the 1.3 kb PCR products were executed using the QIAquick® PCR Purification Kit from QIAGEN (cat. no. 28104). Three volumes of gel dissolving buffer QG were added to the excised gel slice containing the DNA of interest. The resulting mixture was incubated at 50 °C until the gel was completely dissolved. Then 1 gel volume of isopropanol was added and the resulting solution was mixed by vortexing. Afterwards the solution was applied to a QIAquick spin column in a 2.0 ml collection tube. In order to bind DNA to the silicia membrane of the spin column the mixture was centrifuged for 1 min. at 13,000 rpm. After removing the flow-through, bound DNA was washed with 750 µl of Buffer PE and centrifuged again for 1 min. at 13,000 rpm. Then the QIAquick spin column was placed into a fresh 1.5 ml tube and DNA was eluted by adding 30 µl of distilled water to the center of the silicia gel membrane and further centrifugation for 1 min. at 13,000 rpm.

Ligation of DNA into pCR® II TOPO® vector

Purified PCR products were subcloned into the pCR® II TOPO® vector according to the protocol of the TOPO TA cloning® kit from Invitrogen.

- 2.0 µl…….DNA (PCR product)
- 1.0 µl…….Salt solution
- 2.0 µl…….Water (aqua dest.)
- 1.0 µl…….pCR II TOPO vector

Both, TOPO vector and salt solution were components of the cloning kit. Incubation time of the ligation mix was up to 30 min. 2µl of the ligation mix were used for transformation of *E.coli* DH5α.

Transformation of *E.coli* DH5α

For transformation One Shot® MAX Efficiency® DH5 α ™ Chemically Competent Cells (cat.no.12297-016) purchased from Invitrogen were used. After the cells were put on ice, 2-6 µl of the ligation reaction were added. The cells were incubated on ice for 30 min. before a heat shock of 30 sec. at 42°C was executed. In the next step 250 µl of SOC-medium (pre warmed at 37°C) were added to the cells and the resulting mixture was shaken at 37°C and 225 rpm for 1 h. Afterwards, the mixture was plated onto LB-plates supplemented with kanamycin. The plates were incubated at 37°C overnight. Next day single colonies were picked from the plates by pipette tips and overnight cultures were started by placing the tips into tubes containing 4.0 ml LB-medium and adding kanamycin (30 mg/ml) at a ratio of 1:1000 (final concentration of kanamycin:30 µg/ml). Isolation of plasmids carrying the gene of interest was done according the plasmid miniprep protocol as described above.

Restriction digestion of TOPO vectors

DNA ligated into pCR® II TOPO® vector was supposed to contain the recognition sites for endonucleases XhoI (CTCGAG) and SalI (GTCGAC) on the 5`end and the 3`end respectively. In order to cut the DNA of interest out of the TOPO vector a restriction digest using the endonucleases XhoI and SalI was performed. The restriction endonucleases were meant to create sticky ends for ligation into the vector pIRES2-EGFP. The composition of the reaction mix was as follows:

- 30.0 µl…….DNA
- 1.0 µl…….RNase
- 1.5 µl…….XhoI
- 1.5 µl…….SalI
- 0.5 µl…….BSA (at a ratio of 1:100 to the total volume)
- 5.0 µl…….10 x buffer (NEBuffer 2; at a ratio of 1:10 to the total volume)
- 10.5 µl…….water (aqua dest.)

All reagents used for digestion were purchased from New England BioLabs Inc. The digestion was carried out for at least 3 h up to 16 h. Before the reaction mix was applied to the 1% agarose gel containing ethidium bromide, 5.0 µl of loading dye were added.
The expected 1.3kb products were extracted and purified according to the protocol of QIAquick® PCR Purification Kit from QIAGEN (cat. no. 28104).

Ligation of DNA into pIRES2-EGFP and transformation of *E.coli* DH5α

HOXA3 DNA possessing sticky ends created by restriction digestion with the restriction endonucleases XhoI and SalI had to be cloned into the multiple cloning site of the expression vector pIRES2-EGFP (Clontech Laboratories Inc., CA, USA, discontinued). In order to ensure ligation, the expression vector needed to have sticky ends compatible to those of the HOXA3 insert. Thus the empty vector had to be treated with the same restriction endonucleases as the HOXA3 gene. Ligation of the coding sequence of HOXA3 into pIRES2-EGFP was catalysed by T4 DNA-ligase (Invitrogen). The ligation reaction mix was composed of:

- 6.0 µl…….HOXA3 DNA
- 2.0 µl…….pIRES2-EGFP
- 1.0 µl…….10 x ligase buffer
- 1.0 µl…….T4 DNA-Ligase

Ligation was executed at 16 °C overnight. Transformation of E.coli DH5α was done with 5 µl of ligated DNA as described above.

Capillary sequencing

Capillary sequencing was performed in order to control, whether pIRES2-EGFP was carrying the coding sequence of the HOXA3 gene. First, cycle sequencing reactions were executed to generate ddNTP labelled DNA fragments which could be detected afterwards by the ABI Prism 377 sequencing detection system. Primers used for the cycle sequencing reaction were pIRES sequencing forward and reverse primer purchased from Invitrogen. The composition of the cycle sequencing reaction mix was as follows:

- 5.0 µl…….Water (aqua dest.)
- 2.0 µl…….Primer (pIRES sequencing forward **or** reverse primer)
- 2.0 µl…….Big Dye ™ Reaction Mix (Applied Biosystems)
- 1.0 µl…….DNA

For each sample that had to be sequenced two cycle sequencing reaction mixes were prepared which differed in added primers. One mix contained pIRES sequencing forward primer whereas the other cycle sequencing reaction mix contained pIRES sequencing reverse primer. DNA polymerase needed for primer extension as well as ddNTPs were contained in the added Big Dye ™ Reaction Mix.
Cycle sequencing reaction program:

96°C	1 min.	
96°C	12 sec.	29 cycles
56°C	7 sec.	
60°C	2 min.	
4°C	forever	

After finishing the cycle sequencing reaction unincorporated ddNTPs were removed from the reaction mix by using the DyeEx 2.0 Spin Kit (cat. no. 63206) purchased from QIAGEN. Columns filled with Sephadex G50 were used to remove unbound ddNTPs. DNA fragments labelled with ddNTPs were eluted in 20 µl of water. Before sequencing was finally started 20 µl of formamide were added to the samples.

Endotoxin free plasmid midipreparation

Endotoxin free plasmid midipreparation was executed using the QIAfilter™ Midi Kit (25) from QIAGEN (cat. no. 1224). Initially, 5 µl of the glycerol stock of transformed bacterial cells were added to 50 ml LB medium supplemented with 50 µl kanamycin. The resulting mixture was incubated on a shaker at 37°C and 225 rpm overnight. The next day, the bacterial cell suspension was centrifuged for 20 min. at 6000 x g at 4°C and the resulting bacterial cell pellet was dissolved in 4 ml of RNase A-containing buffer P1. After addition of lysis buffer P2 and an incubation time of 5 min., neutralization buffer P3 was added. The resulting mixture was poured into the barrel of a QIAfilter Cartridge and after 10 min. of incubation the cell lysate was filtered into a 50 ml Falcon tube. In the next step, 1ml buffer ER was added to

the filtered lysate and after 30 min. of incubation on ice, the lysate was applied to an equilibrated QIAGEN tip where the plasmid DNA was expected to bind to anion-exchange resin. The QIAGEN tip was then washed twice with 10 ml buffer QC. Elution of plasmid DNA was executed with 5 ml of buffer QN. The eluted DNA was collected in a 10 ml endotoxin free polyallomer tube. After addition of 3.5 ml room-temperature isopropanol to the eluate in order to achieve precipitation of plasmid DNA, the mixture was centrifuged for 30 min. at 15,000 x g and 4°C. The resulting DNA pellet was washed with 2 ml of endotoxin free room-temperature 70% ethanol. After further centrifugation for 10 min. at 15,000 x g followed by removal of the supernatant, DNA was dissolved in 100 µl of endotoxin free water. Finally, DNA concentration was measured as described below. Endotoxin free DNA obtained from endotoxin free plasmid midipreparation was used for transfection of iHUVECS in order to study transient overexpression of the HOXA3 gene in an endothelial cell line.

Spectrophotometric measurement of DNA concentration

.A U-2000 Spectrophotometer (Hitachi) was used to determine DNA concentration of a sample by measuring the optical density (absorbance) at 260 nm. Before measurement, dilution of the sample was executed at a ratio of 1:200 by adding 3 µl of the sample to 600 µl of DNase free water.

The measured absorbance was used to determine DNA concentration according to the formula:

c [µg/ml] = OD_{260} x D x F

c ….Concentration of DNA (µg/ml)

OD_{260} ....Absorbance (optical density) at 260 nm

D ….Dilution used

F ….Strandedness of DNA (50 for dsDNA)

Measurement of DNA concentration was executed in order to use appropriate amounts of endotoxin free DNA for transfection of iHUVECs.

Total RNA isolation from transfected cells

Cells successfully transfected with pIRES2-EGFP carrying the gene of interest were centrifuged for 2 min. at 2,800 rpm and 4 °C. The cell pellet was then dissolved in 1ml of RLT buffer supplemented with 1% β-mercaptoethanol. In preparation for total RNA isolation, the mixture was applied to QIAshredder^{TM} (50) from QIAGEN (cat. no. 79654) in order to

homogenize the cell lysate by centrifugation for 2 min. at 13,000 rpm. Total RNA isolation was executed using the Rneasy® Mini Kit (50) from QIAGEN (cat. no. 74104). In the beginning, 350 µl of RNase-free 70 % ethanol were added to the homogenized sample and the resulting mixture was applied to an RNeasy spin column. The loaded RNeasy spin column was centrifuged for 2 min. at 13,000 rpm in order to achieve binding of total RNA to the silicia gel membrane. Buffer RW1 was used to wash RNA bound to the silicia gel membrane and to remove unwanted excess material. Degradation of unwanted genomic DNA was accomplished by incubation of the silicia gel membrane with DNase I diluted with buffer RDD at a ratio of 1:8. Two further washing steps were carried out using buffer RPE before 30 µl of RNase-free water were added to elute RNA.

Reverse transcription

Reverse transcription of total RNA isolated from successfully transfected iHUVECs was carried out in order to produce cDNA that was applied to TaqMan Low Density Custom Arrays for high throughput real time PCR.

For reverse transcription 20 µl of total RNA were added to Sprint™ PowerScript™ PrePrimed Single Shots (Clontech) containing lyophilized master mix composed of reverse transcriptase, random hexamer or oligo$(dT)_{18}$ primers (20 µM), BSA (10mg/ml), DTT (1M), dNTP mix (10mM each), 10x reaction buffer, cryoprotectant and stabilizers. Reverse transcription was carried out using GeneAmp PCR System 9600.

The thermal cycler program for reverse transcription was as follows:

42 °C	90 min.	1 cycle
70 °C	10 min.	
4 °C	forever	

Multiplex PCR

Multiplex PCR was executed in order to control the quality and integrity of cDNAs produced by reverse transcription. The four housekeeping genes BCR, β2-microglobulin, ABL and PBGD were chosen for amplification. Multiplex PCR was carried out using AmpliTaq Gold®, 5 x 1000 U, with GeneAmp® 10X PCR Gold Buffer and $MgCl_2$ Solution from Applied Biosystems (cat. no. 4311818). Furthermore, GeneAmp dNTPs, also purchased from Applied Biosystems, (cat. no. N808-0007) were added to the PCR reaction mix. Primer pairs for the four housekeeping genes were mixed together and diluted at a ratio of 1:10.

The multiplex PCR reaction mix was composed of as follows:

- 32.75 µl…….Water (aqua dest.)
- 5.0 µl…….10X PCR Gold Buffer
- 3.0 µl…….$MgCl_2$ Solution (1.5 mM)
- 4.0 µl…….dNTPs (final concentration 200 µM)
- 3.0 µl…….Rapid load
- 0.25 µl…….AmpliTaq Gold® (1.25 Units)
- 1.0 µl…….Primer (from 1:10 dilution, final concentration: 2 µM)
- 1.0 µl…….cDNA

The thermal cycler program for multiplex PCR was as follows:

95°C	5 min.	
95°C	1 min.	40 cycles
56°C	1 min.	
72°C	90 sec.	
4°C	forever	

GeneAmp PCR System 9600 was used in order to perform multiplex PCR. The sample was applied to a 2% agarose gel containing ethidium bromide and the PCR products were separated according to their length (BCR: 377 bp, β2-microglobulin: 287 bp, ABL: 193 bp, PBGD: 128 bp) by agarose gel electrophoresis.

High throughput real time PCR

The aim of high throughput real time PCR was to investigate the effects of overexpression of the HOXA3 gene on the expression of 125 candidate genes relevant to diabetic microangiopathy. TaqMan® Low Density Custom Arrays (Applied Biosystems) were constructed in order to enable 128 simultaneous quantitative real time PCR reactions. More precisely, 128 candidate gene specific primers and probes were spotted onto a total of two micro-fluidic cards referred to as DMA1 and DMA2. Each of these 384-well micro-fluidic cards contained two series of 64 pre-made assays that were applied in triplicates. GAPDH specific primers and probes were located on both TaqMan® Low Density Custom Arrays. In addition, DMA2 contained assays for the housekeeping genes NARS and TARDBP which

were not part of the candidate gene set but were chosen for normalization as described below. Thus, both TaqMan® Low Density Custom Arrays comprised a total of 128 pre-made assays (Table 1).

For quantitative real time PCR 100 µl of a reaction mix composed of 20 µl cDNA, 405 µl water (Aqua dest.) and 425 µl 2 x TaqMan Universal PCR Master Mix were applied to 4 from 8 loading ports of DMA1 and DMA2 respectively. Subsequent centrifugation of the micro-fluidic cards at 330 g for 2 min. was executed in order to achieve migration of the samples into the wells. Finally, high throughput PCR was carried out using the ABI Prism 7700 sequence detection system (Applied Biosystems).

Table 1. List of candidate genes that were represented in the form of pre-made assays spotted on TaqMan® Low Density Custom Arrays.

Number	Gene symbol	Number	Gene symbol	Number	Gene symbol	Number	Gene symbol
1	ABL2	33	EBF	65	MAP4	97	PTK2
2	ACE	34	EGF	66	MAPK11	98	PXN
3	ADH1A	35	EPHA4	67	MAPK12	99	RAMP3
4	ADH1B	36	ET	68	MAPK14	100	RHOJ
5	AGT	37	F2	69	MCFP	101	RPIB9
6	ALDOA	38	FBXO7	70	MINPP1	102	RPL13
7	ANGPT1	39	FGF1	71	MMP2	103	RPLP0
8	ANGPT2	40	FLT1	72	MMP9	104	SERPINE1
9	AQP1	41	FN1	73	MT1A	105	SLC2A1
10	ARF4	42	FZD4	74	NARS	106	SLCO2B1
11	ATP6	43	GAPDH	75	NDST1	107	SMAD2
12	BCL2	44	GAPDH	76	NFKB1	108	SMAD3
13	BMX	45	GCA	77	NOP5/NOP58	109	SOD1
14	BTF3	46	GDI2	78	NOS3	110	SORBS1
15	C13orf10	47	GJA1	79	NOX5	111	SRRM1
16	C1S	48	GNAS	80	OASL	112	STAT3
17	C7	49	GTPBP4	81	OSBPL10	113	STOM
18	CALM2	50	HOXA3	82	OSBPL1A	114	TAF7
19	CASP3	51	HPN	83	PARK7	115	TARDBP
20	CD59	52	ICAM1	84	PARP1	116	TGFB1
21	CDYL2	53	IER3	85	PCK1	117	TGFBR2
22	CFH	54	IGF1	86	PCK2	118	TH1L
23	CFL1	55	IGF2	87	PDGFA	119	THBD
24	CMAH	56	IL8	88	PHGDH	120	TIMP2
25	COL4A1	57	ITGA1	89	PLAGL1	121	TNC
26	CRP	58	ITM1	90	PLD1	122	TOR3A
27	CSPG2	59	JUN	91	PPAP2A	123	UBE4A
28	CTGF	60	KLF6	92	PPP1CB	124	UGDH
29	CTSZ	61	LAMB1	93	PRG1	125	USP34
30	CXCL12	62	LEPR	94	PRKACA	126	VCAM1
31	CYR61	63	LEREPO4	95	PRKCB1	127	VEGF
32	DGKE	64	LMCD1	96	PRSS23	128	VIM

GAPDH specific primers and probes were found on DMA1 as well as DMA2. Housekeeping genes NARS and TARDBP were chosen for normalization.

4.4 Bioinformatics

Analysis of data obtained from high throughput real time PCR

Tresholds were set manually within regions of linear increase of sigmoid curves generated by analysis of high throughput real time PCR with SDS 2.2 software (Applied Biosystems). Finally, data were exported and calculation of the fold change was done using the ΔΔCt method. In the beginning, Ct values of the sample were normalized to Ct values of GAPDH, in order to compensate differences in measurements of the sample between DMA1 and DMA2. Ct values normalized to those of GAPDH were then normalized to Ct values of two housekeeping genes (NARS and TARDBP) in order to be able to compare overexpression experiments carried out with different genes. Finally, Ct values of the sample were compared to those of the calibrator sample obtained by transfection of iHUVECs with the empty vector. Building the difference between the sample to be measured and the calibrator sample allowed for determining the fold change ratio.

Construction of a gene network relevant to diabetic microangiopathy

The fold change ratio (FC) was determined according to the formula:

$FC = 2^{-\Delta Ct} = x_{ij}/x_i^0$

x_i^0 …gene expression of the i-th gene

x_{ij} …gene expression of the i-th gene when the j-th gene is perturbed

Next, the influence matrix (D) was built in order to describe the effect of perturbation of gene j on the expression of gene i:

$D_{ij} = \ln (x_{ij}/x_i^0)$

Building of D was expected to yield one of the three possible results:

$$D_{ij} = \begin{cases} > 0 & \text{…perturbation of gene j leads to overexpression of gene i} \\ < 0 & \text{…perturbation of gene j leads to downregulationof gene i} \\ = 0 & \text{…perturbation of gene j has no effect on the expression of gene i} \end{cases}$$

The next step was carried out according to following consideration: In a given gene network represented by the adjacency matrix (A) it was necessary to find all the direct and indirect regulatory links between gene i and gene j. The connection between the influence matrix (D) and adjacency matrix (A) is given with the following equation:

$A_{ji} = \ln (D+I)$, where $\ln(D+I)$ is a matrix logarithm.

Finally, a threshold was set, corresponding to in advance given network connectivity, to select significant link weights. The non-significant ones, below the threshold, were set to zero.

4.5 Cell biology methods

Cells

Immortalized human umbilical vein endothelial cells (iHUVECs) were a kind gift from Professor Miertinnen (University of Helsinki, Finland). These cells were immortalized with the human telomerase catalytic protein (hTERT). Immortalized human umbilical vein endothelial cells have previously been shown to largely maintain their endothelial character, a property necessary for the studies of diabetic microangiopathy. Another reason for choosing iHUVECs was technical feasibility including a reasonable transfection efficiency (30-75 % with pIRES2-EGFP) that would be important for later transfection studies. Cells were maintained in RPMI 1640 medium (GIBCO, cat. no. 51800-035) supplemented with 10 % FBS (fetal bovine serum, GIBCO, cat. no.10108-157) and 1% penicillin/streptomycin (GIBCO, cat. no.15140-122). Incubation of iHUVECs was carried out at 37 °C in an incubator with a CO_2 content of 5 % and 90 % relative humidity.

Transfections

Transfection was carried out when iHUVECs maintained in in RPMI 1640 medium (GIBCO, cat. no. 51800-035) supplemented with 10 % FBS (fetal bovine serum, GIBCO, cat. no.10108-157) and 1% penicillin/streptomycin (GIBCO, cat. no.15140-122) were grown to 90-95% confluence. The amount of endotoxin free plasmid DNA, Lipofectamine2000™ (Invitrogen, cat. no. 11668-027) and OptiMEM® (Invitrogen) used for successful transfection was adapted according to the effective growth area of the culture dishes where the cells were grown. At the beginning, endotoxin free plasmid DNA (0.4 μg/cm^2) and the cationic lipid-based reagent Lipofectamine2000™ (0.5 μl/cm^2) were separately incubated in tubes containing OptiMEM® (25 μl/ cm^2) for 5 min. at room temperature. Prior to transfection, the contents of both tubes were combined and incubated at least for further 20 min. at room temperature. The transfection mix was then added to the grown cells and after 2-4 h of incubation at 37°C the mixture was removed and RPMI 1640 medium supplemented with 10 % FBS (fetal bovine serum) and 1% penicillin/streptomycin was added to the cells. After 24 h of incubation at 37°C fluorescence microscopy was used to identify iHUVECs that were successfully transfected with pIRES2-EGFP carrying the gene of interest. According to the

manufacturer the EGFP encoded by the plasmid was expected to have its excitation maximum at 488 nm and its emission maximum at 507 nm.

Flow cytometry

Flow cytometry was carried out by the Division of Rheumatology/Department of Internal Medicine III in cooperation with the Core Unit Cell Sorting, both from the Medical University of Vienna. Flow cytometric cell sorting was performed in order to isolate and quantify successfully transfected cells. Cells were harvested 48 h after transfection by addition of 1x trypsine/EDTA and immediate centrifugation for 4 min. at 1800 rpm. The resulting pellet was resuspended in 1 ml of RPMI 1640 medium supplemented with 10 % FBS (fetal bovine serum) and 1% penicillin/streptomycin and 7-amino-actinomycin D (7-AAD, Fluka, Buchs SG, Switzerland, cat. no. 06648) was added at 1 µg/ml. Flow cytometric cell sorting was then carried out using a BD FACSAria™ flow cytometer, EGFP emission being detected via FL1 channel using a bandpass filter at 530±15nm. Sort criteria combined a generously wide scatterlight region excluding small particles (cell fragments and debris) with positivity for EGFP as well as negativity for 7-AAD. Furthermore, transfection efficiencies and EGFP half-life were determined using a BD FACSCalibur™ flow cytometer. The sorted EGFP-positive, 7-AAD negative cells were lysed in 350µl of RLT buffer supplemented with 1% β-mercaptoethanol and stored at -80°C until RNA isolation was executed. For isolation of sufficient RNA, the sorting had to yield at least 300,000 EGFP-positive cells.

Immunefluorescence staining of HOXA3 proteins

The purpose of immunefluorescence staining was to analyze the distribution of the HOXA3 protein in the cell under several conditions including transient expression of the protein to be analyzed, overexpression of another protein or normal conditions. Prior to immune fluorescence staining iHUVECs maintained RPMI 1640 medium supplemented with 10 % FBS (fetal bovine serum) and 1% penicillin/streptomycin were grown in 9.6 cm^2 petri dishes. On the day of staining the medium was removed and the cells were fixed in 4% PFA in PBS for a minimum of 10 min at room temperature. After removal of 4% PFA/PBS the cells were washed three times with PBS and 0.1% Triton-X-100 in PBS was added for permeabilization of the cell membrane. After 10 min. of incubation at room temperature Triton-X-100 was removed and 200 µl of goat serum diluted in PBS at a ratio of 1:10 were added to each 9.6 cm^2 dish for 20 min. in order to block unspecific binding sites. Prior to use, the primary antibody (Anti-HOXA3) was diluted in PBS at a ratio of 1:100. The antibody of choice

against HOXA3 was the unconjugated polyclonal antibody anti-homeobox protein Hox-A3 (AVIVA SYSTEMS BIOLOGY; cat. no. ARP36056_T200) produced in rabbits. Anti-Hoxa3 was delivered in a state lyophilised from PBS buffer with 2% sucrose. After addition of 100 µl distilled water the final antibody concentration was 2 mg/ml.

The primary antibody was added to the cells for 45 min. at room temperature. Afterwards, the cells were washed with PBS before the secondary antibody diluted in PBS at a ratio of 1:1000 was added. In case of rabbit anti-human HOXA3 polyclonal antibody serving as primary antibody, the secondary antibody of choice was Alexa Fluor 594 goat anti-rabbit antibody (MolecularProbes) labelled with red-fluorescent dye. The secondary antibody was added for 45 min. at room-temperature. After washing with PBS, DAPI-staining (1:50,000) was executed for 1 min. in order to visualize cell nuclei. After the final wash step with PBS, cells were covered with GelTol mounting medium (Thermo Electron Corporation, PA, USA, cat. no. 484950) and a cover glass. Analysis of immunostained cells was performed under the microscope. AxioCam (ZEISS, Germany) was used for taking pictures of the cells.

4.6 Protein chemistry methods

Protein assay in Laemmi buffer

This method was executed according to the article of Karlsson et al. (1994) in order to determine protein concentrations within cell samples. At the beginning, cell samples were solubilized in Laemmli buffer and heated at 96°C for 3 min. before centrifugation at 10,000 x g for 5 min. was performed. Next, 9 µl aliquots of the samples were applied to a microtiter plate and diluted at a ratio of 1:10 by addition of 81 µl of Laemmli buffer.

Different concentrations (500 µg/ml, 250 µg/ml, 100 µg/ml, 50 µg/ml, 25 µg/ml and 10 µg/ml) of bovine serum albumin (BSA) solubilized in Laemmli buffer were prepared in order to determine protein concentrations of the samples by a BSA standard curve. Then, 90 µl of the respective BSA solutions were also applied to the microtiter plate.

Finally, 60 µl of 60% TCA were added to the samples and the BSA solutions and the yellow turned mixtures were incubated for 10-30 min. at room temperature.

Microplate reader Synergy-HT (BIO-TEK) was used for measuring turbidity of the samples and the BSA-solutions at 570 nm. Furthermore, a BSA standard curve was built in order to determine protein concentrations (µg/ml). In order to obtain correct protein concentrations it was necessary to take the dilution of the samples (1:10) into account.

Western blot analysis

Western blots of transfected and nontransfected iHUVECs were probed for HOXA3. Western blot analysis of HOXA3 protein was done for CFL1, CASP3 and HOXA3 transfected iHUVECs as well as for nontransfected cells. At the beginning 20µg of total protein isolated from transfected and nontransfected cells were applied to SDS-PAGE carried out at 120V. The running gel used for separation of proteins contained 12% acrylamide. Transfer of proteins to nitrocellulose membranes was carried out at 20V overnight. After transfer, the nitrocellulose membrane was stained with Ponceau S red in order to visualize proteins. The membrane was then blocked with 5% milk powder in 1xTBST for at least 20 min. The primary antibody was added at room temperature for 1 h. The antibody of choice against HOXA3 was Mouse Anti-Human HOXA3 Polyclonal Antibody, Unconjugated from ABR-Affinity BioReagents (cat. no. PA1-52660). Prior to use, anti-HOXA3 was diluted at a ratio of 1:1000 in 2.5% milk powder in 1xTBST. After 1 h of incubation with the primary antibody the membrane was washed three times for 5 min. each with1xTBST. The secondary antibody (HRP rabbit anti-mouse) diluted at a ratio of 1:4000 in 2.5% milk powder in 1xTBST was then added to the blots at room temperature for at least 1 h. Afterwards, several washing steps using TBST were carried out for 50 min. Finally, ECL plus™ Western Blotting Detection Reagent (Amersham Biosciences) was added to the blot prior to detection of HOXA3 by chemiluminescence using Lumi-Imager F1™ (Rocher). Analysis of images acquired by Lumi-Imager F1™ was carried out using LumiAnalyst™ software (Rocher).

5 Results

5.1 Flow cytometry

Separation and counting of iHUVECs successfully transfected with the cloned coding sequence of HOXA3 were executed by flow cytometric cell sorting. Thereby, we collected of a total number of 307,423 intact, viable EGFP-positive cells for subsequent isolation of total RNA.

5.2 RNA-isolation and Multiplex PCR

Total RNA isolated from iHUVECs transiently expressing HOXA3 was reverse- transcribed in order to obtain cDNA that could be applied to quantitative real time PCR. Before cDNA was loaded onto TaqMan® Low Density Custom Arrays, multiplex PCR of four housekeeping genes (BCR, β2-microglobulin, ABL and PBGD) was performed, providing information about quality and integrity of cDNAs produced by reverse transcription. Multiplex PCR products separated on a 2 % agarose gel yielded four bands of different size (Figure 6). In order to exclude technical failures concerning the method, multiplex PCR was carried out for a control sample as well (data not shown).

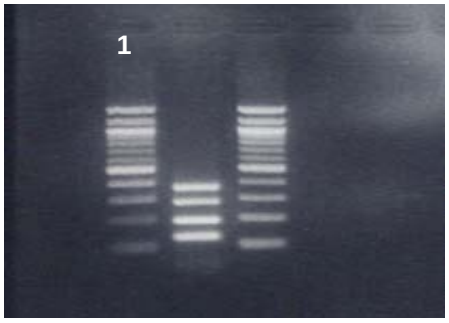

Figure 6. Control of quality and integrity of cDNA sample
Multiplex PCR of the four housekeeping genes (BCR, β2-microglobulin, ABL and PBGD) and subsequent separation of the PCR products by 2 % agarose gel electrophoresis yielded four bands (lane 2) of different size (BCR: 377 bp, β2-microglobulin: 287 bp, ABL: 193 bp, PBGD: 128 bp). The 100 bp ladder (lanes 1 and 3) was used as size marker.

5.3 Quantitative real time PCR

5.3.1 Determination of fold change and correlation in expression patterns

The aim of high throughput real time PCR was to investigate the effects of transient expression of the HOXA3 gene on the expression of the 125 candidate genes relevant to diabetic microangiopathy. Therefore, cDNA obtained from reverse transcription of total RNA isolated from iHUVECs transiently expressing HOXA3 was loaded onto two TaqMan® Low Density Custom Arrays (referred to as DMA1 and DMA2). A total of 128 pre-made assays were spotted on both micro-fluidic cards enabling 128 simultaneous quantitative real time PCR reactions (as already described in Materials and Methods sections).

Analysis of quantitative real time PCR with SDS 2.2 software generated sigmoid curves representing the increase of the respective PCR products. In order to obtain precise C_t values, thresholds were set manually within regions of linear increase of these curves. After normalization of C_t values to these of GAPDH, the two housekeeping genes NARS and TARDBP and the calibrator sample, the fold change was determined according to the formula:

$$FC = 2^{-\Delta Ct} = x_{ij}/x_i^{\,0}$$

Software developed within our group (Stokic et al., 2008) was able to create four different profiles for analysis of functional interactions between members of the candidate gene set as well as correlations in expression patterns. On the one hand, this software was used to generate global profiles of both, expression and correlation, but on the other hand profiles of single gene expression and correlation were created.

Global profiles of correlation allowed for analysis of correlation between transiently expressed genes concerning their effects on the expression of the candidate gene set.

The global profile of expression was built in order to demonstrate the upregulating and downregulating effects of a transiently expressed gene on candidate gene expression.

The expression pattern of a certain gene within the candidate gene set as a result of the respective experiments of transient gene expression was demonstrated by the single gene expression profile. The single gene profile of correlation allowed for analysis of correlation between all candidate genes within the set concerning their expression as a result of transient gene expression.

In order to obtain reliable results, three replicates of transient expression of HOXA3 followed by RNA-isolation, cDNA synthesis and quantitative real time PCR were executed. Transfected iHUVECs of the first trial emerged to be contaminated by mycoplasms whereas cells used for transfection during the second and the third trials were free from contamination. Since the experimental conditions of the third trial of transient expression of HOXA3 were most favourable, data obtained from this trial were considered to be significant for examination of the role of HOXA3 in a gene network relevant to diabetic microangiopathy.

1) The **global profile** of **correlation** was used to compare the respective effect on the candidate gene set of every transiently expressed gene to the effect of transient expression of HOXA3 on candidate gene expression (Figure 7). More precisely, the global profile of correlation built for HOXA3 allowed for analysis of correlation between transiently expressed HOXA3 and the other overexpressed genes in terms of their effects on candidate gene expression. Values close to +1 indicated a high degree of correlation whereas values close to 0 reflected poor correlation. Table 2 outlines correlations that emerged between transient HOXA3 expression and overexpression of 44 genes concerning the influence on the candidate gene set.

Concerning the effect on the candidate gene set, HOXA3-new was found to show highest correlation with overexpression of RPIB1 (correlation value: 0.864). The RPIB1 gene encodes ribose-5-phosphate isomerase, an enzyme that converts ribulose 5-phosphate to ribose-5-phosphate in the pentose phosphate pathway (Huck et al., 2004).

Furthermore, transient expression of the gene encoding the intercellular adhesion molecule ICAM1 showed high correlation with transiently expressed HOXA3-new in terms of the effects on the expression of the candidate gene set (correlation value: 0.738).

Comparison of the three trials of transient expression of HOXA3 with respect to the influence on the expression pattern of the candidate genes delivered interesting results. Correlation found between transiently expressed HOXA3 of the second (HOXA3-2.Versuch) and the third (HOXA3-new) trial accounted for almost 72% (correlation value: 0.717). Both trials of transient HOXA3 expression were carried out under similar conditions using iHUVECs free from any contamination. Nevertheless, small differences concerning the effects on candidate gene expression between HOXA3-2.versuch and HOXA3- new were detected. This result was acceptable however, since small variations concerning gene expression in iHUVECs after two trials of transfection with HOXA3 were expected to occur. Comparison of transiently expressed HOXA3 of the first trial (HOXA3-old) to HOXA3-new yielded a significant

difference in terms of the effects on the candidate gene expression. Cells used for transient exogenous expression of HOXA3 in the first trial turned out to be contaminated with mycoplasms. Correlation found between HOXA3-old and HOXA3-new accounted for 13% (correlation value: 0.131). As expected, this result strongly suggests that mycoplasm contamination has significant influence on the gene expression profile of cells affected.

Concerning the influence on the expression of the candidate gene set, transient expression of two more genes was found to yield a correlation value greater than 0.7 when compared to HOXA3-new. One of them, UGDH (correlation value: 0.707) encodes the enzyme UDP-glucose dehydrogenase that is known to catalyze two oxidations of UDP-glucose to generate UDP-glucuronic acid required for synthesis of extracellular matrix polysaccharides (Sommer et al., 2004). The other one, PLD (correlation value: 0.703) codes for phospholipase D, an enzyme that hydrolyzes phosphatidylcholine to yield the lipid second messenger phosphatidic acid and free choline (Whatmore et al., 1996).

Table 2. Correlations between transient HOXA3 expression and overexpression of 44 genes concerning the effect on the candidate gene set.

Position	Gene symbol	Correlation value	Position	Gene symbol	Correlation value
1	HOXA3-new	1.000	24	TGFb1	0.378
2	RPIB1	0.864	25	CXCL12	0.309
3	ICAM1	0.738	26	GTPBP4	0.295
4	HOXA3-2.Versuch	0.717	27	RHOJ	0.277
5	UGDH	0.707	28	TOR3A	0.273
6	PLD	0.703	29	PHGDH	0.269
7	GAPDH	0.687	30	CFH	0.191
8	CXCR4	0.676	31	PRG	0.187
9	Endothelin1	0.673	32	CALM2	0.186
10	IFITM	0.668	33	FZD4	0.179
11	NOS3	0.598	34	IMPA	0.149
12	GDI2	0.531	35	PRSS23	0.139
13	SMAD3	0.520	36	HOXA3-old	0.131
14	CD99	0.509	37	RPL3	0.128
15	AQP1	0.491	38	CDYL12	0.116
16	FGF1	0.439	39	CYR61	0.114
17	SMAD2	0.431	40	KLF6	0.107
18	TGFb-R2	0.427	41	BTF3	0.097
19	PKA	0.426	42	RAMP3	0.065
20	CFL1	0.420	43	CSPG	0.050
21	GNAS2	0.404	44	ATP6VOD1	-0.030
22	GCA	0.398	45	CASP3	-0.065
23	c-Jun	0.395			

The respective genes involved are listed according to their correlation value, starting with the highest degree of positive correlation. The gene symbols HOXA3-old, HOXA3-2.Versuch and HOXA3-new were used in reference to the first, the second and the third trial respectively of transient HOXA3 expression followed by RNA-isolation, reverse transcription and quantitative real time PCR.

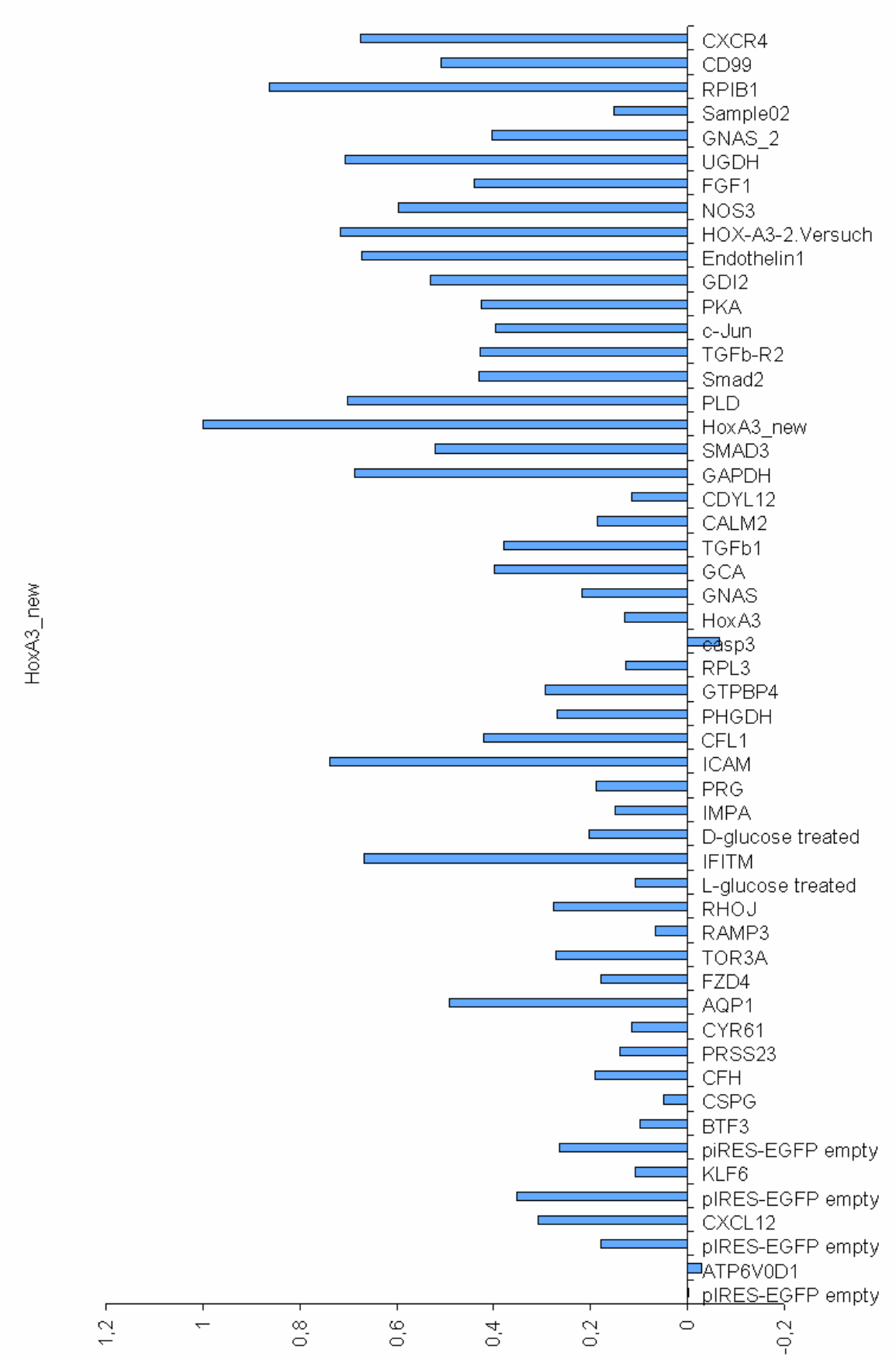

Figure 7. Global profile of correlation built for HOXA3. Values close to +1 indicate a high degree of correlation whereas values close to 0 reflect poor correlation.

2) The **global profile** of **expression** was used to analyze the upregulating and downregulating effects of transient HOXA3-expression on the expression of the candidate gene set (Figure 8). The magnitude of change in candidate gene expression as a result of HOXA3 overexpression was displayed by determination of the fold change. Table 3 summarizes the most upregulated as well as the most downregulated candidate genes as a result of transient expression of HOXA3.

Transient expression of HOXA3 was found to result in almost 44600 fold elevated levels of HOXA3 transcripts.

The majority of genes notably upregulated upon transient HOXA3 expression were found to encode proteins acting in adipocytes or being involved in reorganization of the actin cytoskeleton.

Overexpression of HOXA3 resulted in enormously increased expression of the EBF gene encoding the early B-cell factor. Early B-cell factor is a DNA binding protein that activates transcription of several B-cell specific genes and plays a critical role in early B-cell development (Hagman et al., 1991). Furthermore, the EBF gene product was found to act as transcription factor in olfactory neurons (Kudrycki et al., 1993). The EBF gene was also shown to be expressed during adipogenesis, a process by which adipocytes are formed (Jimenez et al., 2007).

Expression of sorbin and SH3-domain-containing-1 (SORBS1) gene known to participate in insulin signaling in adipocytes and thereby playing a critical role in the regulation of glucose uptake (Baumann et al., 2000) was elevated as a result of HOXA3 overexpression. According to previous studies, defects in SORBS1 may play a critical role in the pathology of human disorders with insulin resistance including the development of obesity and type 2 diabetes (Lin et al., 2001).

The RHOJ gene encoding a member of the family of small Rho GTPases was upregulated upon transient HOXA3 expression. Rho GTPases are known to affect actin cytoskeleton reorganization by regulation of actin dynamics. Proteins of the Rho family of small GTPases switch between an active GTP-bound and an inactive GDP-bound state (Vignal et al., 2003). The Rho GTPase encoded by the RHOJ gene has been found to act as an essential regulator of the early endocytic pathway (de Toledo et. al, 2003). Furthermore, RHOJ plays a critical role in early adipocyte differentiation (Nishizuka et al., 2003).

Overexpression of HOXA3 was found to result in elevated expression of the EPHA4 gene encoding the EPHA4 receptor that belongs to the Eph family of receptor tyrosine kinases. Eph receptors and their ligands, the ephrins are known to act in the developing and the mature

nervous system (Kullander and Klein, 2002) by reorganization of the actin cytoskeleton leading to modification of cell shape and movement (Henkemeyer et al., 2003). The EPHA4 receptor has been shown to affect β_1-integrin signaling pathways in neuronal cells by inhibiting β_1-integrin activity (Bourgin et al., 2008).

The expression of the NOS3 gene coding for endothelial nitric oxide synthase was found to be upregulated as a result of transient HOXA3 expression. Nitric oxide synthases are known to catalyze the synthesis of nitric oxide (NO). Formation of nitric oxide results in its diffusion into the smooth muscle where it activates soluble guanylate cyclase (sGC), an enzyme catalyzing the synthesis of 3', 5'- cyclic guanosine monophosphate (cGMP) leading to smooth muscle relaxation and vasodilation. Nitric oxide derived from NOS3 is thought to be the most important regulator of the vascular tone (Alderton, Cooper and Knowles, 2001).

Transient expression of HOXA3 resulted in elevated expression of the IL-8 gene encoding the chemokine interleukin 8. Furthermore, the expression of the gene coding for gap junction protein alpha 1 (GJA1) was upregulated as a result of HOXA3 overexpression.

Among the candidate genes notably downregulated upon transient HOXA3 expression the encoded proteins differ to a great extent in terms of function.

The ITGA1 gene encoding the integrin alpha subunit and the gene Parkinson disease (autosomal recessive, early onset) 7, also known as PARK7 were downregulated as a consequence of HOXA3 overexpression.

Overexpression of HOXA3 was found to result in downregulated expression of the VEGF gene coding for the vascular endothelial growth factor. Members of the VEGF gene family including VEGF have been shown to be critical for growth and differentiation of vascular as well as lymphatic endothelial cells (Korpelainen and Alitalo, 1998). VEGF has been found to play a crucial role in the early development of the vasculature. Furthermore, VEGF is considered to be the major regulator of angiogenesis (Leung et al., 1989).

Downregulated expression of the PHGDH gene encoding the enzyme 3-phosphoglycerate dehydrogenase was found to occur as a result of transient HOXA3 expression. The PHGDH gene product catalyzes the conversion of 3-phosphoglycerate into 3-phosphohydroxypyruvate during L-serine biosynthesis (Snell, 1986). L-serine is an important precursor for the synthesis of proteins, membrane lipids, glycine and D-serine (Snell, 1984). PHGDH deficiency is associated with defective L-serine biosynthesis. Furthermore, it has been found that the PHGDH gene product and L-serine are crucial for metabolism, development and function of the central nervous system (Klomp et al., 2000).

The expression of the GAPDH gene encoding the glycolytic enzyme glyceraldehyde-3-phosphate dehydrogenase was downregulated upon overexpression of HOXA3. The GAPDH protein catalyzes the conversion of glyceraldehyde-3-phosphate into 1, 3-diphosphogycerate. Overproduction of superoxide O_2^- induced by hyperglycaemia has been shown to result in activation of the enzyme poly (ADP-ribose) polymerase (PARP) which in turn inhibits the enzyme GAPDH by poly-ADP ribosylation resulting in accumulation of glycolytic metabolites upstream of GAPDH leading to activation of the four biochemical pathways that are known to contribute to hyperglycaemia-induced damage (Du et al., 2003).

The family of FBXO genes encode proteins, all of them possessing a protein motif also referred to as the F-box. F-box proteins are known to be components of the SCF ubiquitin-ligase complexes. The function of F-box proteins within these complexes is to provide a site for protein-protein interaction via their F-box motifs (Kipreos and Pagano, 2000). Upon transient expression of HOXA3, the expression of the FBXO7 gene was found to be downregulated.

The C1s gene encodes a serine protease that is known to be a subunit of the multimeric C1 protein complex of the complement system (Arlaud, Colomb and Gagnon, 1987). C1s cleaves and activates C4 and C2 resulting in formation of the C3 convertase (Schumaker, Zavodszky and Poon, 1987). Downregulated expression of the C1s gene was found to be the consequence of HOXA3 overexpression.

Another gene notably downregulated upon transient expression of HOXA3 was the GCA gene encoding the Ca^{2+} binding protein grancalcin found in neutrophils, monocytes and lymphocytes (Boyhan et al., 1991).

Table 3. List of the most upregulated and the most downregulated candidate genes upon transient HOXA3 expression.

Gene symbol	Fold change	upregulation or downregulation	Gene symbol	Fold change	upregulation or downregulation
EBF	4.86812E+12	upregulation	GAPDH	0.005	downregulation
HOXA3	44566.06	upregulation	ITGA1	0.052	downregulation
SORBS1	18.89	upregulation	PARK7	0.098	downregulation
RHOJ	15.49	upregulation	VEGF	0.098	downregulation
EPHA4	14.01	upregulation	PHGDH	0.123	downregulation
GJA1	13.53	upregulation	FBXO7	0.145	downregulation
IL-8	13.08	upregulation	C1S	0.160	downregulation
NOS3	10.81	upregulation	GCA	0.222	downregulation

The fold change was determined in order to analyze the magnitude of change in candidate gene expression as a result of transient HOXA3 expression.

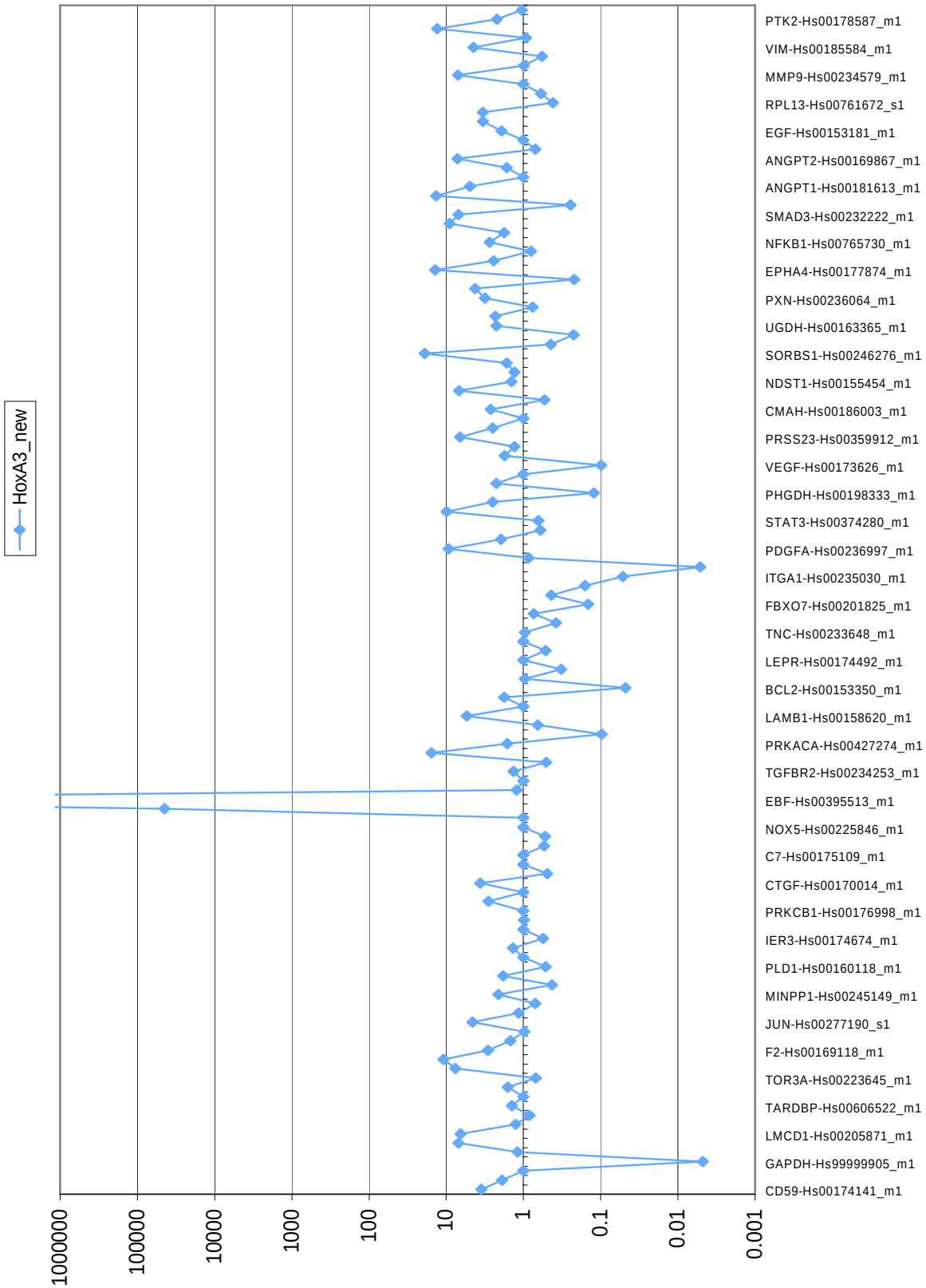

Figure 8. Global profile of expression built for HOXA3. Determination of the fold change was executed in order to display the magnitude of change in candidate gene expression as a result of HOXA3 overexpression. A fold change greater than 1 indicates upregulated candidate gene expression. Downregulated candidate gene expression is indicated by a fold change smaller than 1.

3) The **single gene** profile of **expression** of HOXA3 was built in order to analyze the effects of transient expression of the candidate genes including HOXA3 on the expression pattern of HOXA3 within the candidate gene set (Figure 9). Changes in HOXA3 expression as a result of overexpression of the respective candidate genes were displayed by determination of the fold change. Table 4 lists the candidate genes that were found to have the most significant influence upon transient expression on the expression pattern of HOXA3.

As previously described, transient expression of HOXA3 was found to result in elevated transcription of HOXA3.

Transient expression of CFL1 encoding the protein cofilin1 resulted in enormously increased expression of endogenous HOXA3. Cofilin1 belongs to the family of actin depolymerising factor (ADF)/cofilins. Members of this family are actin binding proteins that are known to promote depolymerization of actin filaments, thereby playing a critical role in cytokinesis, cell motility and morphogenesis in mammals. The proteins cofilin1 and ADF are coexpressed in nonmuscle cells where they contribute to cytoskeletal dynamics with overlapping functions (Hotulainen et al., 2005).

Endogenous HOXA3 expression was elevated as a result of transient KLF6 expression. The protein encoded by KLF6 is the Krüppel-like factor 6, a member of the Krüppel-like family of transcription factors. Proteins of this family possess highly conserved carboxy terminal zinc finger domains enabling specific DNA binding to GC rich sites within the promoter region of target genes. The transcription activation domain is located at the amino terminus (Dang, Pevsner and Yang, 2000). KLF6 has been found to act as tumor suppressor gene that is mutated in human prostate cancer (Narla et al., 2001). Furthermore, KLF6 has turned out to promote adipocyte differentiation by inhibition of the proto-oncogene Delta-like1 (DLK1) in preadipocytes (Dan Li et al., 2005).

Another gene found to result in increased expression of endogenous HOXA3 upon transient expression was CXCL12 encoding the chemokine that is also referred to as the stromal cell-derived factor 1. The gene product of CXCL12 has been shown to promote angiogenesis by mediating recruitment and migration of endothelial progenitor cells as well as endothelial cells in response to ischemic injuries. Binding of the CXCL12 protein to the CXCR4-receptor induces the proangiogenic signaling pathway (Askari et al., 2003; Deshane et al., 2007). An angiogenesis promoting activity by induction of endothelial cell migration has been also demonstrated for HOXA3. Studies revealed that constitutive expression of HOXA3 accelerated the healing process of diabetic wounds in mice (Kimberly et al., 2005).

HOXA3 expression was downregulated upon transient expression of CASP3 coding for caspase 3. Caspases are cysteine-aspartyl specific proteases that are known to be crucial for apoptosis (Creagh, Conroy and Martin, 2003). Caspase3 is an effector caspase that has been found to mediate apoptosis of β-cells of the pancreas, a process known to be significant for the occurrence of type 1 diabetes (Liadis et al., 2005).

Downregulated expression of endogenous HOXA3 was found to occur in untransfected cells treated with medium containing high concentrations of D-glucose. Since elevated expression of HOXA3 protein has been found in sera of patients suffering from diabetes mellitus (Wick et al., unpublished data), this result was unexpected.

Transient expression of FZD4 encoding frizzled homolog 4 resulted in downregulated expression of HOXA3. FZD4 belongs to the frizzled gene family whose members are known to code for transmembrane proteins acting as receptors for Wnt ligands (Reya and Clevers, 2005). The gene product encoded by FZD4 has been found to bind the non-Wnt ligand norrin (Nichrs, 2004) that appears to have an angiogenesis promoting activity (Ohlmann et al., 2005). Studies have revealed that mutations in the FZD4 gene result in familial exudative vitreoretinopathy (FEVR), a disorder characterized by defects in retinal vascular development (Robitaille et al., 2002).

Furthermore, downregulated expression of HOXA3 occurred as a result of transient expression of ATP6VOD1, a gene encoding the D1 subunit of the transmembrane VO domain of the enzyme ATPase.

Table 4. List of the candidate genes having the most significant influence upon transient expression on HOXA3 expression within the candidate gene set.

Gene symbol	Fold change	upregulation or downregulation	Gene symbol	Fold change	upregulation or downregulation
HOXA3	44566.06	upregulation	CASP3	0.002	downregulation
CFL1	10177.78	upregulation	D-glucose	0.079	downregulation
KLF6	16.87	upregulation	FZD4	0.188	downregulation
CXCL12	12.36	upregulation	ATP6VOD1	0.374	downregulation

Determination of the fold change was performed in order to indicate the magnitude of change in HOXA3 expression as a result of transient expression of the respective candidate genes including HOXA3. The gene symbol D-glucose refers to untransfected iHUVECs that were treated with D-glucose.

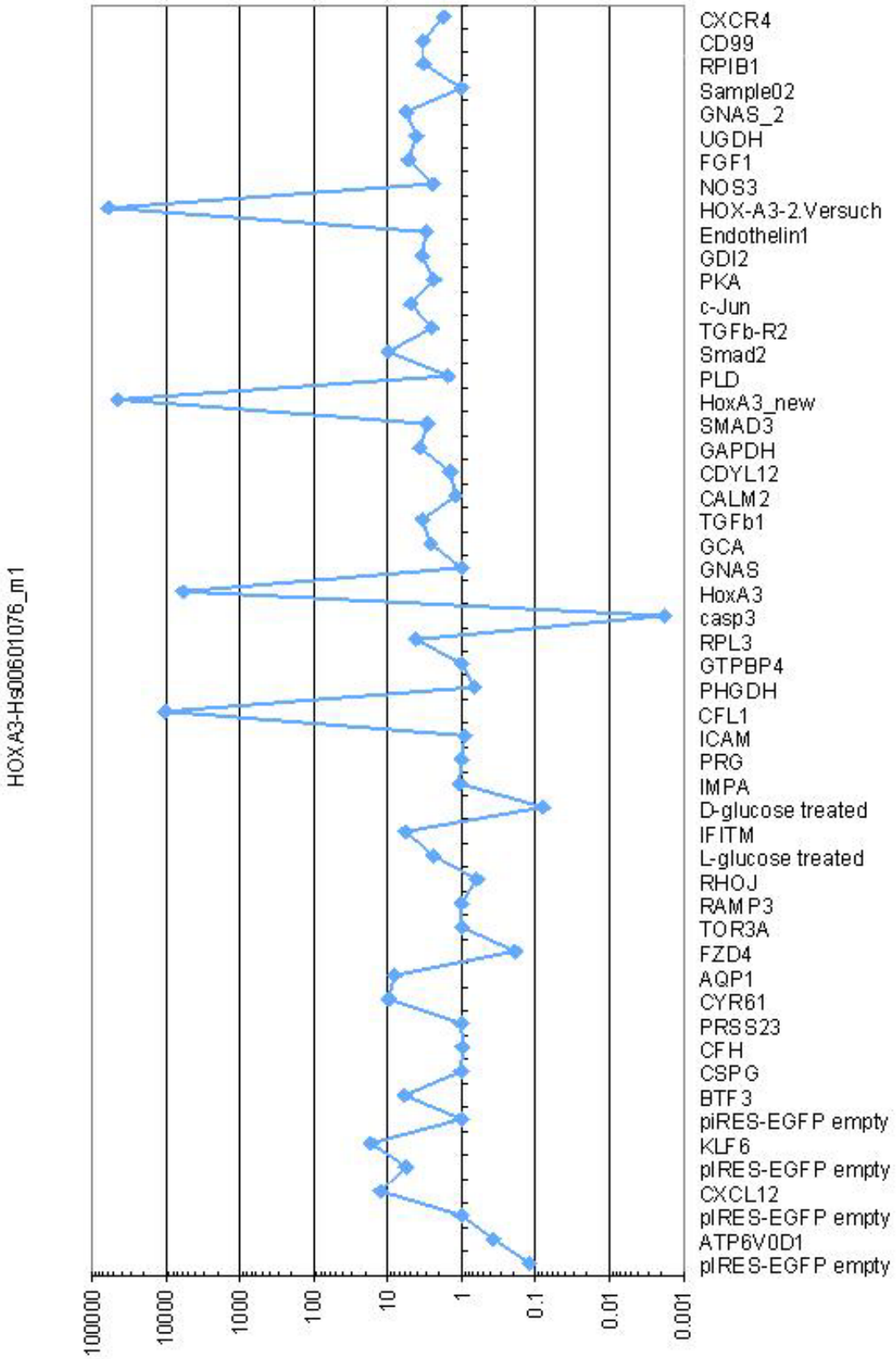

Figure 9. Single gene profile of expression built for HOXA3. Determination of the fold change was executed in order to display the magnitude of change of HOXA3 RNA expression as a result of transient expression of the respective candidate genes. A fold change greater than 1 indicates upregulated HOXA3 expression. Downregulated HOXA3 expression is indicated by a fold change smaller than 1.

4) The **single gene profile** of **correlation** built for HOXA3 allowed for analysis of correlation between HOXA3 and all the other candidate genes within the set concerning their expression as a result of transient candidate gene expression (Figure 10). Values close to +1 indicated high correlation in expression. On the other hand values close to 0 indicated poor correlation. Table 5 lists genes that were found to show highest correlation with HOXA3 concerning their expression upon transient expression of the respective candidate genes.

Values found for correlation between HOXA3 and the other candidate genes concerning their expression pattern as a result of transient expression of the respective candidate genes were smaller than 0.5. These data indicate correlation below 50% between HOXA3 and the other genes within the set in terms of expression in response to the overexpression experiments.

The gene SERPINE1 encoding the plasminogen activator inhibitor 1, a serine proteinase inhibitor protein was found to show highest correlation (correlation value: 0.468) with HOXA3 in terms of expression upon overexpression of the respective candidate genes. Plasminogen activator inhibitor 1 (PAI-1) has been found to cause detachment of cells from extracellular matrices by binding to urokinase plasminogen activator (uPA) in complexes mediating attachment of cells to the extracellular matrix. These complexes are composed of uPA, its receptor uPAR and integrins (Czekay et al., 2003). Previous studies have revealed a link between uPAR and HOXA3 since constitutive expression of HOXA3 leads to upregulated expression of uPAR in HMEC-1, an immortalized human dermal microvascular endothelial cell line (Kimberly et al., 2005).

GJA1 coding for the gap junction protein alpha 1 and found to be upregulated upon transient HOXA3 expression showed 46% correlation (correlation value: 0.464) with HOXA3 concerning the expression in response to the overexpression experiments.

Correlation found between HOXA3 and SMAD3 in terms of expression upon transient candidate gene expression accounted for 45% (correlation value: 0.453). The SMAD3 gene encodes a protein that belongs to the R-Smads or receptor regulated Smads. TGF-β signaling leads to activation of the SMAD3 protein by phosphorylation followed by heterodimerization with the SMAD4 protein. These heterodimers translocate to the nucleus where they regulate target gene transcription (Heldin, Miyazono and Dijke, 1997).

Correlation accounting for 42% was found between HOXA3 and CASP3 (correlation value: 0.429) in terms of expression in response to the overexpression experiments. CASP3 coding for an effector caspase was already shown to result in downregulated expression of HOXA3 upon transient expression of the CASP3 gene.

Genes found to show correlation of 40% with HOXA3 concerning their expression upon overexpression of the candidate genes were EPHA4 (correlation value: 0.406), PRSS23 (correlation value: 0.404) and IL-8 (correlation value: 0.396).

EPHA encoding the EPHA4 receptor, a member of the Eph family of receptor tyrosine kinases was already found to be upregulated upon transient HOXA3 expression.

PRSS23, also known as protease serine 23 encodes a serine protease that has been found to act as critical ovarian protease in vertebrates (Miyakoshi et al., 2006).

IL-8 coding for the chemokine interleukin 8 was also found to be upregulated as a result of transient HOXA3 expression.

Table 5. List of genes found to show highest correlation with HOXA3 concerning their expression as a result of transient candidate gene expression.

Position	Gene symbol	Correlation value	Position	Gene symbol	Correlation value
1	HOXA3	1.000	5	CASP3	0.429
2	SERPINE1	0.468	6	EPHA4	0.406
3	GJA1	0.464	7	PRSS23	0.404
4	SMAD3	0.453	8	IL-8	0.396

The respective genes are listed according to their correlation value, starting with the highest degree of correlation.

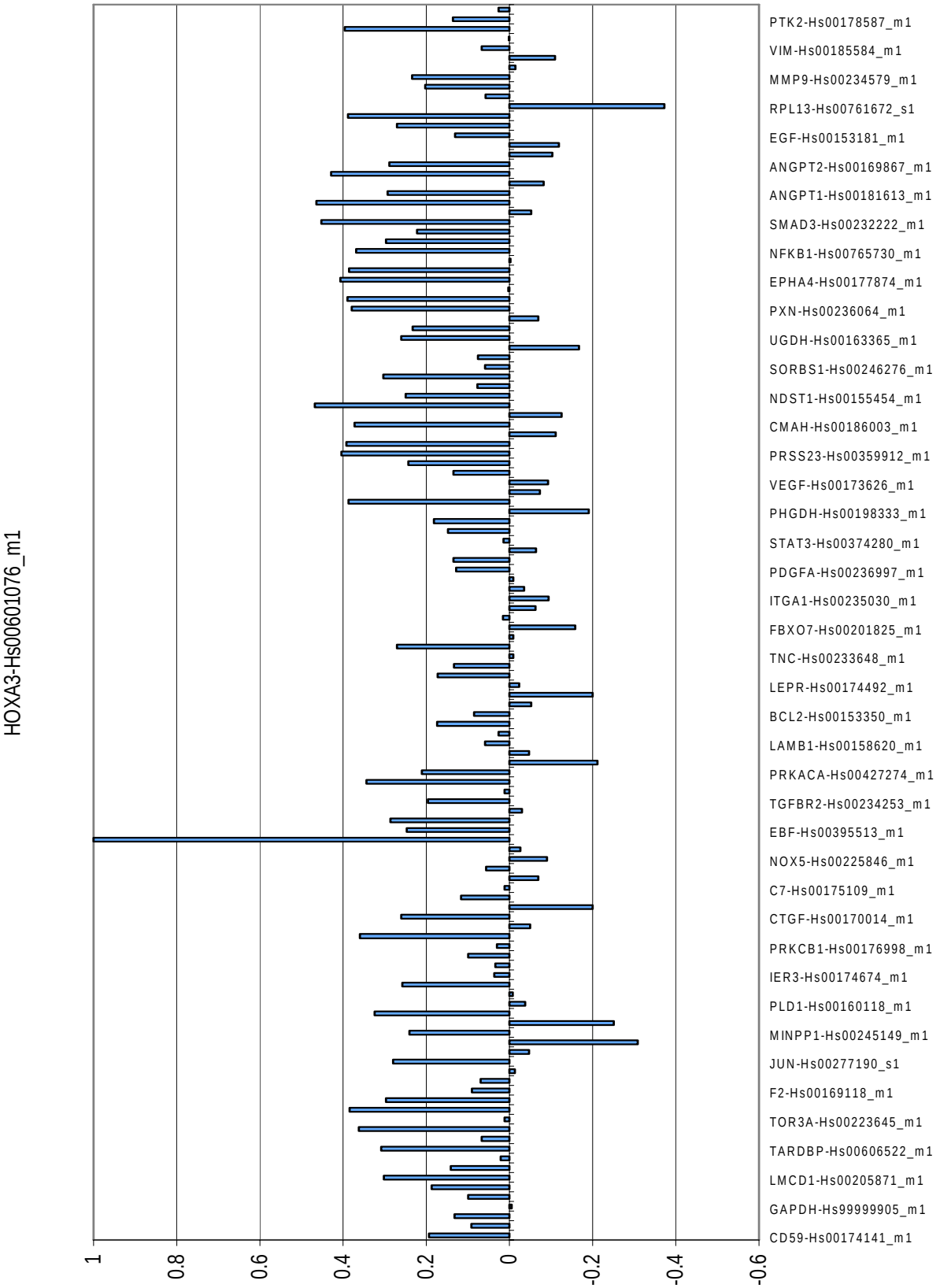

Figure 10. Single gene profile of correlation built for HOXA3. Values close to +1 indicated high correlation in expression whereas values close to 0 indicated poor correlation. Values found for correlation between HOXA3 and the other candidate genes in terms of expression in response to the overexpression experiments were smaller than 0.5.

5.4 HOXA3 in a gene network relevant to diabetic microangiopathy

In the course of the project aiming at identification of a gene network relevant to diabetic microangiopathy, a total of 37 candidate genes including HOXA3 were cloned into the expression vector pIRES2-EGFP and transiently expressed in iHUVECs prior to RNA-isolation from successfully transfected cells, reverse transcription and quantitative real time PCR of cDNA samples. Determination of the fold change was executed to analyze the effects of transient expression of a certain gene on the expression of the candidate gene set as it was shown in global and single gene profiles of both, expression and correlation without revealing direct or indirect regulatory interactions. In order to build a gene network represented by the adjacency matrix A, it was necessary to identify all the direct functional links between the candidate genes according to the formula:

$$A = \ln (D+I)$$

On the basis of regulatory interactions found between transiently expressed candidate genes (see appendix), it was possible to create a network comprising 37 genes (Figure 11), which was assumed to be of relevance to diabetic microangiopathy. This network demonstrated the most significant functional links between genes that might play a critical role in the occurrence of diabetic microvascular complications. The relative position of each gene within this network was determined according to the number of functional links between the respective gene and other genes. Functional links found between genes constituting the network represented activating or inhibitory effects. In addition, significant effects of the respective genes on their own expression were also demonstrated in this gene network relevant to diabetic microangiopathy. In order to be incorporated into the gene network, interactions between the candidate genes had to be greater than a certain threshold in terms of strength.

Table 6 describes the strength of direct functional links of HOXA3 to all the other candidate genes that were transiently expressed in the course of the project. The genes CFL1 and CASP3 were identified to be significantly involved in regulatory interactions with HOXA3. CFL1 encoding the protein cofilin1 was found to have an upregulating effect on the expression of HOXA3, whereas CASP3 coding for an effector caspase was described to have a downregulating effect on HOXA3 expression. Furthermore, a notable activating effect of HOXA3 on its own expression was demonstrated. Further significant

interactions of HOXA3 with candidate genes transiently expressed were not identified. Therefore, HOXA3 was found to take a peripheral position in the gene network, where its functional links to CFL1 and CASP3 as well as the activating effect on its own expression were demonstrated.

Table 6. Summary of direct interactions found between HOXA3 and all the other transiently expressed candidate genes.

from	to	strenght of interaction	effect	from	to	strenght of interaction	effect
CFL1	HOXA3	3.861057	upregulation	HOXA3	FZD4	0.239946	no effect
CASP3	HOXA3	-3.037106	downregulation	FGF1	HOXA3	0.239667	no effect
HOXA3	HOXA3	2.284825	upregulation	HOXA3	CFL1	0.238254	no effect
Endothelin1	HOXA3	-1.073105	no effect	HOXA3	KLF6	0.232501	no effect
CALM2	HOXA3	-0.977092	no effect	BTF3	HOXA3	-0.226815	no effect
PLD	HOXA3	-0.969137	no effect	RPIB9	HOXA3	0.219708	no effect
TGFb-R2	HOXA3	0.742079	no effect	HOXA3	RAMP3	-0.206556	no effect
PRSS23	HOXA3	0.740413	no effect	HOXA3	FGF1	0.203323	no effect
TGFb1	HOXA3	0.735693	no effect	RAMP3	HOXA3	0.183082	no effect
HOXA3	GAPDH	-0.721046	no effect	HOXA3	UGDH	0.166775	no effect
GTPBP4	HOXA3	0.644008	no effect	HOXA3	BTF3	-0.147050	no effect
TOR3A	HOXA3	0.612508	no effect	HOXA3	CASP3	0.129217	no effect
CFH	HOXA3	0.571996	no effect	ATP6VOD1	HOXA3	0.122829	no effect
FZD4	HOXA3	0.545993	no effect	HOXA3	TOR3A	-0.122777	no effect
HOXA3	PRSS23	0.526719	no effect	HOXA3	CSPG	-0.120706	no effect
HOXA3	AQP1	-0.494100	no effect	HOXA3	SMAD2	-0.116524	no effect
RHOJ	HOXA3	0.486262	no effect	HOXA3	TGFb1	0.116499	no effect
KLF6	HOXA3	0.469992	no effect	c-JUN	HOXA3	0.109867	no effect
HOXA3	RPIB9	-0.458962	no effect	HOXA3	CDYL12	-0.109686	no effect
GCA	HOXA3	0.457223	no effect	UGDH	HOXA3	0.106492	no effect
HOXA3	SMAD3	0.426192	no effect	CSPG	HOXA3	0.071653	no effect
SMAD2	HOXA3	0.417238	no effect	HOXA3	Endothelin1	0.069464	no effect
HOXA3	PLD	-0.411843	no effect	AQP1	HOXA3	0.068006	no effect
GAPDH	HOXA3	0.385663	no effect	HOXA3	GCA	0.066035	no effect
PHGDH	HOXA3	0.367620	no effect	CYR61	HOXA3	-0.064949	no effect
HOXA3	c-JUN	0.347007	no effect	HOXA3	ATP6VOD1	0.061754	no effect
ICAM1	HOXA3	0.337033	no effect	HOXA3	ICAM1	-0.057733	no effect
GNAS2	HOXA3	-0.329482	no effect	HOXA3	CFH	0.052311	no effect
SMAD3	HOXA3	0.324979	no effect	HOXA3	GTPBP4	-0.042365	no effect
HOXA3	NOS3	0.317200	no effect	CXCL12	HOXA3	0.041873	no effect
HOXA3	CXCL12	0.299946	no effect	HOXA3	GDI2	-0.039585	no effect
GDI2	HOXA3	-0.293912	no effect	HOXA3	TGFb-R2	0.028100	no effect
HOXA3	RHOJ	0.284675	no effect	HOXA3	PRG	-0.015214	no effect
HOXA3	CYR61	0.277071	no effect	NOS3	HOXA3	-0.011407	no effect
CDYL12	HOXA3	0.268072	no effect	HOXA3	GNAS2	-0.008812	no effect
HOXA3	PHGDH	-0.255345	no effect	HOXA3	CALM2	-0.003165	no effect
PRG	HOXA3	0.242248	no effect				

Only the most significant functional links of HOXA3 to other genes were incorporated into the gene network composed of 37 genes. Positive values greater than a certain threshold of 1.334 were considered to indicate activating effects whereas negative values smaller than a threshold of -1.130 were thought to reflect inhibitory effects.

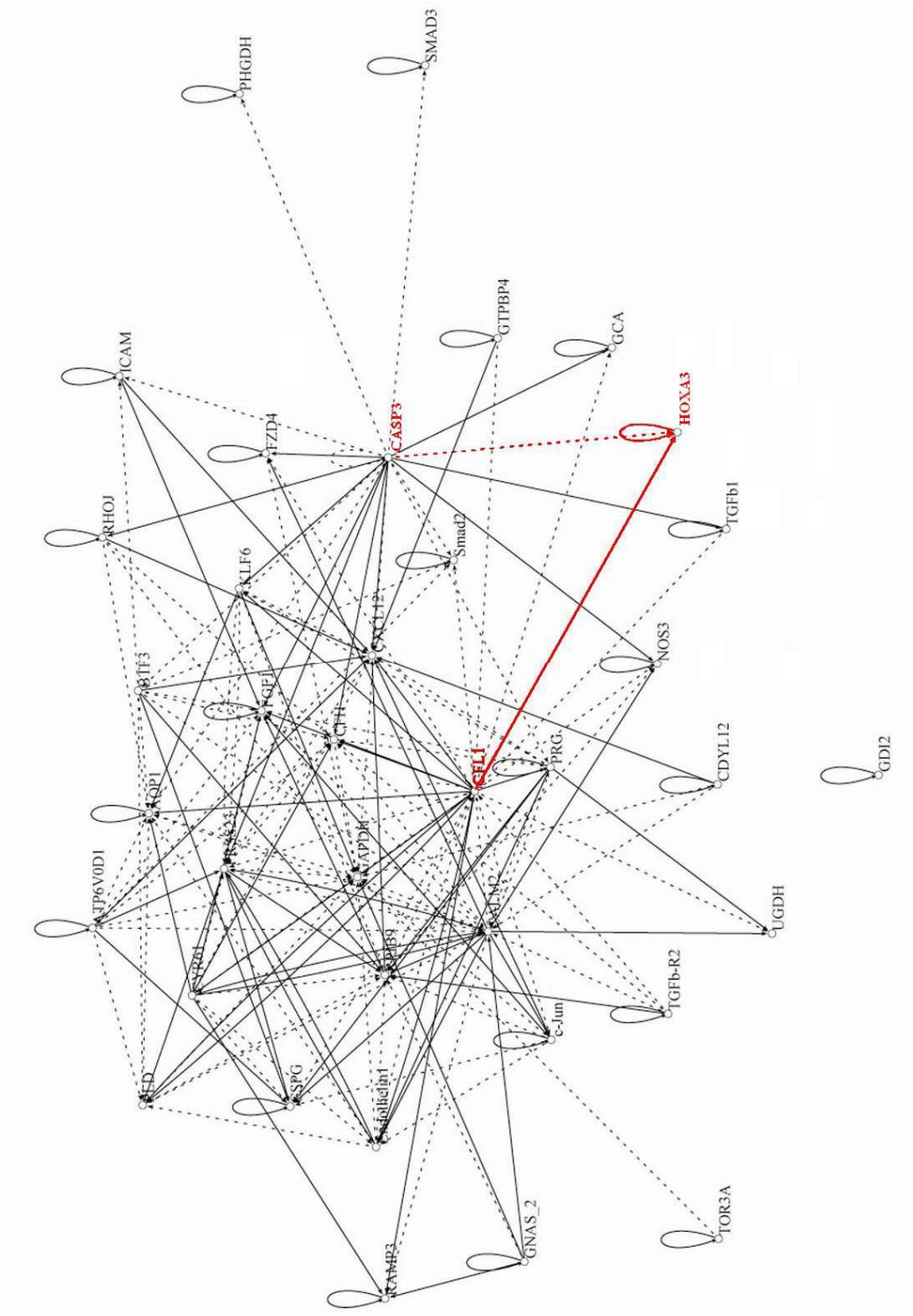

Figure 11. HOXA3 in a gene network of possible relevance for diabetic microangiopathy. HOXA3 takes a peripheral position in the gene network since there is a smaller number of significant functional links between HOXA3 and the other genes involved. In this network, HOXA3 expression is demonstrated to be activated by CFL1 and inhibited by CASP3. Furthermore, an activating effect of HOXA3 on its own expression is demonstrated. In this illustration of the gene network, arrows indicate the direction of regulatory action. Upregulating effects are illustrated by continuous lines between interacting genes, Downregulating effects are indicated by discontinuous lines between interacting genes.

5.5 Western blot analysis and immunofluorescence staining of HOXA3

As mentioned above HOXA3 was found to be functionally linked to the genes CFL1 and CASP3 in a network that comprises 37 genes and is assumed to be of relevance to diabetic microangiopathy. Furthermore, a significant positive effect of HOXA3 on its own expression was identified. In order to verify these findings, Western blot analysis and immunofluorescence staining of HOXA3 protein were carried out comparing iHUVECs transiently expressing HOXA3, CFL1 and CASP3, respectively, to untransfected cells.

5.5.1 Western blot analysis of HOXA3 protein

Western blot analysis of HOXA3 protein was done using cell lysates of untransfected and transfected iHUVECs, where transfected cells were transiently expressing HOXA3 or CFL1 or CASP3. When compared to untransfected iHUVECs elevated expression of HOXA3 protein was detected upon transient expression of HOXA3 and CFL1 (Figure 12). A downregulating effect of CASP3 on HOXA3 expression as it was demonstrated in the gene network was not confirmed since overexpression of CASP3 was not found to result in decreased levels of HOXA3 protein.

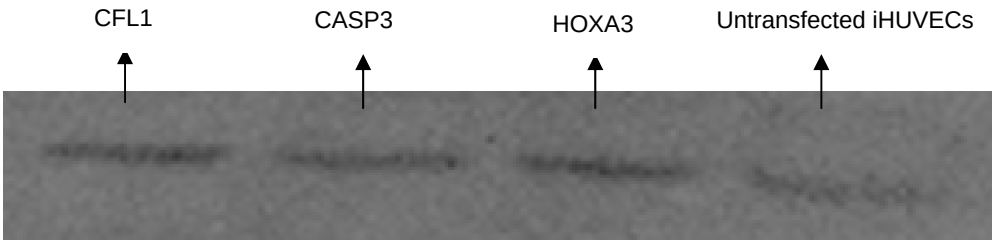

Figure 12. Western blot analysis of HOXA3 expression in transfected and untransfected iHUVECs. HOXA3 expression is shown as a result of transient expression of CFL1 (lane 1) CASP3 (lane 2) and HOXA3 (lane3). When compared to untransfected iHUVECs (lane 4), HOXA3 expression was found to be upregulated upon transient expression of CFL1 and HOXA3. Note that overexpression of CASP3 did not result in downregulated expression of HOXA3.

5.5.2 Immunofluorescence staining of HOXA3 protein

Cells successfully transfected with expression vector pIRES2-EGFP carrying the respective gene of interest showed a green signal as a result of EGFP expression.

When compared to untransfected cells (Figure 4d) immunofluorescence staining of protein encoded by HOXA3 in iHUVECs transiently expressing CFL1 (Figures 4a-1, 4a-2) revealed increased concentrations of HOXA3 protein in the cytoplasm and in the nucleus confirming the upregulating effect of CFL1 on the expression of HOXA3 as it was demonstrated in the gene network relevant to diabetic microangiopathy.

Elevated levels of HOXA3 protein were also found in iHUVECs transiently expressing HOXA3 (Figures 4b-1, 4b-2). In these cells especially the nucleus showed high concentrations of HOXA3 protein.

In contrast to Western blot analysis, immunofluorescence staining of HOXA3 protein was found to demonstrate a downregulating effect of CASP3 on HOXA3. When compared to untransfected cells decreased levels of HOXA3 protein were found in the cytoplasms and in the nuclei of iHUVECs transiently expressing CASP3 (Figures 4c-1, 4c-2).

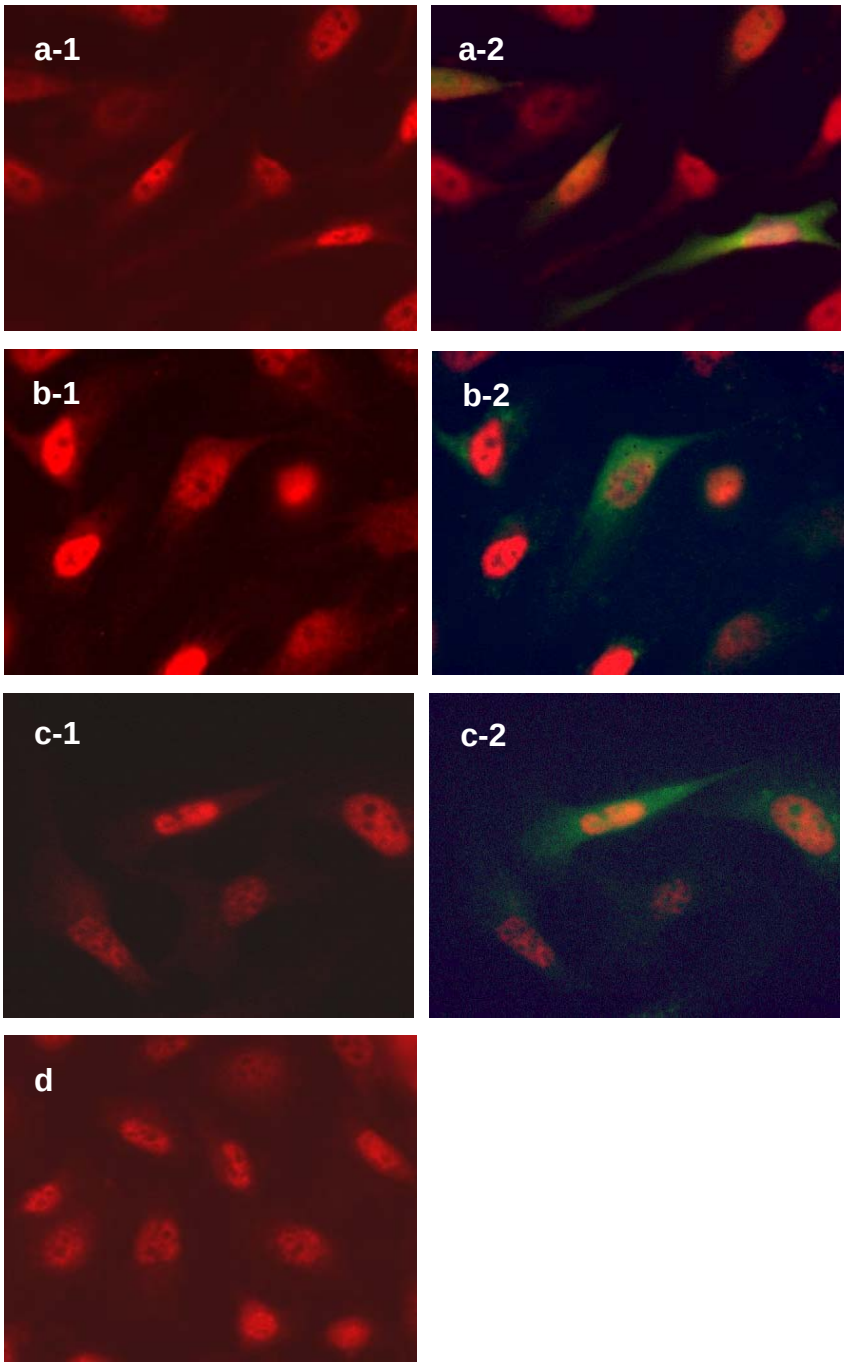

Figure 4. Immunofluorescence staining of HOXA3 protein.
The concentrations of HOXA3 protein in the cytoplasms and in the nuclei of iHUVECs transiently expressing CFL1 (a-1, a-2) or HOXA3 (b-1, b-2) or CASP3 (c-1, c-2) were compared to the levels of HOXA3 protein in untransfected cells (d). On the left side single channel images of iHUVECs in red show the cellular distribution of HOXA3 protein represented by the red signal. Images of the same cells on the right side additionally depict in green the result of EGFP expression, indicating successful transfection with expression vector pIRES2-EGFP carrying the respective gene of interest. Cells transiently expressing CFL1 were found to have elevated levels of HOXA3 protein in the cytoplasm and in the nucleus. Increased concentrations of HOXA3 protein were detected in the nuclei of iHUVECs transiently expressing HOXA3. Decreased levels of HOXA3 protein were found in the cytoplasms and in the nuclei of cells overexpressing the CASP3 gene.

6 Discussion

The idea of creating a gene network for diabetic microangiopathy was to demonstrate the interactions of functional relevance between candidate genes assumed to control the occurrence and course of microvascular complications. We could build a network composed of 37 candidate genes that had previously been identified in an *ex vivo* screen for transcripts regulated in BECs of diabetic *versus* non-diabetic capillaries. The position of each gene was determined by the number of its functional links to other genes involved and thereby provided information about the possible role of a gene in microvascular complications. Genes taking a central position within the network were considered to be key players in the occurrence of diabetic microangiopathy since they had a higher number of functional links than genes occupying a peripheral position.

Initially, a total of 125 candidate genes hypothesized to control microvascular complications was identified by gene expression profiling comparing (i) blood vascular endothelial cells (BECs) derived from tissue samples of diabetic and non-diabetic patients and (ii) BECs cultured *in vitro* under diabetic conditions, as well as by (iii) literature search. However, the fact that our final gene network was built from only 37 of these 125 identified candidate genes gives rise to doubts concerning the biological relevance of the network. The major point of criticism is that some important gene regulatory interactions may remain obscured as a result of the small number of genes constituting the network. Thus, it is unlikely that the regulatory interactions identified between the 37 genes within our network suffice to understand the whole process of gene regulation contributing to diabetic microangiopathy. However, this gene network can be considered as an important step to reveal the secrets of gene regulatory interactions controlling the occurrence of microvascular complications.

One reason for restricting the final gene network to barely 30 % of all identified candidate genes was the time consuming biological methods to obtain the data required for gene network construction. Each of the candidate genes had to be cloned into the expression vector pIRES2-EGFP and be transiently expressed in iHUVECs. Successfully transfected cells were sorted by flow cytometry which had to yield at least 300,000 enhanced green fluorescent protein (EGFP) -positive cells for subsequent RNA-isolation. Isolated RNA was reverse transcribed and the resulting cDNA-sample was subjected to quantitative real time PCR, which was expected to deliver data essential for the construction of our gene network. Sometimes technical difficulties were found to delay the progression of the project. For example, for some of the candidate genes several unsuccessful attempts of cloning had to be

overcome, which were the result of problems occurring during PCR amplification or failure in restriction enzyme digestion.

As already mentioned, the candidate genes were cloned into pIRES2-EGFP prior to transient transfection of iHUVECs. The reason for choosing this expression vector was the highly efficient detection of successfully transfected cells by flow cytometric cell sorting. The characteristic of pIRES2-EGFP is the presence of an internal ribosomal entry site (IRES) located between the multiple cloning site and the coding region of the EGFP. The consequence of this construction is translation of the gene that is cloned into the multiple cloning site and the EGFP gene from a single bicistronic mRNA.

Although diabetic microangiopathy seems to be the consequence of altered gene expression over a long period of time, the short duration of downstream effects upon transient candidate gene expression was considered appropriate to study the role of the respective candidate genes in the microvascular complications. This decision was a consequence of the fact that stable transfections of iHUVECs in order to analyze the long-term effects of permanent overexpression of the candidate genes on the gene expression patterns of endothelial cells would have meant unrealistically great expenditure of time.

Human umbilical vein endothelial cells (HUVECs) immortalized with the human telomerase catalytic protein (hTERT) were used for our transfection experiments. These cells were shown to largely maintain their endothelial character and therefore making them appropriate for the studies of diabetic microangiopathy (Aurea Burchard, personal communication). Moreover, iHUVECs could be transfected at a reasonably high efficiency of up to 75 % with pIRES2-EGFP; which was in contrast to much lower results when using microvascular BECs. Still, the origin of iHUVECs from the umbilical vein that normally is not subjected to diabetic complications is a drawback worth to mention. However, in principal we tested gene interactions that should be found in any condition, if gene products were of appropriate relative levels, i.e. not necessarily diabetes-specific. Thus, the iHUVECs seemed to be a good compromise between technical feasibility and biological representativity.

Quantitative real time PCR was the method of choice in order to detect changes in candidate gene transcripton upon transient gene expression in iHUVECs. An alternative approach for measurement of changes in expression levels could have been the use of DNA chips. However, the higher costs of DNA chips as well as the lower accuracy and lower sensitivity of hybridization were the reason for choosing quantitative real time PCR for analysis of candidate gene transcription in response to the overexpression experiments. Moroever, from

the bioinformatical point of view quantitative real time PCR was more favorable for gene network construction than DNA chips, since this approach was expected to deliver more bits of information per data point than DNA chips. Thus, fewer data points were required in case of using real time PCR to accomplish the same accuracy when working with DNA chips (D'haeseleer et al., 2000).

In this diploma thesis a peripheral position of the HOXA3 gene within our 37 genes comprising network is reported. According to the gene network HOXA3 expression was directly regulated by the genes CFL1 and CASP3. Furthermore, an activating effect of HOXA3 on its own expression was suggested. CFL1 encoding cofilin1 that is known to contribute to cytoskeletal dynamics in nonmuscle cells (Hotulainen et al., 2005) activated HOXA3 expression. On the other hand, CASP3 coding for caspase 3, an effector caspase mediating apoptosis of pancreatic β-cells (Liadis et al., 2005), seemed to have a downregulating effect on the expression of the HOXA3 gene. In order to verify these findings Western blot analysis and immunofluorescence staining of HOXA3 protein were carried out. Both approaches involved transient transfection of iHUVECs with pIRES2-EGFP carrying the coding sequence of the gene suggested to regulate the expression of HOXA3. The levels of HOXA3 protein detected in cells transiently expressing CFL1, CASP3 and HOXA3, respectively, were compared to endogenous HOXA3 expression in untransfected cells. Western blot analysis and immunofluorescence staining of HOXA3 protein were not carried out for iHUVECs transiently transfected with empty pIRES2-EGFP However, an empty vector control would have been reasonable for two reasons: First, initial determination of the fold change in gene expression was executed by comparison of Ct values obtained from quantitative real time PCR to those of a calibrator sample which was derived from iHUVECs transfected with empty pIRES2-EGFP. Second, effects of plasmid backbone on gene expression cannot be excluded. However, according to the single gene profile of HOXA3, no significant differences to untransfected cells treated with RPMI medium containing L-glucose were found to occur in terms of HOXA3 expression. Therefore, we still feel to be able to interpret correctly the possible role of HOXA3 within the gene network.
Specifically, three different experiments were carried out:
First, not unexpected, transient HOXA3 expression was also found to result in elevated levels of HOXA3 protein. On the one hand these higher amounts of HOXA3 protein could be the result of the additional exogenous expression of HOXA3 without any effect on the expression of endogenous HOXA3. On the other hand an autoinducive effect of HOXA3 on its own

expression could be the reason for the elevated levels of HOXA3 protein in cells transiently expressing HOXA3.
Second, Western blot and immunofluorescence analyses revealed activated HOXA3 expression in iHUVECs transiently expressing CFL1 when compared to untransfected cells. Third, Western blot analysis and immunofluorescence staining of iHUVECs transiently expressing CASP3 delivered different results concerning the effect on HOXA3 expression. Western blot analysis of cells transiently expressing CASP3 revealed levels of HOXA3 protein equal to those in untransfected cells. This unexpected result may be explained by the fact that cells used in these confirmation experiments were not subjected to flow cytometric cell sorting after transfection and therefore it is likely that a great amount of these iHUVECs assumed to be successfully transfected did not contain the expression vector carrying the CASP3 gene. On contrary, microscopic inspection of cells transiently expressing the CASP3 gene after immunofluorescence staining of HOXA3 protein revealed downregulated HOXA3 expression, when compared to untransfected iHUVECs. This latter result seems more significant, since the green signal of the EGFP protein detected in analyzed iHUVECs allowed identification of cells that were successfully transfected with pIRES2-EGFP carrying CASP3 coding sequence and exclusion of negative ones.

Three trials of transient HOXA3 expression followed by RNA-isolation, reverse transcription and quantitative real time PCR were compared with respect to the effects on candidate gene expression. Cells transiently transfected in the first trial were contaminated with mycoplasms, whereas iHUVECs used in the other two trials were free from contamination. Considerable differences in candidate gene expression between contaminated and non-contaminated cells were observed upon transient transfection with pIRES2-EGFP carrying HOXA3 coding sequence. Small variations concerning the effect on the candidate gene set were found even between the second and the third trial of transient HOXA3 expression. These findings demonstrated the sensitivity of a cell line in terms of gene expression. However, these small variations between the second and the third trial of HOXA3 overexpression were found in expression of those candidate genes that were only slightly affected by transient expression of HOXA3.

Besides of the three interactions of HOXA3 with other proteins within the gene network, analysis of the effects of transient expression of HOXA3 on the 125 candidate gene set delivered interesting results. HOXA3 overexpression was found to result in activated

expression of genes encoding proteins that act in adipocytes. Adipocytes are known to serve as energy reservoirs by storing free fatty acids. Furthermore, these cells have been found to be of broader importance for health. Studies have revealed that adipocytes release various proteins that are critical for the regulation of metabolism. For example, enlarged adipocytes of obese individuals promote insulin resistance by production of proinflammatory factors and increased recruitment of macrophages (Greenberg and Obin, 2006). The expression of the genes EBF, SORBS1 and RHOJ was notably upregulated as a result of transient HOXA3 expression. The Rho GTPase encoded by the RHOJ gene is known to play a critical role in early adipocyte differentiation (Nishizuka et al., 2003). The EBF gene encoding the early B-cell factor has been shown to be expressed during adipogenesis, the process by which adipocytes are formed from preadipocytes (Jimenez et al., 2007). Studies have revealed a critical role of the SORBS1 gene in the regulation of glucose uptake by participating in insulin signaling in adipocytes (Baumann et al., 2000). The finding that HOXA3 activates the expression of genes regulating adipogenesis or being involved in insulin signaling in adipocytes suggests an important role of HOXA3 in the regulation of these processes.

Furthermore, HOXA3 might be involved in reorganization of the actin cytoskeleton since transient expression of HOXA3 was found to result in activated expression of the genes RHOJ (Vignal et al., 2003) and EPHA4 (Henkemeyer et al., 2003) which are known to regulate actin dynamics.

Vice versa HOXA3 was also found to be positively regulated by genes acting in adipocytes and contributing to actin dynamics, respectively, indicating that HOXA3 seems to be embedded in the regulation of these processes. Within the candidate gene set HOXA3 expression was notably elevated upon overexpression of CFL1 and KLF6 respectively. As already mentioned, CFL1 encoding cofilin 1 plays an important role in the regulation of cytoskeletal dynamics in nonmuscle cells (Hotulainen et al., 2005). KLF6 coding for transcription factor Krüppel-like factor 6 has been found to inhibit the proto-oncogene Delta-like1 (DLK1) in preadipocytes and thereby promoting adipocyte differentiation (Dan Li et al., 2005).

Previous studies revealed an angiogenesis promoting activity of HOXA3 by induction of endothelial cell migration. Constitutive expression of HOXA3 was found to accelerate the healing process of diabetic wounds in mice (Kimberly et al., 2005). These findings are supported by the activating effect of transiently expressed CXCL12 on endogenous HOXA expression as it was found in this diploma thesis. CXCL12 encoding the chemokine that is also known as stromal cell-derived factor 1 has been shown to mediate recruitment and

migration of endothelial progenitor cells as well as endothelial cells in response to ischemic injuries and thereby promoting angiogenesis. The proangiogenic signaling pathway is induced by binding of the CXCL12 protein to the CXCR4-receptor (Askari et al., 2003; Deshane et al., 2007).

In this diploma thesis, functional links of HOXA3 to the genes CFL1 and CASP3 within a 37 gene comprising network created by interdisciplinary cooperation between physicists, physicians and biologists were suggested.
In addition, a potential role of HOXA3 in biological processes including adipocyte differentiation and insulin signaling in adipocytes as well as reorganization of the actin cytoskeleton was found. Beside its function in embryonic development HOXA3 was known to be involved in angiogenesis and wound repair so far. Therefore, the results presented in this diploma thesis might open new perspectives concerning the function of HOXA3 in diabetic microangiopathy that could be analyzed in further studies.

References

1. **Alderton, W. K., Cooper, C. E., Knowles, R. G.** (2001). Nitric oxide synthases: structure, function and inhibition. *Biochem J.* **357:** 593–615.

2. **American Diabetes Association** (2007). Diagnosis and Classification of Diabetes Mellitus. *Diabetes Care* **30***, Suppl* **1:** S42-S47.

3. **Arlaud, G. J.;Colomb, M. G.; Gagnon, J.** (1987). A functional model of the human C1 complex. *Immunol. Today.* **8:** 106–111.

4. **Askari, A. T., Unzek, S., Popovic, Z. B., Goldman, C. K., Forudi, F., Kiedrowski, M., Rovner, A., Ellis, S. G., Thomas, J. D., DiCorleto, P. E., Topol, E. J., Penn, M. S.** (2003). Effect of stromal-cell-derived factor 1 on stem-cell homing and tissue regeneration in ischaemic cardiomyopathy. *Lancet* **362:** 697–703.

5. **Baumann, C.A., Ribon, V., Kanzaki, M., Thurmond, D.C., Mora, S., Shigematsu, S., Bickel, P.E., Pessin, J.E. and Saltiel, A.R.** (2000). CAP defines a second signalling pathway required for insulin-stimulated glucose transport. *Nature* **407:** 202–207.

6. **Bourajjaj, M., Stehouwer, C. D., van Hinsbergh, V. W., Schalkwijk, C. G.** (2003). Role of methylglyoxal adducts in the development of vascular complications in diabetes mellitus. *Biochem. Soc. Trans.* **31:** 1400-1402.

7. **Bourgin, C., Murai, K. K., Richter, M., Pasquale, E. B.** (2007). The EphA4 receptor regulates dendritic spine remodeling by affecting beta1-integrin signaling pathways. *J Cell Biol.* **178(7):** 1295-307.

8. **Boyhan, A., Casimir, C. M., French, J. K., Teahan, C. G., and Segal, A. W.** (1992). Molecular cloning and characterization of grancalcin, a novel EF-hand calcium-binding protein abundant in neutrophils and monocytes. *J. Biol. Chem.* **267:** 2928-2933.

9. **Brownlee, M.** (1990). Advanced products of nonenzymatic glycosylation and the pathogenesis of diabetic complications. In *Diabetes Mellitus, Theory and Practise* (Rifkin, H., and Porte, D., Jr., eds) pp. **279-291,** Elsevier, New York.

10. **Brownlee, M.** (2001). Biochemistry and molecular cell biology of diabetic complications. *Nature* (London) **414:** 813-820.

11. **Charonis, A. S., Reger, L. A., Dege, J. E., Kouzii-Koliakos, K., Furcht, L. T., Wohlhueter, R. M., Tsilibary, E. C.** (1990). Laminin alterations after in vitro nonenzymatic glucosylation. *Diabetes* **39:** 807-814.

12. **Creagh, E. M., Conroy, H., Martin, S. J.** (2003). Caspase-activation pathways in apoptosis and immunity. *Immunol. Rev.* **193:** 10-21.

13. **Czekay, R. P., Aertgeerts, K., Curriden, S. A., Loskutoff, D. J.:** (2003). Plasminogen activator inhibitor-1 detaches cells from extracellular matrices by inactivating integrins. *J Cell Biol* **160:** 781-791.

14. **Dahl-Jørgensen, K** (1998). Diabetic microangiopathy. *Acta Paediatr Suppl* **425:** 31-34.

15. **Dang, D. T., Pevsner, J., Yang, V. W.** (2000).The biology of the mammalian Kruppel-like family of transcription factors. *Int J Biochem Cell Biol.* 32**:** 1103–1121.

16. **Degenhardt, T. P., Thorpe, S. R., Baynes, J. W.** (1998). Chemical modification of proteins by methylglyoxal. *Cell Mol. Biol.* **44:** 1139-1145.

17. **Deshane, J., Chen, S., Caballero, S., Grochot-Przeczek, A., Was, H., Li Calzi, S., Lach, R., Hock, T. D., Chen, B., Hill-Kapturczak, N., Siegal, G. P., Dulak, J., Jozkowicz, A., Grant, M. B., Agarwal, A.** (2007). Stromal cell-derived factor 1 promotes angiogenesis via a heme oxygenase 1-dependent mechanism. *J Exp Med.* **204(3):** 605-18.

18. **Desplan, C., Theis, J., O'Farrel, P. H.** (1988). The sequence specificity of homeodomain-DNA interaction. *Cell* **54:** 1081–1090.

19. **D'Haeseleer, P., Liang, S., Somogyi, R.** (2000). Genetic network inference: from co-expression clustering to reverse engineering. *Bioinformatics* **16:** 707-26.

20. **Du, X. L., Edelstein, D., Rossetti, L., Fantus, I. G., Goldberg, H., Ziyadeh, F., Wu, J., Browlee, M.** (2000). Hyperglycemia-induced mitochondrial superoxide overproduction activates the hexosamine pathway and induces plasminogen activator inhibitor-1 expression by increasing Sp1 glycosylation. *Proc. Natl. Acad. Sci. USA* **97:** 12222-12226.

21. **Du, X. L., Edelstein, D., Dimmeler, S., Ju, Q., Sui, C., Brownlee, M.** (2001). Hyperglycemia inhibits endothelial nitric oxide synthase activity by posttranslational modification at the Akt site. *J. Clin. Invest.* **108:** 1341-1348.

22. **Du, X., Matsumura, T., Edelstein, D., Rossetti, L., Zsengeller, Z., Szabo, C., Brownlee, M.** (2003). Inhibition of GAPDH activity by poly(ADP-ribose) polymerase activates three major pathways of hyperglycaemic damage in endothelial cells. *J. Clin. Invest.* **112:** 1049–1057.

23. **Feener, E. P., Xia, P., Inoguchi, T., Shiba, T., Kunisaki, M., King, G. L.** (1996). Role of protein kinase C in glucose- and angiotensin II-induced plasminogen activator inhibitor expression. *Contrib. Nephrol.* **118:** 180-187.

24. **Glogowski, E. A., Tsiani, E., Zhou, X. P., Fantus, I. G., Whiteside C. I.** (1999). High glucose alters the response of mesangial cell protein kinase C isoforms to endothelin-1. *Kidney Int.* **55:** 486-499.

25. **Greenberg, A.S., Obin, M.S.** (2006). Obesity and the role of adipose tissue in inflammation and metabolism. *American Journal of Clinical Nutrition.* **83(2):** 461S-465S.

26. **Greer, J. M., Puetz, J., Thomas, K. R., Capecchi, M. R.** (2000). Maintenance of functional equivalence during paralogous Hox gene evolution. *Nature* **403:** 661–664.

27. **Hagman, J., Travis, A., Grosschedl, R.** (1991). A novel lineage-specific nuclear factor regulates mb-1 gene transcription at the early stages of B cell differentiation. *EMBO J.* **10:** 3409–3417.

28. **Heldin, C. H., Miyazono, K., ten Dijke, P.** (1997). TGF-beta signalling from cell membrane to nucleus through SMAD proteins. *Nature* **390:** 465–471.

29. **Henkemeyer, M., Itkis, O. S., Ngo, M., Hickmott, P. W., Ethell, I. M.** (2003). Multiple EphB receptor tyrosine kinases shape dendritic spines in the hippocampus. *J. Cell Biol.* **163:** 1313–1326.

30. **Hotulainen, P., Paunola, E., Vartiainen, M. K., Lappalainen, P.** (2005). Actin-depolymerizing factor and cofilin-1 play overlapping roles in promoting rapid F-actin depolymerization in mammalian nonmuscle cells. *Mol. Biol. Cell.* **16:** 649–664.

31. **Huck, J. H. J., Verhoeven, N. M., Struys, E. A., Salomons, G. S., Jakobs, C., van der Knaap, M. S.,** (2004). Ribose-5-Phosphate Isomerase Deficiency: New Inborn Error in the Pentose Phosphate Pathway Associated with a Slowly Progressive Leukoencephalopathy. *Am. J. Hum. Genet.* **74:** 745-751.

32. **Ingham, P.W.** (1988) The Molecular genetics of embryonic pattern formation in Drosophila. *Nature* **335:** 25-34.

33. **Jimenez, M. A., Akerblad, P., Sigvardsson, M., Rosen, E. D.** (2007). Critical role for Ebf1 and Ebf2 in the adipogenic transcriptional cascade. *Mol Cell Biol.* **27(2):** 743-57.

34. **Kappen, C., Schughart, K., Ruddle, F. H.** (1989). Two steps in the evolution of Antennapedia-class vertebrate homeobox genes. *Proc Natl Acad Sci U S A.* **86:** 5459–5463.

35. **Kipreos, E. T., Pagano, M.** (2000). The F-box protein family. *Genome Biol* **1(5):** REVIEWS3002.1-REVIEWS3002.7.

36. **Kissinger, C. R., Liu, B., Martin-Blanco, E., Kornberg, T. B., Pabo, C. O.** (1990). Crystal structure of an engrailed homeodomain-DNA complex at 2.8A resolution: a framework for understanding homeodomain-DNA interactions. *Cell* **63:** 579–590.

37. **Klomp, L. W., de Koning, T. J., Malingre, H. E., van Beurden, E. A., Brink, M., Opdam, F. L., Duran, M., Jaeken, J., Pineda, M., van Maldergem, L., Poll-The, B. T., van den Berg, I. E., Berger R.** (2000) Molecular characterization of 3-phosphoglycerate dehydrogenase deficiency–A neurometabolic disorder associated with reduced L-serine biosynthesis. *Am J Hum Genet* **67:** 1389–1399.

38. **Kolm-Litty, V., Sauer, U., Nerlich, A., Lehmann, R., Schleicher, E. D.** (1998). High glucose-induced transforming growth factor beta1 production is mediated by the hexosamine pathway in porcine glomerular mesangial cells. *J. Clin Invest.* **101:** 160–169.

39. **Korpelainen, E. I., Alitalo, K.** (1998). Signaling angiogenesis and lymphangiogenesis. *Curr Opin Cell Biol* **10:** 159–164.

40. **Koya, D., Jirousek, M. R., You-Wei, L., Ishii, H., Kuboki, K., King, G. L.** (1997). Characterization of protein kinase C beta isoform activation on gene expression of transforming growth factor-beta, extracellular matrix components, and prostanoids in the glomeruli of diabetic rats. *J Clin Invest* **100:** 115 –126.

41. **Koya, D., King, G. L.** (1998). Protein kinase C activation and the development of diabetic complications. *Diabetes* **47:** 859-866.

42. **Kuboki, K., Jiang, Z. Y., Takahara, N., Ha, S. W., Igarashi, M., Yamauchi, T., Feener, E. P., Herbert, T. P., Rhodes, C. J., King, G. L.** (2000). Regulation of endothelial constitutive nitric oxide synthase gene expression in endothelial cells and in vivo: a specific vascular action of insulin. *Circulation* **101:** 676–681.

43. **Kudrycki, K., Stein-Izsak, C., Behn, C., Grillo, M., Akeson, R., Margolis, F. L.** (1993). Olf-1-binding site: characterization of an olfactory neuronspecific promoter motif. *Mol. Cell. Biol.* **13:** 3002–3014.

44. **Kullander, K., Klein, R.** (2002). Mechanisms and functions of Eph and ephrin signalling. *Nat. Rev. Mol. Cell Biol.* **3:** 475–486.

45. **Kuziora, M. A., McGinnis, W.** (1989). A homeodomain substitution changes the regulatory specificity of the deformed protein in *Drosophila* embryos. *Cell* **59:** 563–571.

46. **Lander, H. M., Tauras, J. M., Ogiste, J. S., Hori, O., Moss, R. A., and Schmidt, A. M.** (1997). Activation of the receptor for advanced glycation end products triggers a p21(ras)-dependent mitogen-activated protein kinase pathway regulated by oxidant stress. *J Biol Chem.* **28**, 17810–17814.

47. **Lee, A.Y., Chung, S.S.** (1999). Contributions of polyol pathway to oxidative stress in diabetic cataract. *FASEB J.* **13:** 23-30.

48. **Leung, D. W., Cachianes, G., Kuang, W. J., Goeddel, D. V., Ferrara, N.** (1989). Vascular endothelial growth factor is a secreted angiogenic mitogen. *Science* **246:** 1306–1309.

49. **Levine, M., Hoey, T.** (1988). Homeobox proteins as sequence-specific transcription factors. *Cell* **55:** 537-540.

50. **Lewis, E. B.** (1978). A gene complex controlling segmentation in *Drosophila*. *Nature* **276:** 565–570.

51. **Li, Y. M., Mitsuhashi, T., Wojciechowicz, D., Shimizu, N., Li, J., Stitt, A., He, C., Banerjee, D., Vlassara, H.** (1996). Molecular identity and cellular distribution of advanced glycation end product receptors: relationship of p60 to OST-48 and p90-80K-H membrane proteins. *Proc. Natl Acad. Sci. USA* **93:** 11047-11052.

52. **Li, D., Yea, S., Li, S., Chen, Z., Narla, G., Banck, M., Laborda, J., Tan, S., Friedman, J. M., Friedman, S. L., Walsh, M. J.** (2005). Kruppel-like factor-6 promotes preadipocyte differentiation through histone deacetylase 3-dependent repression of DLK1. *J Biol Chem,* **280:** 26941-52.

53. **Liadis, N., Murakami, K., Eweida, M., Elford, A. R., Sheu, L., Gaisano, H. Y., Hakem, R., Ohashi, P. S., Woo, M.** (2005). Caspase-3-dependent beta-cell apoptosis in the initiation of autoimmune diabetes mellitus. *Mol. Cell. Biol.* **25:** 3620–3629.

54. **Lin, W. H., Chiu, K. C., Chang, H. M., Lee, K. C., Tai, T. Y., Chuang, L. M.** (2001). Molecular scanning of the human sorbin and SH3-domain-containing-1 (SORBS1) gene: positive association of the T228A polymorphism with obesity and type 2 diabetes. *Hum Mol Genet* **10:** 1753-1760.

55. **Lu, M., Kuroki, M., Amano, S., Tolentino, M., Keough, K., Kim, I., Bucala, R., Adamis, A. P.** (1998). Advanced glycation end products increase retinal vascular endothelial growth factor expression. *J. Clin. Invest.* **101:** 1219-1224.

56. **Mace, K. A., Hansen, S. L., Myers, C., Young, D.M., Boudreau, N.** (2005). HOXA3 induces cell migration in endothelial and epithelial cells promoting angiogenesis and wound repair. *Journal of Cell Science* **118:** 2567-2577.

57. **Manley, N. R., Capecchi, M. R.** (1995) The role of Hoxa-3 in mouse thymus and thyroid development. *Development* **121:** 1989–2003.

58. **Manley, N. R., Capecchi, M. R.** (1998). *Hox* group 3 paralogs regulate the development and migration of the thymus, thyroid and parathyroid glands. *Dev. Biol.* **195:** 1-15.

59. **McGinnis, W., Krumlauf, R.** (1992). Homeobox genes and axial patterning. *Cell* **68:** 283–302.

60. **Miyakoshi, K., Murphy, M. J., Yeoman, R. R., Mitra, S., Dubay, C. J., Hennebold, J. D.** (2007). The identification of novel ovarian proteases through the use of genomic and bioinformatic methodologies. *Biol. Reprod.* **75(6):** 823–35.

61. **Narla, G., Heath, K. E., Reeves, H. L., Li, D., Giono, L. E., Kimmelman, A. C., Glucksman, M. J., Narla, J., Eng, F. J., Chan, A. M., Ferrari, A. C., Martignetti, J. A., Friedman, S. L.** (2001). KLF6, a candidate tumor suppressor gene mutated in prostate cancer. *Science* **294:** 2563–2566.

62. **Neeper, M., Schmidt, A. M., Brett, J., Yan, S. D., Wang, F., Pan, Y. C., Elliston, K., Stern, D., Shaw, A.** (1992). Cloning and expression of RAGE: a cell surface receptor for advanced glycosylation end products of proteins. *J. Biol. Chem.* **267:** 14998-15004.

63. **Nichrs, C.** (2004). Norrin and frizzled; a new vein for the eye. *Dev Cell.* **6:** 453–454.

64. **Nishizuka, M.; Arimoto, E.; Tsuchiya, T.; Nishihara, T., Imagawa, M.** (2003). Crucial role of TCL/TC10beta L, a subfamily of Rho GTPase, in adipocyte differentiation. *J Biol Chem.* **278(17):** 15279–15284.

65. **Ohlmann, A., Scholz, M., Goldwich, A., Chauhan, B. K., Hudl, K., Ohlmann, A. V., Zrenner, E., Berger, W., Cvekl, A., Seeliger, M. W., Tamm, E. R.** (2005). Ectopic norrin induces growth of ocular capillaries and restores normal retinal angiogenesis in Norrie disease mutant mice. *J Neurosci.* **25:** 1701–1720.

66. **Otting, G., Qian, Y. Q., Billeter, M., Muller, M., Affolter, M., Gehring, W. J., Wüthrich, K.** (1990). Protein-DNA contacts in the structure of a homeodomain-DNA complex determined by nuclear magnetic resonance spectroscopy in solution. *EMBO J* **9:** 3085–3092.

67. **Pieper, G. M., Riaz-ul-Haq, G.** (1997). Activation of nuclear factor-κB in cultured endothelial cells by increased glucose concentration: prevention by calphostin C. *J. Cardiovasc. Pharmacol.* **30:** 528−532.

68. **Qian, Y. Q., Billeter, M., Otting, G., Muller, M., Gehring, W. J., Wuthrich, K.** (1989). The structure of the Antennapedia homeodomain determined by NMR spectroscopy in solution: comparison with prokaryotic repressors. *Cell* **59:** 573–580.

69. **Reya, T., Clevers, H.** (2005). Wnt signaling in stem cell and cancer. Review Article. *Nature.* **434:** 843–850.

70. **Robitaille, J., MacDonald M. L., Kaykas, A., Sheldahl, L. C., Zeisler, J., Dube, M. P., Zhang, L. H., Singaraja, R. R., Guernsey, D. L., Zheng, B., Siebert, L. F., Hoskin-Mott, A., Trese, M. T., Pimstone, S. N., Shastry, B. S., Moon, R. T., Hayden, M. R., Goldberg, U. P., Samuels, M. E.** (2002). Mutant frizzled-4 disrupts retinal angiogenesis in familial exudative vitreoretinopathy. *Nature Genet.* **32:** 326–330.

71. **Schalkwijk, C.G., Stehouwer, C.D.A.** (2005). Vascular complications in diabetes mellitus: the role of endothelial dysfunction. *Clinical Science* **109:** 143-159.

72. **Schmidt, A. M., Hori, O., Chen, J. X., Li, J. F., Crandall, J., Zhang, J., Cao, R., Yan, S. D., Brett, J., Stern, D.** (1995). Advanced glycation endproducts interacting with their endothelial receptor induce expression of vascular cell adhesion molecule-1 (VCAM-1) in cultured human endothelial cells and in mice: a potential mechanism for the accelerated vasculopathy of diabetes. *J. Clin. Invest.* **96:** 1395-1403.

73. **Schumaker, V. N.;Zavodszky, P.; Poon, P. H.** (1987). Activation of the first component of the complement system. *Annu. Rev. Immunol.* **5:** 21–42.

74. **Scott, M. P.** (1992). Vertebrate homeobox gene nomenclature. *Cell* **71**: 551–553.

75. **Smedsrod, B., Melkko, J., Araki, N., Sano, H., Horiuchi, S.** (1997). Advanced glycation end products are eliminated by scavenger-receptor-mediated endocytosis in hepatic sinusoidal kupffer and endothelial cells. *Biochem J.* **322:** 567-573.

76. **Snell, K.** (1984). Enzymes of serine metabolism in normal, developing and neoplastic rat tissues. *Adv Enzyme Regul* **22:** 325–400.

77. **Snell, K., Weber, G.** (1986). The duality of pathways for serine biosynthesis is a fallacy. *Trends Biochem Sci* **11:** 241–243.

78. **Sommer, B. J., Barycki, J. J., Simpson, M. A.** (2004). Characterization of human UDP-glucose dehydrogenase. CYS-276 is required for the second of two successive oxidations. *J. Biol. Chem.* **279:** 23590-23596.

79. **Stokic, D., Hanel, R., Thurner, S.** (2008). A fast and efficient gene-network reconstruction method from multiple over-expression experiments. *arXiv:0806.3048v1*

80. **Su, D. M., Manley, N. R.** (2000). Hoxa3 and Pax1 transcription factors regulate the ability of fetal thymic epithelial cells to promote thymocyte development. *J Immunol.* **164:** 5753–5760.

81. **Svingen, T. Tonissen, KF.** (2006). Hox transcription factors and their elusive mamalian gene targets. *Heredity* **97:** 88-96.

82. **Tanaka, S., Avigad, G., Brodsky, B., Eikenberry, E. F.** (1988). Glycation induces expansion of the molecular packing of collagen. *J. Mol. Biol.* **203:** 495-505.

83. **Tsilibary, E. C., Charonis, A. S., Reger, L. A., Wohlhueter, R. M., Furcht, L. T.** (1988). The effect of nonenzymatic glycosylation on the binding of the main noncollagenous NC1 domain to type IV collagen. *J. Biol. Chem.* **263:** 4302-4308.

84. **Ulijaszek, S. J., Johnston, F. E., Preece, M. A.** (1998). *The Cambridge Encyclopedia of Human Growth and Development*. Cambridge University Press: Cambridge.

85. **Vignal, E., Blangy, A., Fort, P.** (2003). Signaling networks of Rho GTPases. In: Rho GTPases, ed. M. Symons, Austin, TX: R.G. Landes Co. **323:** 253–262.

86. **Vlassara, H., Li, Y. M., Imani, F., Wojciechowicz, D., Yang, Z., Liu, F. T., Cerami, A.** (1995). Identification of galectin-3 as a high-affinity binding protein for advanced glycation end products (AGE): a new member of the AGE-receptor complex. *Mol. Med.* **1:** 634-646.

87. **Wells-Knecht K. J., Zyzak, D. V., Lichtfeld, J. E., Thorpe, S. R., Baynes, J. W.** (1995). Mechanism of autoxidative glycosylation: identification of glyoxal and arabinose as intermediates in the autoxidative modification of proteins by glucose. *Biochemistry* **34:** 3702-3709.

88. **Whatmore, J., Morgan, C. P., Cunningham, E., Collison, K. S., Willison, K. R., Cockcroft, S.** (1996). ADP-ribosylation factor 1-regulated phospholipase D activity is localized at the plasma membrane and intracellular organelles in HL60 cells. *Biochem J.* **320:** 785–794.

89. **Williams, B., Gallacher, B., Patel, H., Orme, C.** (1997). Glucose-induced protein kinase C activation regulates vascular permeability factor mRNA expression and peptide production by human vascular smooth muscle cells in vitro. *Diabetes* **46:** 1497–1503.

90. **Williamson, J. R., Tilton, R. G., Chang, K., Kilo, C.** (1988). Basement membrane abnormalities in diabetes mellitus: relationship to clinical microangiopathy. *Diabetes/Metabolism Rev.* **4:** 339-370.

91. **Yan, S. D.**, **Schmidt, A. M., Anderson G. M., Zhang, J., Brett, J., Zou, Y. S., Pinky, D., Stern, D.** (1994). Enhanced cellular oxidant stress by the interaction of advanced glycation end products with their receptors/binding proteins. *J. Biol. Chem.* **269:** 9889-9897.

Appendix

Table 7. Interactions between all candidate genes transiently expressed in the course of the project aiming at identification of a gene network in diabetic microangiopathy.

Position	from	to	Strength of interaction	Position	from	to	Strength of interaction
1	BTF3	CXCL12	8.242679	41	CASP3	PRSS23	2.727602
2	PRSS23	RPIB9	7.857261	42	AQP1	AQP1	2.722051
3	CASP3	ICAM1	-7.712362	43	CFH	GAPDH	-2.719102
4	CASP3	SMAD2	-6.414143	44	CASP3	NOS3	2.708902
5	PRG	RPIB9	6.210309	45	CFL1	GAPDH	2.696649
6	CASP3	PRG	-5.738937	46	CFL1	Endothelin1	-2.678154
7	ATP6V0D1	CXCL12	5.265143	47	PRG	CXCL12	-2.66132
8	CALM2	GAPDH	-4.815197	48	CASP3	AQP1	-2.656819
9	CALM2	RPIB9	4.66573	49	CFL1	PRSS23	-2.629604
10	CFL1	PLD	4.656133	50	PRG	Endothelin1	2.617896
11	CALM2	PLD	-4.478745	51	CASP3	RHOJ	2.60178
12	CASP3	CASP3	-3.999093	52	PRG	FGF1	-2.585011
13	CFL1	**HOXA3**	3.861057	53	KLF6	GAPDH	2.549512
14	CALM2	Endothelin1	3.835349	54	PRSS23	FGF1	-2.538473
15	CFL1	FGF1	3.782886	55	FGF1	FGF1	2.515363
16	CALM2	CALM2	-3.732761	56	RHOJ	RHOJ	2.49185
17	CSPG	CSPG	3.731625	57	RPIB9	CXCL12	2.479657
18	BTF3	AQP1	-3.652131	58	CFL1	RAMP3	2.458638
19	RAMP3	RAMP3	3.575295	59	CFL1	CXCL12	2.419278
20	PRSS23	CXCL12	-3.413204	60	CYR61	CFH	2.369235
21	CFL1	PRG	3.395434	61	CFL1	CSPG	-2.344377
22	BTF3	CSPG	3.306348	62	SMAD3	SMAD3	2.33675
23	ATP6V0D1	GAPDH	-3.279249	63	CALM2	NOS3	2.3354
24	CFL1	CYR61	-3.263373	64	CYR61	RPIB9	-2.333872
25	CALM2	CYR61	3.233838	65	ATP6V0D1	ATP6V0D1	2.325257
26	BTF3	RPIB9	3.182712	66	CFL1	c-Jun	-2.3076
27	CALM2	FGF1	-3.181601	67	GNAS2	RPIB9	-2.293562
28	CASP3	CFH	3.117886	68	**HOXA3**	**HOXA3**	2.284825
29	ATP6V0D1	AQP1	-3.08974	69	CFL1	GCA	-2.242516
30	CFL1	CFL1	-3.081079	70	CALM2	RAMP3	-2.231726
31	CASP3	CXCL12	3.062254	71	GNAS2	RAMP3	2.226801
32	CALM2	AQP1	-3.046736	72	CYR61	CSPG	-2.217062
33	CASP3	**HOXA3**	-3.037106	73	CYR61	GAPDH	2.192965
34	CALM2	PRSS23	3.02272	74	GNAS2	GNAS2	2.187287
35	CYR61	RAMP3	2.999542	75	c-Jun	RPIB9	-2.183915
36	CALM2	CSPG	2.96628	76	CASP3	FGF1	2.179099
37	CALM2	UGDH	2.927373	77	Endothelin1	RPIB9	-2.168576
38	PRSS23	Endothelin1	2.842801	78	PRSS23	CALM2	-2.163368
39	PLD	RPIB9	-2.768838	79	TGFb-R2	CFH	-2.136859
40	CASP3	SMAD3	-2.728214	80	BTF3	CALM2	-2.130973

Position	from	to	Strength of interaction	Position	from	to	Strength of interaction
81	FZD4	FZD4	2.128543	126	ICAM1	ICAM1	1.642936
82	c-Jun	c-Jun	2.125499	127	PLD	PRSS23	1.642682
83	NOS3	NOS3	2.098091	128	PRG	KLF6	-1.637824
84	CYR61	CXCL12	-2.091655	129	TGFb1	TGFb1	1.633198
85	CALM2	c-Jun	2.078061	130	RPIB9	FGF1	1.620557
86	ATP6V0D1	CSPG	2.07361	131	CALM2	FZD4	1.619776
87	CASP3	FZD4	2.062084	132	PLD	CFL1	1.604756
88	CFL1	UGDH	-2.052853	133	CASP3	GCA	1.576945
89	ATP6V0D1	CFH	-2.044165	134	CFL1	KLF6	1.576523
90	TGFb-R2	TGFb-R2	2.036906	135	BTF3	SMAD2	-1.555074
91	Endothelin1	CFL1	2.024652	136	CASP3	BTF3	-1.546986
92	GCA	GCA	1.996602	137	c-Jun	FGF1	1.54171
93	GNAS2	GAPDH	1.987186	138	ATP6V0D1	PRSS23	1.535841
94	RHOJ	GAPDH	-1.982485	139	c-Jun	CXCL12	1.532972
95	CFL1	CFH	1.979011	140	Endothelin1	PLD	-1.523676
96	ATP6V0D1	CALM2	-1.974402	141	CYR61	CALM2	1.517557
97	BTF3	FGF1	-1.968983	142	ATP6V0D1	PLD	-1.496417
98	SMAD2	SMAD2	1.966927	143	CDYL12	CXCL12	1.487483
99	FZD4	GAPDH	-1.96532	144	CDYL12	GAPDH	-1.482582
100	CFL1	NOS3	-1.962628	145	GTPBP4	CFL1	-1.480965
101	CYR61	FGF1	1.954061	146	CASP3	PHGDH	-1.457463
102	Endothelin1	PRSS23	1.94045	147	GTPBP4	CXCL12	1.457217
103	CALM2	CFH	-1.92955	148	PRG	PRG	1.456033
104	CFL1	AQP1	1.92925	149	CASP3	KLF6	1.4507
105	RHOJ	CXCL12	1.921979	150	PRG	CFH	-1.450461
106	TOR3A	TOR3A	1.904106	151	CDYL12	CALM2	-1.443827
107	TGFb-R2	RPIB9	1.903911	152	GNAS2	CALM2	1.438364
108	GTPBP4	GTPBP4	1.89768	153	TGFb1	CFL1	-1.433114
109	CDYL12	CDYL12	1.897598	154	PRSS23	CFH	-1.425859
110	TOR3A	GAPDH	-1.895986	155	TGFb-R2	CALM2	-1.424873
111	KLF6	CXCL12	-1.892251	156	Endothelin1	AQP1	-1.423115
112	GDI2	GDI2	1.886837	157	CASP3	TGFb1	1.402141
113	PHGDH	PHGDH	1.853456	158	CASP3	GAPDH	-1.386159
114	BTF3	CFH	-1.81942	159	PLD	GAPDH	-1.376722
115	PRSS23	CSPG	1.817921	160	PRSS23	KLF6	-1.375956
116	CALM2	PRG	-1.799347	161	PRG	UGDH	1.348567
117	CALM2	SMAD2	-1.782508	162	ICAM1	CXCL12	1.345553
118	BTF3	PLD	-1.748211	163	TGFb-R2	CFL1	-1.336576
119	BTF3	ICAM11	-1.74477	164	ICAM1	FGF1	1.334682
120	CYR61	AQP1	1.733734	165	PRSS23	UGDH	1.333416
121	PRG	CSPG	1.721634	166	KLF6	RPIB9	-1.329022
122	CFL1	RPIB9	-1.715203	167	PHGDH	FGF1	1.327598
123	KLF6	AQP1	1.664461	168	PRSS23	GAPDH	-1.317217
124	PRG	CALM2	-1.656693	169	CYR61	ICAM1	1.315667
125	CFL1	FZD4	-1.654806	170	Endothelin1	GAPDH	-1.313102

Position	from	to	Strength of interaction	Position	from	to	Strength of interaction
171	UGDH	UGDH	1.310948	216	Endothelin1	**HOXA3**	-1.073105
172	KLF6	CALM2	1.30467	217	Endothelin1	NOS3	1.072445
173	PLD	AQP1	-1.304656	218	GTPBP4	PRG	1.068494
174	CASP3	CYR61	1.290601	219	CXCL12	CXCL12	1.068447
175	KLF6	CSPG	1.286562	220	KLF6	ICAM1	1.068114
176	GAPDH	AQP1	-1.285852	221	CALM2	KLF6	-1.06752
177	PRG	CYR61	1.282092	222	GTPBP4	FGF1	1.067299
178	RHOJ	AQP1	-1.280362	223	TOR3A	CALM2	-1.060599
179	KLF6	PRSS23	-1.269263	224	PRSS23	CFL1	-1.05331
180	FZD4	CXCL12	1.262295	225	GNAS2	FGF1	1.052674
181	GNAS2	CFH	1.257652	226	CALM2	ICAM1	-1.051629
182	c-Jun	CSPG	-1.254964	227	TGFb1	CXCL12	1.041784
183	PRSS23	CYR61	1.253514	228	CYR61	CFL1	1.035112
184	PLD	CALM2	1.249145	229	GNAS2	Endothelin1	-1.031415
185	ATP6V0D1	SMAD2	-1.246196	230	TOR3A	CXCL12	1.026558
186	Endothelin1	c-Jun	1.243444	231	KLF6	CFH	1.022732
187	ATP6V0D1	FGF1	-1.242175	232	CFL1	SMAD2	1.019112
188	SMAD3	CSPG	1.235187	233	CDYL12	AQP1	-1.017664
189	NOS3	RPIB9	-1.233677	234	TGFb-R2	CSPG	1.016944
190	Endothelin1	SMAD3	1.230222	235	RPIB9	CFH	1.010395
191	BTF3	BTF3	1.229077	236	PRSS23	AQP1	1.008426
192	KLF6	KLF6	1.226434	237	TOR3A	CFL1	-1.00681
193	PLD	SMAD3	1.219833	238	ICAM1	PRG	0.999998
194	KLF6	PLD	1.211519	239	CALM2	GCA	0.996761
195	c-Jun	GAPDH	-1.179839	240	FZD4	CALM2	-0.994436
196	CYR61	Endothelin1	-1.162037	241	PHGDH	PLD	0.992965
197	RHOJ	CFH	-1.151993	242	ATP6V0D1	c-Jun	0.988746
198	CYR61	PRSS23	-1.150767	243	ICAM1	PLD	0.987355
199	c-Jun	Endothelin1	-1.147760	244	SMAD2	CXCL12	0.985341
200	CFL1	GDI2	1.145122	245	PRG	PLD	-0.980209
201	AQP1	CSPG	1.141788	246	CXCL12	AQP1	0.979658
202	CASP3	ATP6V0D1	1.140607	247	TGFb-R2	TGFb1	-0.978712
203	c-Jun	PRG	1.136098	248	CALM2	**HOXA3**	-0.977092
204	RPIB9	Endothelin1	-1.131415	249	RPIB9	KLF6	0.974219
205	CYR61	SMAD2	1.122306	250	CALM2	SMAD3	0.970076
206	TGFb1	CSPG	1.12179	251	CASP3	UGDH	0.97002
207	Endothelin1	CYR61	1.118653	252	PLD	**HOXA3**	-0.969137
208	CALM2	PHGDH	-1.105632	253	CFL1	TGFb1	-0.968707
209	FZD4	CFL1	-1.100342	254	GAPDH	PRSS23	0.968161
210	BTF3	PRSS23	1.095389	255	PLD	c-Jun	0.965911
211	KLF6	SMAD2	1.0852	256	RHOJ	CFL1	-0.96468
212	CALM2	RHOJ	1.081526	257	GTPBP4	PLD	0.964364
213	CALM2	BTF3	-1.077063	258	NOS3	CXCL12	0.962163
214	CALM2	TGFb1	1.074866	259	CFH	CALM2	-0.960891
215	BTF3	CYR61	1.073831	260	TGFb-R2	CXCL12	0.954057

Position	from	to	Strength of interaction	Position	from	to	Strength of interaction
261	CASP3	CSPG	0.953982	306	TGFb-R2	GAPDH	-0.819272
262	RPIB9	RPIB9	-0.947515	307	KLF6	BTF3	0.813969
263	PHGDH	CFL1	-0.946539	308	BTF3	Endothelin1	0.813671
264	CYR61	UGDH	-0.938486	309	TOR3A	CFH	-0.813397
265	FZD4	GCA	-0.936292	310	ATP6V0D1	CYR61	0.81192
266	PRSS23	SMAD3	-0.935454	311	ATP6V0D1	PHGDH	-0.808789
267	c-Jun	KLF6	0.933512	312	CALM2	CXCL12	0.807208
268	BTF3	CFL1	-0.933266	313	ATP6V0D1	RHOJ	0.806569
269	RPIB9	AQP1	-0.930272	314	Endothelin1	PRG	-0.803353
270	CFH	AQP1	-0.929077	315	CYR61	PLD	0.799185
271	KLF6	PRG	0.926734	316	CASP3	CFL1	0.798349
272	ATP6V0D1	CFL1	-0.920006	317	GAPDH	c-Jun	0.79265
273	CYR61	BTF3	0.91894	318	NOS3	FGF1	0.792039
274	ATP6V0D1	UGDH	0.917983	319	ATP6V0D1	Endothelin1	0.790161
275	RPIB9	CSPG	-0.916101	320	CALM2	GNAS2	-0.789899
276	KLF6	Endothelin1	-0.913173	321	PLD	CYR61	0.784333
277	BTF3	NOS3	0.909243	322	GDI2	NOS3	0.782998
278	BTF3	UGDH	0.904876	323	UGDH	FGF1	0.781267
279	ATP6V0D1	ICAM1	0.89925	324	GTPBP4	CALM2	-0.780322
280	ICAM1	CFL1	-0.898077	325	CFH	PRSS23	0.780167
281	CFL1	SMAD3	-0.894491	326	RPIB9	GAPDH	-0.777969
282	ATP6V0D1	NOS3	0.893727	327	GAPDH	SMAD3	0.777137
283	GCA	CFL1	-0.892572	328	CASP3	RAMP3	-0.776737
284	CASP3	CALM2	0.888856	329	RHOJ	CSPG	0.776246
285	RHOJ	CALM2	-0.887787	330	RPIB9	SMAD3	0.769392
286	PLD	NOS3	0.887649	331	KLF6	CYR61	-0.761481
287	Endothelin1	RAMP3	-0.880815	332	CDYL12	CFL1	-0.757179
288	PRSS23	RAMP3	-0.880577	333	UGDH	RPIB9	-0.756906
289	PRG	GCA	0.880418	334	CYR61	PHGDH	0.753908
290	PRG	AQP1	0.879461	335	UGDH	CSPG	-0.752372
291	TOR3A	RPIB9	0.872244	336	CASP3	RPIB9	0.744745
292	SMAD3	CXCL12	0.865239	337	RPIB9	PHGDH	-0.74399
293	PLD	FGF1	0.863824	338	GDI2	PRSS23	0.7428
294	BTF3	PRG	-0.863597	339	TGFb-R2	**HOXA3**	0.742079
295	RPIB9	PRG	0.863141	340	GNAS2	CYR61	-0.74119
296	Endothelin1	FZD4	0.861509	341	PRSS23	**HOXA3**	0.740413
297	SMAD2	FGF1	0.856169	342	PHGDH	PRG	0.739949
298	FZD4	AQP1	-0.853477	343	Endothelin1	CALM2	0.738925
299	TOR3A	AQP1	-0.847746	344	TOR3A	GCA	-0.736713
300	PRSS23	PRSS23	0.847285	345	ICAM1	RPIB9	-0.735808
301	GDI2	RPIB9	-0.841091	346	TGFb1	**HOXA3**	0.735693
302	GNAS2	CFL1	0.836314	347	KLF6	UGDH	-0.72825
303	GCA	CXCL12	0.836269	348	GAPDH	CALM2	-0.721993
304	PRG	RAMP3	-0.82963	349	**HOXA3**	GAPDH	-0.721046
305	FZD4	CFH	-0.826351	350	CFL1	TOR3A	0.720497

Position	from	to	Strength of interaction	Position	from	to	Strength of interaction
351	PLD	CSPG	-0.720347	396	GAPDH	CXCL12	0.62672
352	CFH	CFL1	-0.718437	397	CDYL12	PRSS23	0.626512
353	TGFb-R2	Endothelin1	0.715016	398	CYR61	PRG	0.620565
354	SMAD2	PRG	0.712885	399	ICAM1	CFH	0.620361
355	PLD	PLD	-0.709276	400	BTF3	GAPDH	-0.619802
356	BTF3	TGFb-R2	-0.707906	401	ATP6V0D1	GCA	-0.619129
357	BTF3	c-Jun	0.704005	402	GDI2	PLD	-0.619083
358	GTPBP4	GCA	-0.702158	403	CALM2	CFL1	0.616158
359	TGFb1	RPIB9	0.701872	404	PRSS23	BTF3	0.613626
360	CYR61	c-Jun	-0.699378	405	TOR3A	**HOXA3**	0.612508
361	RAMP3	GAPDH	-0.697487	406	PHGDH	KLF6	0.611256
362	PHGDH	CXCL12	0.691945	407	CDYL12	BTF3	-0.610371
363	NOS3	CSPG	-0.688913	408	TOR3A	CSPG	0.609698
364	PLD	RAMP3	-0.686776	409	c-Jun	CALM2	0.607867
365	GDI2	CFL1	0.684758	410	CASP3	CDYL12	-0.604778
366	RHOJ	PRSS23	0.683442	411	GAPDH	PLD	-0.604335
367	RHOJ	GCA	-0.682826	412	BTF3	RAMP3	-0.603226
368	RPIB9	BTF3	-0.682635	413	CFH	CSPG	0.601111
369	PRSS23	PLD	-0.680746	414	CDYL12	PLD	-0.599745
370	ICAM1	CSPG	-0.677438	415	PLD	CXCL12	0.594866
371	ATP6V0D1	CDYL12	-0.676129	416	TGFb-R2	GCA	-0.593891
372	PRG	PHGDH	0.672652	417	GNAS2	UGDH	-0.593696
373	PRSS23	CDYL12	0.672295	418	GAPDH	CASP3	0.592818
374	TGFb1	KLF6	0.67219	419	ICAM1	GCA	-0.59269
375	PLD	FZD4	0.67139	420	GNAS2	KLF6	0.592359
376	BTF3	RHOJ	0.665645	421	BTF3	PHGDH	-0.591673
377	RHOJ	BTF3	-0.663887	422	ATP6V0D1	PRG	-0.589468
378	CYR61	FZD4	-0.658798	423	TGFb1	PRG	0.588396
379	BTF3	FZD4	0.657172	424	Endothelin1	RHOJ	0.586128
380	RPIB9	GCA	-0.654921	425	PRG	CDYL12	0.581995
381	ICAM1	KLF6	0.653758	426	c-Jun	GCA	-0.581458
382	CFH	GCA	-0.652579	427	FZD4	PRG	0.579215
383	TGFb1	PLD	0.651457	428	CFH	CXCL12	0.578945
384	TGFb-R2	AQP1	-0.650353	429	CALM2	TOR3A	-0.578279
385	PLD	KLF6	0.646984	430	CFH	**HOXA3**	0.571996
386	PLD	RHOJ	0.644232	431	CFL1	ICAM1	0.571748
387	GTPBP4	**HOXA3**	0.644008	432	c-Jun	CFH	0.566377
388	PHGDH	CSPG	-0.641865	433	CALM2	GDI2	-0.565448
389	CDYL12	PHGDH	-0.64088	434	GTPBP4	KLF6	0.565255
390	Endothelin1	GCA	0.636822	435	NOS3	GAPDH	-0.562523
391	ICAM1	Endothelin1	-0.63608	436	PRG	SMAD3	-0.562137
392	CFL1	TGFb-R2	-0.633826	437	PLD	CFH	0.559681
393	TGFb1	CALM2	-0.633426	438	RPIB9	RHOJ	0.554255
394	GNAS2	AQP1	0.631276	439	CFH	Endothelin1	0.552145
395	ATP6V0D1	FZD4	0.629283	440	c-Jun	UGDH	-0.55193

Position	from	to	Strength of interaction	Position	from	to	Strength of interaction
441	TGFb1	GCA	-0.54898	486	CYR61	TGFb-R2	0.488599
442	AQP1	CXCL12	-0.548603	487	CFH	PHGDH	-0.488553
443	TGFb-R2	RHOJ	0.547531	488	KLF6	RAMP3	0.488305
444	FZD4	CSPG	0.546913	489	RHOJ	**HOXA3**	0.486262
445	FZD4	**HOXA3**	0.545993	490	c-Jun	SMAD3	0.485082
446	BTF3	CASP3	-0.545044	491	GDI2	GAPDH	-0.484308
447	CASP3	GTPBP4	0.542718	492	TOR3A	PHGDH	-0.483153
448	ICAM1	PHGDH	-0.537722	493	CYR61	GNAS2	0.48172
449	FZD4	RPIB9	0.537328	494	CDYL12	SMAD2	-0.480506
450	CDYL12	NOS3	0.53664	495	NOS3	PRSS23	0.48024
451	GCA	GAPDH	-0.534175	496	KLF6	c-Jun	-0.479879
452	KLF6	NOS3	-0.532306	497	BTF3	GCA	-0.479607
453	CXCL12	RPIB9	0.532244	498	CASP3	GDI2	0.478653
454	PHGDH	CFH	0.530371	499	BTF3	TGFb1	-0.478121
455	PLD	PHGDH	-0.530245	500	TGFb-R2	FGF1	-0.477687
456	**HOXA3**	PRSS23	0.526719	501	SMAD2	CSPG	-0.477231
457	CYR61	NOS3	-0.525726	502	RPIB9	UGDH	-0.476633
458	PLD	Endothelin1	-0.523273	503	SMAD2	Endothelin1	-0.476078
459	GDI2	AQP1	-0.522203	504	GCA	FGF1	0.475266
460	SMAD3	CALM2	-0.51931	505	CXCL12	ICAM1	0.473598
461	CSPG	GAPDH	-0.514425	506	CXCL12	CFL1	0.470731
462	GCA	CALM2	-0.514125	507	SMAD3	AQP1	-0.470039
463	GTPBP4	BTF3	-0.511736	508	KLF6	**HOXA3**	0.469992
464	RHOJ	PHGDH	-0.509805	509	SMAD3	PRG	0.46935
465	RPIB9	CYR61	-0.509635	510	RPIB9	CDYL12	-0.466737
466	GDI2	SMAD3	0.509539	511	FZD4	PRSS23	0.465435
467	GAPDH	Endothelin1	0.506889	512	TGFb-R2	ICAM1	-0.463773
468	CFL1	CASP3	0.506538	513	TOR3A	Endothelin1	0.463403
469	AQP1	FGF1	-0.505472	514	GTPBP4	CYR61	-0.46138
470	PLD	GCA	0.504969	515	KLF6	CASP3	0.459868
471	c-Jun	PLD	0.504646	516	**HOXA3**	RPIB9	-0.458962
472	TGFb-R2	BTF3	-0.504576	517	SMAD2	RPIB9	-0.457652
473	FZD4	PHGDH	-0.503613	518	CFL1	GNAS2	0.45734
474	RPIB9	PLD	0.50319	519	GCA	**HOXA3**	0.457223
475	GNAS2	PLD	0.501432	520	FZD4	BTF3	-0.456124
476	ICAM1	c-Jun	-0.499641	521	PHGDH	GCA	-0.455638
477	GTPBP4	PHGDH	-0.499135	522	CFL1	CALM2	0.452025
478	PHGDH	CYR61	-0.497396	523	BTF3	GNAS2	-0.450612
479	TGFb-R2	UGDH	0.496391	524	Endothelin1	TGFb1	0.450065
480	TOR3A	RHOJ	0.496005	525	CDYL12	RHOJ	0.449222
481	SMAD2	CFL1	-0.494962	526	CDYL12	UGDH	0.448834
482	GAPDH	CYR61	0.494133	527	CFH	FGF1	-0.447435
483	**HOXA3**	AQP1	-0.4941	528	Endothelin1	Endothelin1	0.44604
484	ICAM1	CYR61	-0.493526	529	GDI2	c-Jun	0.446012
485	KLF6	CFL1	0.492448	530	c-Jun	CYR61	-0.444088

Position	from	to	Strength of interaction	Position	from	to	Strength of interaction
531	SMAD2	KLF6	0.44373	576	CDYL12	RPIB9	0.397418
532	SMAD2	CFH	0.44157	577	CYR61	TGFb1	0.39706
533	ATP6V0D1	SMAD3	0.441503	578	GNAS2	ICAM1	0.39632
534	SMAD2	PLD	0.437831	579	SMAD2	GCA	-0.393349
535	ATP6V0D1	TOR3A	-0.43736	580	TGFb-R2	GDI2	0.392268
536	SMAD3	CFL1	-0.436647	581	GTPBP4	TGFb1	-0.392196
537	GNAS2	PRSS23	-0.436322	582	Endothelin1	CXCL12	0.391085
538	CXCL12	CSPG	-0.433789	583	GTPBP4	GDI2	0.389734
539	GTPBP4	c-Jun	-0.433004	584	TGFb1	GDI2	0.388874
540	NOS3	SMAD3	0.431952	585	UGDH	CFH	0.388493
541	CDYL12	GCA	-0.429901	586	RHOJ	NOS3	0.386474
542	ATP6V0D1	RAMP3	-0.429829	587	CYR61	RHOJ	-0.386008
543	CFH	UGDH	0.429609	588	GAPDH	**HOXA3**	0.385663
544	GAPDH	UGDH	0.428592	589	CFH	c-Jun	0.384285
545	ICAM1	BTF3	-0.42817	590	PHGDH	RAMP3	0.383569
546	KLF6	TGFb-R2	0.427413	591	PHGDH	RPIB9	-0.383497
547	PLD	TGFb1	0.427115	592	c-Jun	BTF3	-0.381775
548	PHGDH	Endothelin1	-0.426788	593	ICAM1	RAMP3	0.381481
549	**HOXA3**	SMAD3	0.426192	594	RHOJ	RPIB9	0.380013
550	CFH	RHOJ	0.426008	595	TOR3A	PRG	0.37954
551	CFH	RPIB9	0.424983	596	SMAD2	CYR61	-0.378648
552	PRSS23	TOR3A	0.423672	597	ATP6V0D1	BTF3	-0.376401
553	FZD4	CASP3	0.423494	598	CSPG	FGF1	0.37619
554	PRG	BTF3	0.422625	599	RAMP3	CXCL12	0.373445
555	PHGDH	c-Jun	-0.421911	600	GCA	PRG	0.373063
556	GNAS2	NOS3	-0.421791	601	ICAM1	GDI2	0.372268
557	GAPDH	ICAM1	0.419292	602	TGFb1	BTF3	-0.371438
558	SMAD3	CASP3	0.417966	603	AQP1	CASP3	0.369031
559	SMAD2	**HOXA3**	0.417238	604	CFL1	BTF3	-0.368529
560	SMAD3	KLF6	0.417051	605	Endothelin1	KLF6	0.367888
561	CXCL12	SMAD2	0.416041	606	PHGDH	**HOXA3**	0.36762
562	BTF3	ATP6V0D1	0.414528	607	KLF6	FZD4	-0.367284
563	ATP6V0D1	GNAS2	-0.414404	608	UGDH	CALM2	0.367226
564	PRSS23	TGFb1	-0.414377	609	GCA	PHGDH	-0.367007
565	TOR3A	BTF3	-0.413956	610	PRSS23	PHGDH	0.365794
566	RPIB9	CFL1	-0.412118	611	CALM2	TGFb-R2	0.365716
567	**HOXA3**	PLD	-0.411843	612	RPIB9	RAMP3	0.362849
568	GTPBP4	RAMP3	0.41166	613	TGFb1	c-Jun	-0.361341
569	TOR3A	PRSS23	0.410234	614	UGDH	PRG	0.359132
570	GDI2	CYR61	0.409766	615	GTPBP4	CFH	0.357408
571	TGFb1	PHGDH	-0.407542	616	NOS3	Endothelin1	-0.357291
572	TGFb-R2	NOS3	0.402942	617	TGFb-R2	PRSS23	0.355099
573	CDYL12	SMAD3	0.401069	618	RAMP3	CALM2	-0.354093
574	GAPDH	CSPG	0.400566	619	CXCL12	CALM2	0.352665
575	PLD	PRG	-0.397471	620	TGFb-R2	SMAD2	-0.349989

Position	from	to	Strength of interaction	Position	from	to	Strength of interaction
621	NOS3	CFH	0.34896	666	PHGDH	GDI2	0.317786
622	**HOXA3**	c-Jun	0.347007	667	GAPDH	RAMP3	-0.317611
623	CFH	CFH	0.345406	668	**HOXA3**	NOS3	0.3172
624	Endothelin1	GDI2	-0.345289	669	RHOJ	UGDH	0.316683
625	TOR3A	UGDH	0.344782	670	TGFb1	RHOJ	0.316043
626	UGDH	SMAD3	0.344669	671	FZD4	GDI2	0.315538
627	RHOJ	PRG	0.342943	672	RHOJ	SMAD3	0.313565
628	CFH	CASP3	0.341853	673	UGDH	PLD	0.312842
629	CYR61	KLF6	0.34182	674	PRSS23	PRG	-0.311732
630	GNAS2	c-Jun	-0.341702	675	ICAM1	RHOJ	0.311002
631	ICAM1	UGDH	-0.339851	676	CFH	BTF3	-0.309593
632	PLD	CDYL12	-0.338918	677	GAPDH	FZD4	0.308799
633	GCA	PLD	0.337256	678	UGDH	CDYL12	0.307307
634	ICAM1	**HOXA3**	0.337033	679	PLD	GDI2	-0.307012
635	GDI2	RAMP3	-0.336962	680	PLD	TOR3A	-0.303559
636	GAPDH	CFH	-0.336479	681	Endothelin1	TOR3A	-0.303502
637	GNAS2	GCA	-0.335394	682	CDYL12	c-Jun	0.303417
638	GNAS2	PRG	0.335174	683	AQP1	CFH	-0.30251
639	GNAS2	SMAD2	0.334785	684	SMAD3	RPIB9	-0.302382
640	RHOJ	SMAD2	-0.33421	685	AQP1	ICAM1	0.301902
641	PRG	FZD4	0.333999	686	BTF3	CDYL12	-0.301147
642	TGFb-R2	FZD4	0.332204	687	CDYL12	Endothelin1	0.300286
643	CFL1	RHOJ	-0.332018	688	**HOXA3**	CXCL12	0.299946
644	GCA	KLF6	0.331737	689	PRG	CFL1	-0.298701
645	KLF6	RHOJ	-0.331237	690	Endothelin1	UGDH	0.298661
646	GAPDH	FGF1	-0.330092	691	TGFb1	PRSS23	-0.298462
647	GNAS2	**HOXA3**	-0.329482	692	UGDH	SMAD2	0.298387
648	UGDH	NOS3	-0.32921	693	GDI2	FZD4	0.298291
649	CFL1	CDYL12	-0.328737	694	PRG	TOR3A	0.298233
650	GAPDH	NOS3	0.326284	695	RHOJ	c-Jun	0.295836
651	SMAD3	**HOXA3**	0.324979	696	FZD4	Endothelin1	0.295482
652	PRG	GNAS2	-0.324713	697	GDI2	**HOXA3**	-0.293912
653	FGF1	CSPG	-0.324237	698	NOS3	KLF6	0.293661
654	FZD4	RHOJ	0.322986	699	FGF1	PLD	0.293499
655	GAPDH	CFL1	-0.322811	700	AQP1	c-Jun	0.293258
656	CDYL12	PRG	0.322572	701	RPIB9	CASP3	0.292656
657	CXCL12	TGFb-R2	0.322165	702	RHOJ	FGF1	-0.292086
658	TGFb1	ICAM1	-0.32212	703	PRSS23	GNAS2	-0.291544
659	TGFb1	FGF1	0.321726	704	SMAD3	BTF3	-0.290751
660	GAPDH	PHGDH	-0.321702	705	GAPDH	BTF3	-0.290265
661	c-Jun	PHGDH	-0.321302	706	RAMP3	CFH	-0.289608
662	UGDH	ICAM1	0.320821	707	TOR3A	CASP3	0.289129
663	Endothelin1	PHGDH	-0.320208	708	PRG	NOS3	0.288936
664	SMAD2	PHGDH	-0.320187	709	CXCL12	Endothelin1	0.28751
665	CDYL12	KLF6	0.319906	710	GCA	RPIB9	0.286851

Position	from	to	Strength of interaction	Position	from	to	Strength of interaction
711	**HOXA3**	RHOJ	0.284675	756	SMAD2	RAMP3	0.255614
712	UGDH	AQP1	0.284509	757	FGF1	PRG	0.255403
713	GCA	BTF3	-0.284124	758	**HOXA3**	PHGDH	-0.255345
714	AQP1	CFL1	0.283436	759	CXCL12	CDYL12	0.254639
715	CFH	SMAD3	0.28332	760	AQP1	SMAD3	0.253928
716	FZD4	SMAD3	0.283262	761	PLD	BTF3	-0.252284
717	PHGDH	PRSS23	-0.283235	762	Endothelin1	SMAD2	-0.251569
718	BTF3	GDI2	0.280371	763	CDYL12	CSPG	0.250842
719	RHOJ	GDI2	0.277609	764	PHGDH	TGFb-R2	-0.25053
720	PLD	SMAD2	-0.277574	765	TGFb-R2	KLF6	0.250044
721	FZD4	PLD	0.277162	766	GTPBP4	CSPG	-0.249621
722	**HOXA3**	CYR61	0.277071	767	RHOJ	ICAM1	-0.249554
723	CYR61	ATP6V0D1	-0.276139	768	RPIB9	NOS3	0.249131
724	TOR3A	GDI2	0.275635	769	GAPDH	RHOJ	0.248126
725	PHGDH	ICAM1	-0.27431	770	SMAD3	c-Jun	0.248093
726	ATP6V0D1	TGFb-R2	-0.273231	771	RPIB9	TGFb1	0.247692
727	RAMP3	CFL1	-0.273036	772	SMAD2	UGDH	-0.247075
728	TGFb1	CYR61	-0.272378	773	CDYL12	TGFb1	0.246506
729	CFH	PRG	0.272365	774	PHGDH	TOR3A	0.245874
730	TGFb-R2	PHGDH	-0.271544	775	c-Jun	CDYL12	-0.245587
731	GTPBP4	NOS3	-0.270796	776	UGDH	CASP3	0.245382
732	AQP1	CYR61	0.270721	777	CFH	GNAS2	-0.244501
733	PRG	PRSS23	-0.270675	778	GTPBP4	RHOJ	0.242985
734	RHOJ	CASP3	0.268817	779	CFH	NOS3	0.242949
735	CDYL12	**HOXA3**	0.268072	780	PHGDH	UGDH	-0.242587
736	CASP3	PLD	-0.267839	781	GCA	GDI2	0.242542
737	GTPBP4	RPIB9	0.267293	782	PRG	**HOXA3**	0.242248
738	RHOJ	FZD4	0.26688	783	FGF1	CFL1	-0.241329
739	TGFb1	RAMP3	0.265818	784	ICAM1	CDYL12	-0.241314
740	SMAD2	BTF3	-0.265004	785	**HOXA3**	FZD4	0.239946
741	GTPBP4	FZD4	-0.262349	786	FGF1	**HOXA3**	0.239667
742	CDYL12	FZD4	0.261701	787	UGDH	Endothelin1	-0.239631
743	SMAD3	PHGDH	-0.261475	788	CXCL12	KLF6	-0.239119
744	NOS3	PHGDH	-0.261336	789	CALM2	ATP6V0D1	0.239007
745	RAMP3	AQP1	-0.260592	790	CFH	FZD4	0.238589
746	PHGDH	TGFb1	-0.260175	791	SMAD3	PRSS23	0.238448
747	KLF6	CDYL12	0.259899	792	FGF1	KLF6	0.23843
748	GCA	RHOJ	0.259841	793	**HOXA3**	CFL1	0.238254
749	SMAD3	GCA	-0.259429	794	NOS3	BTF3	-0.237475
750	PRSS23	RHOJ	-0.258409	795	PRSS23	GDI2	0.236799
751	SMAD2	RHOJ	0.258073	796	FZD4	UGDH	0.236679
752	KLF6	GNAS2	0.258047	797	CSPG	CXCL12	0.234863
753	PHGDH	RHOJ	0.257652	798	GTPBP4	PRSS23	-0.234567
754	GTPBP4	CDYL12	-0.257282	799	GDI2	CALM2	0.234539
755	c-Jun	GNAS2	0.255923	800	Endothelin1	BTF3	-0.234424

Position	from	to	Strength of interaction	Position	from	to	Strength of interaction
801	RPIB9	TOR3A	-0.234201	846	PHGDH	NOS3	-0.205624
802	PHGDH	BTF3	-0.234119	847	CYR61	GCA	-0.204767
803	CDYL12	ICAM1	-0.232719	848	NOS3	PRG	0.204702
804	PRSS23	GCA	0.232562	849	**HOXA3**	FGF1	0.203323
805	**HOXA3**	KLF6	0.232501	850	GTPBP4	Endothelin1	-0.202608
806	FZD4	TGFb-R2	-0.231483	851	GAPDH	KLF6	0.202552
807	GNAS2	TGFb1	0.231002	852	c-Jun	CASP3	0.202097
808	TGFb-R2	CYR61	0.230689	853	RAMP3	CSPG	0.201877
809	RHOJ	TGFb-R2	-0.229026	854	AQP1	RAMP3	-0.201398
810	CXCL12	GCA	0.2288	855	CFH	TGFb1	0.201212
811	PRG	RHOJ	-0.228541	856	FZD4	GNAS2	-0.199054
812	RHOJ	KLF6	0.227239	857	GCA	AQP1	-0.198923
813	BTF3	**HOXA3**	-0.226815	858	AQP1	UGDH	0.19852
814	BTF3	SMAD3	-0.225375	859	ICAM1	TOR3A	0.198179
815	GAPDH	PRG	0.224281	860	RHOJ	Endothelin1	0.197263
816	TGFb-R2	GNAS2	-0.223673	861	FGF1	CDYL12	0.196979
817	TOR3A	FGF1	-0.223439	862	CYR61	CASP3	0.196327
818	TOR3A	GNAS2	-0.222805	863	TOR3A	c-Jun	0.194724
819	GDI2	RHOJ	0.221758	864	GDI2	CASP3	0.19451
820	GAPDH	TOR3A	-0.220995	865	NOS3	AQP1	0.194468
821	SMAD2	SMAD3	0.220741	866	CXCL12	GAPDH	-0.193411
822	PRG	c-Jun	-0.220247	867	PHGDH	AQP1	0.192622
823	RHOJ	GNAS2	-0.21972	868	ICAM1	TGFb-R2	-0.192266
824	RPIB9	**HOXA3**	0.219708	869	GTPBP4	TOR3A	0.191929
825	AQP1	SMAD2	0.219555	870	CSPG	CALM2	-0.191271
826	UGDH	KLF6	0.21904	871	TOR3A	SMAD2	-0.190656
827	SMAD3	ICAM1	0.218015	872	AQP1	PLD	-0.189371
828	CYR61	GDI2	-0.216719	873	TGFb1	Endothelin1	-0.18914
829	GNAS2	TOR3A	-0.214781	874	CXCL12	PHGDH	0.189017
830	GTPBP4	CASP3	0.214397	875	GNAS2	BTF3	0.186395
831	c-Jun	RAMP3	0.214328	876	GTPBP4	TGFb-R2	-0.185649
832	NOS3	GCA	-0.213649	877	CASP3	c-Jun	0.185592
833	TOR3A	SMAD3	0.213453	878	CDYL12	GNAS2	-0.184377
834	NOS3	RHOJ	0.212726	879	SMAD2	CALM2	-0.183287
835	GDI2	CXCL12	0.211289	880	RAMP3	**HOXA3**	0.183082
836	GDI2	GCA	0.210284	881	TOR3A	NOS3	0.18301
837	NOS3	UGDH	-0.210265	882	RHOJ	CDYL12	-0.182935
838	Endothelin1	CSPG	-0.210143	883	PHGDH	CDYL12	-0.18084
839	PRG	SMAD2	0.209534	884	GDI2	TGFb1	0.180345
840	NOS3	CDYL12	-0.208658	885	RPIB9	PRSS23	0.180337
841	UGDH	GAPDH	0.207119	886	Endothelin1	CASP3	0.180086
842	**HOXA3**	RAMP3	-0.206556	887	RAMP3	PHGDH	-0.180068
843	CFH	GDI2	0.205872	888	RPIB9	GDI2	0.178603
844	TGFb1	SMAD2	-0.205828	889	FZD4	TGFb1	-0.178481
845	SMAD3	PLD	-0.205723	890	NOS3	CALM2	0.178299

Position	from	to	Strength of interaction	Position	from	to	Strength of interaction
891	GTPBP4	ATP6V0D1	0.177547	936	GCA	CSPG	-0.153859
892	PHGDH	FZD4	-0.17661	937	PRG	TGFb1	-0.153684
893	CDYL12	CYR61	0.175548	938	CALM2	CASP3	-0.153562
894	FZD4	KLF6	0.175129	939	TGFb1	GAPDH	0.153084
895	SMAD2	CASP3	0.174729	940	GNAS2	CDYL12	-0.153049
896	SMAD2	GDI2	0.174495	941	ICAM1	FZD4	-0.15303
897	c-Jun	GDI2	0.172997	942	NOS3	c-Jun	0.152776
898	KLF6	TOR3A	0.172837	943	PRG	GAPDH	0.152326
899	SMAD2	AQP1	-0.171812	944	RAMP3	PRG	0.151859
900	CDYL12	CASP3	0.170126	945	TGFb-R2	ATP6V0D1	0.151817
901	CXCL12	CASP3	0.169904	946	CXCL12	TGFb1	0.151731
902	NOS3	FZD4	0.169745	947	FZD4	RAMP3	0.150172
903	c-Jun	RHOJ	0.169692	948	RAMP3	BTF3	-0.150158
904	PHGDH	CALM2	0.168511	949	CFH	TGFb-R2	0.150135
905	PRG	ICAM1	-0.167208	950	UGDH	CYR61	-0.148293
906	KLF6	PHGDH	0.166961	951	NOS3	CYR61	-0.14822
907	GDI2	KLF6	0.166866	952	UGDH	CFL1	0.148204
908	**HOXA3**	UGDH	0.166775	953	AQP1	PRSS23	0.147562
909	AQP1	Endothelin1	0.16569	954	**HOXA3**	BTF3	-0.14705
910	TOR3A	TGFb-R2	-0.165327	955	BTF3	TOR3A	-0.146376
911	KLF6	ATP6V0D1	-0.164714	956	UGDH	TGFb1	0.144615
912	ATP6V0D1	TGFb1	0.164494	957	BTF3	GTPBP4	-0.144592
913	CFH	CYR61	0.164056	958	CSPG	CFL1	-0.144475
914	PLD	TGFb-R2	0.163462	959	BTF3	KLF6	0.144336
915	RPIB9	CALM2	0.162924	960	PRG	GTPBP4	0.143221
916	GTPBP4	GAPDH	-0.162759	961	FGF1	SMAD3	0.143185
917	PRSS23	SMAD2	0.161709	962	SMAD3	RHOJ	0.143075
918	CALM2	GTPBP4	-0.161493	963	TOR3A	FZD4	0.142345
919	TOR3A	ICAM1	-0.16147	964	SMAD2	CDYL12	-0.140778
920	RAMP3	RPIB9	0.160901	965	c-Jun	PRSS23	0.140679
921	ICAM1	ATP6V0D1	0.160282	966	FZD4	SMAD2	-0.139913
922	PHGDH	ATP6V0D1	0.160081	967	PRSS23	NOS3	-0.139539
923	FZD4	c-Jun	0.159408	968	GDI2	PRG	-0.139531
924	AQP1	RPIB9	0.159107	969	PRG	ATP6V0D1	0.139465
925	FGF1	CASP3	0.159011	970	CSPG	GCA	-0.138902
926	GTPBP4	ICAM1	-0.158091	971	TGFb1	CFH	0.137997
927	CDYL12	FGF1	0.157463	972	TOR3A	TGFb1	-0.136906
928	TOR3A	KLF6	0.157412	973	c-Jun	ICAM1	0.136716
929	KLF6	GCA	0.156962	974	GAPDH	GNAS2	-0.136431
930	CYR61	SMAD3	-0.156653	975	ICAM1	SMAD3	0.135896
931	PLD	UGDH	0.156602	976	NOS3	CASP3	0.134759
932	ICAM1	CASP3	0.155861	977	PLD	CASP3	0.134269
933	TGFb1	TGFb-R2	-0.154977	978	AQP1	KLF6	0.134175
934	Endothelin1	CDYL12	-0.154949	979	AQP1	BTF3	0.134059
935	SMAD3	RAMP3	0.154578	980	RPIB9	SMAD2	-0.133732

Position	from	to	Strength of interaction	Position	from	to	Strength of interaction
981	CXCL12	FGF1	-0.132652	1026	UGDH	GNAS2	0.117645
982	RHOJ	CYR61	0.131644	1027	GCA	SMAD3	0.117338
983	CFL1	ATP6V0D1	0.131621	1028	Endothelin1	TGFb-R2	0.117336
984	SMAD3	CFH	-0.13046	1029	ATP6V0D1	KLF6	0.117326
985	ICAM1	PRSS23	-0.12977	1030	CDYL12	ATP6V0D1	0.117312
986	**HOXA3**	CASP3	0.129217	1031	**HOXA3**	SMAD2	-0.116524
987	GCA	ICAM1	-0.128633	1032	**HOXA3**	TGFb1	0.116499
988	c-Jun	FZD4	-0.128566	1033	CSPG	PRSS23	0.116173
989	GAPDH	GCA	0.12856	1034	PLD	ICAM1	-0.115976
990	TOR3A	PLD	0.12787	1035	CASP3	GNAS2	-0.11571
991	GNAS2	PHGDH	0.127728	1036	SMAD3	FZD4	0.115177
992	c-Jun	TOR3A	-0.127674	1037	RAMP3	SMAD3	0.115017
993	CSPG	AQP1	-0.127365	1038	GDI2	PHGDH	-0.114569
994	GNAS2	GDI2	-0.127158	1039	CASP3	Endothelin1	-0.113279
995	AQP1	PRG	0.12705	1040	GDI2	UGDH	0.112341
996	FGF1	GDI2	0.126447	1041	RAMP3	RHOJ	0.11189
997	KLF6	FGF1	0.126154	1042	PLD	GTPBP4	-0.111398
998	GCA	PRSS23	0.125945	1043	c-Jun	TGFb1	0.11057
999	CDYL12	TOR3A	-0.125409	1044	RPIB9	ATP6V0D1	0.110544
1000	CDYL12	GTPBP4	-0.125345	1045	UGDH	RHOJ	0.110438
1001	CASP3	TGFb-R2	0.125311	1046	NOS3	RAMP3	0.110214
1002	SMAD3	FGF1	-0.125278	1047	c-Jun	**HOXA3**	0.109867
1003	RAMP3	CASP3	0.125197	1048	**HOXA3**	CDYL12	-0.109686
1004	TGFb-R2	PRG	0.124962	1049	TGFb1	ATP6V0D1	0.109299
1005	CXCL12	CYR61	0.123507	1050	CXCL12	RAMP3	-0.107473
1006	GNAS2	SMAD3	0.122901	1051	PLD	GNAS2	0.107368
1007	ATP6V0D1	**HOXA3**	0.122829	1052	FGF1	SMAD2	0.107148
1008	**HOXA3**	TOR3A	-0.122777	1053	SMAD2	c-Jun	-0.106852
1009	RHOJ	PLD	-0.122358	1054	CXCL12	GDI2	-0.106753
1010	SMAD3	CYR61	-0.122251	1055	UGDH	**HOXA3**	0.106492
1011	SMAD3	NOS3	0.121789	1056	FZD4	FGF1	-0.106148
1012	RPIB9	ICAM1	-0.121627	1057	GDI2	CFH	-0.105751
1013	RAMP3	PRSS23	0.121545	1058	FGF1	GCA	-0.105136
1014	TGFb-R2	PLD	0.121529	1059	GCA	CDYL12	-0.105097
1015	SMAD3	GAPDH	0.120993	1060	FZD4	CDYL12	-0.104829
1016	c-Jun	CFL1	-0.120851	1061	GCA	CASP3	0.10447
1017	**HOXA3**	CSPG	-0.120706	1062	GNAS2	FZD4	-0.104385
1018	KLF6	GDI2	-0.120326	1063	SMAD3	TGFb-R2	-0.104073
1019	UGDH	CXCL12	-0.119975	1064	PRG	TGFb-R2	0.103448
1020	ATP6V0D1	RPIB9	-0.119441	1065	CXCL12	ATP6V0D1	-0.102499
1021	FGF1	PRSS23	-0.119329	1066	AQP1	TGFb-R2	0.102489
1022	NOS3	TGFb1	0.11867	1067	GDI2	TOR3A	-0.102458
1023	GCA	SMAD2	-0.118574	1068	CXCL12	RHOJ	-0.101821
1024	GDI2	CSPG	-0.118149	1069	TGFb1	TOR3A	0.101178
1025	GAPDH	TGFb1	0.117956	1070	TGFb-R2	c-Jun	0.101163

Position	from	to	Strength of interaction	Position	from	to	Strength of interaction
1071	FZD4	ICAM1	-0.10025	1116	SMAD2	FZD4	-0.080911
1072	AQP1	GAPDH	0.100185	1117	UGDH	GDI2	0.080081
1073	ATP6V0D1	GTPBP4	-0.100111	1118	TGFb-R2	CASP3	0.078106
1074	TOR3A	CDYL12	-0.099789	1119	RAMP3	UGDH	0.077934
1075	TGFb1	CDYL12	-0.099515	1120	GNAS2	CSPG	0.077801
1076	ICAM1	TGFb1	-0.099432	1121	GCA	NOS3	0.077197
1077	GDI2	BTF3	-0.098632	1122	GCA	c-Jun	-0.077142
1078	Endothelin1	CFH	-0.09834	1123	NOS3	ICAM1	0.077071
1079	PHGDH	GNAS2	0.098245	1124	UGDH	TOR3A	0.076896
1080	ICAM1	CALM2	-0.098076	1125	GNAS2	CXCL12	-0.076881
1081	SMAD3	GNAS2	-0.097178	1126	SMAD3	TGFb1	0.076864
1082	GCA	RAMP3	0.096418	1127	PRSS23	CASP3	0.076568
1083	RAMP3	GCA	-0.095663	1128	PRSS23	c-Jun	0.075995
1084	CSPG	PHGDH	-0.095599	1129	AQP1	TOR3A	-0.075687
1085	SMAD3	CDYL12	-0.09506	1130	PLD	ATP6V0D1	0.07524
1086	RAMP3	GDI2	0.095051	1131	CSPG	BTF3	-0.074958
1087	CDYL12	GDI2	0.093695	1132	Endothelin1	FGF1	0.074869
1088	GCA	TGFb-R2	-0.093554	1133	CFH	PLD	0.074743
1089	AQP1	FZD4	0.092528	1134	CXCL12	UGDH	0.073585
1090	NOS3	GTPBP4	-0.092357	1135	RAMP3	ICAM1	-0.073403
1091	RHOJ	ATP6V0D1	0.091783	1136	UGDH	FZD4	0.072966
1092	FGF1	RPIB9	0.091172	1137	SMAD3	GTPBP4	-0.072951
1093	RPIB9	GNAS2	0.090822	1138	RAMP3	SMAD2	-0.072731
1094	FGF1	AQP1	0.090385	1139	CXCL12	PLD	0.072361
1095	SMAD2	PRSS23	-0.090107	1140	SMAD2	TOR3A	0.07211
1096	ATP6V0D1	GDI2	0.089239	1141	CSPG	**HOXA3**	0.071653
1097	SMAD2	GNAS2	0.08878	1142	GNAS2	TGFb-R2	0.071475
1098	RHOJ	TOR3A	-0.088269	1143	PRSS23	GTPBP4	0.070735
1099	ICAM1	GNAS2	0.086516	1144	RHOJ	GTPBP4	-0.070687
1100	FZD4	NOS3	0.086504	1145	UGDH	PHGDH	-0.07038
1101	ATP6V0D1	CASP3	-0.085988	1146	CDYL12	TGFb-R2	-0.070223
1102	RHOJ	TGFb1	-0.08597	1147	CFH	TOR3A	-0.069621
1103	SMAD3	TOR3A	-0.085956	1148	**HOXA3**	Endothelin1	0.069464
1104	PHGDH	GTPBP4	0.085801	1149	FZD4	ATP6V0D1	0.069382
1105	FGF1	CYR61	0.085685	1150	FGF1	ATP6V0D1	0.069161
1106	FGF1	FZD4	0.085373	1151	Endothelin1	ATP6V0D1	0.06901
1107	CFH	SMAD2	-0.085103	1152	TOR3A	ATP6V0D1	0.068918
1108	KLF6	GTPBP4	-0.0846	1153	RAMP3	GNAS2	-0.068126
1109	RPIB9	c-Jun	-0.083738	1154	AQP1	**HOXA3**	0.068006
1110	SMAD2	GAPDH	-0.083507	1155	CYR61	TOR3A	0.067978
1111	CYR61	CDYL12	0.083023	1156	CXCL12	PRSS23	-0.067909
1112	GNAS2	CASP3	-0.082553	1157	RAMP3	TGFb1	-0.067827
1113	TOR3A	CYR61	0.082552	1158	NOS3	GDI2	0.067631
1114	AQP1	GCA	0.081266	1159	GCA	CFH	0.06698
1115	FGF1	RHOJ	0.08113	1160	NOS3	TGFb-R2	-0.06661

Position	from	to	Strength of interaction	Position	from	to	Strength of interaction
1161	FGF1	RAMP3	-0.06658	1206	PRSS23	ATP6V0D1	0.053409
1162	RAMP3	c-Jun	0.066469	1207	FGF1	BTF3	-0.052939
1163	CXCL12	SMAD3	0.066343	1208	ICAM1	NOS3	-0.052836
1164	**HOXA3**	GCA	0.066035	1209	CXCL12	TOR3A	0.052434
1165	CFL1	PHGDH	-0.065913	1210	**HOXA3**	CFH	0.052311
1166	CFH	ATP6V0D1	0.065912	1211	SMAD3	UGDH	0.052293
1167	UGDH	BTF3	0.065391	1212	CDYL12	RAMP3	-0.051987
1168	PRG	GDI2	-0.065074	1213	GAPDH	GAPDH	0.050888
1169	CYR61	**HOXA3**	-0.064949	1214	PRSS23	TGFb-R2	0.050703
1170	RAMP3	PLD	0.064598	1215	NOS3	SMAD2	-0.049944
1171	AQP1	NOS3	0.064439	1216	SMAD2	NOS3	0.049899
1172	c-Jun	AQP1	-0.064146	1217	CXCL12	FZD4	0.049283
1173	CSPG	PRG	0.064071	1218	SMAD3	GDI2	0.048709
1174	UGDH	RAMP3	0.064014	1219	CSPG	RHOJ	0.048541
1175	RAMP3	TGFb-R2	-0.063445	1220	GDI2	Endothelin1	0.048475
1176	GAPDH	ATP6V0D1	0.062921	1221	c-Jun	TGFb-R2	-0.048419
1177	CFH	CDYL12	0.062279	1222	TOR3A	GTPBP4	-0.04841
1178	CASP3	TOR3A	0.062116	1223	CSPG	CFH	0.048031
1179	**HOXA3**	ATP6V0D1	0.061754	1224	TGFb1	AQP1	-0.04787
1180	RPIB9	GTPBP4	-0.061006	1225	GDI2	TGFb-R2	0.047316
1181	PRG	CASP3	0.060645	1226	FGF1	CXCL12	0.047263
1182	NOS3	PLD	0.060515	1227	CSPG	CASP3	0.046823
1183	GCA	CYR61	-0.060192	1228	SMAD2	GTPBP4	-0.046543
1184	GDI2	FGF1	0.059297	1229	FGF1	ICAM1	0.046307
1185	TGFb-R2	CDYL12	0.059089	1230	NOS3	GNAS2	0.046218
1186	TGFb-R2	TOR3A	0.058657	1231	TGFb-R2	GTPBP4	-0.046167
1187	FGF1	PHGDH	-0.058264	1232	GAPDH	RPIB9	-0.045898
1188	GAPDH	TGFb-R2	0.057832	1233	UGDH	PRSS23	-0.04542
1189	KLF6	SMAD3	0.057792	1234	SMAD3	Endothelin1	-0.045374
1190	**HOXA3**	ICAM1	-0.057733	1235	CXCL12	c-Jun	0.044251
1191	GCA	ATP6V0D1	0.057357	1236	GDI2	CDYL12	-0.043086
1192	RAMP3	CDYL12	-0.057261	1237	GNAS2	ATP6V0D1	-0.043007
1193	CSPG	SMAD3	0.057168	1238	**HOXA3**	GTPBP4	-0.042365
1194	FZD4	GTPBP4	-0.057107	1239	TGFb-R2	RAMP3	-0.042349
1195	TOR3A	RAMP3	0.056591	1240	UGDH	GCA	-0.042267
1196	RPIB9	FZD4	0.055868	1241	NOS3	CFL1	0.041936
1197	ICAM1	AQP1	-0.055842	1242	GTPBP4	SMAD2	-0.041879
1198	FGF1	NOS3	0.055732	1243	CXCL12	**HOXA3**	0.041873
1199	RPIB9	TGFb-R2	-0.054799	1244	CSPG	GDI2	0.041696
1200	FGF1	TOR3A	0.054268	1245	GNAS2	GTPBP4	0.040727
1201	RAMP3	FZD4	0.054218	1246	GDI2	ICAM1	0.040684
1202	NOS3	TOR3A	-0.054059	1247	GCA	FZD4	0.040527
1203	FZD4	CYR61	-0.05394	1248	GCA	UGDH	0.040334
1204	FZD4	TOR3A	-0.05375	1249	CXCL12	BTF3	0.040212
1205	AQP1	PHGDH	-0.053721	1250	PRSS23	ICAM1	-0.039704

Position	from	to	Strength of interaction	Position	from	to	Strength of interaction
1251	**HOXA3**	GDI2	-0.039585	1296	CSPG	RPIB9	-0.021518
1252	RAMP3	GTPBP4	-0.03857	1297	CFH	ICAM1	0.021479
1253	TGFb1	UGDH	-0.038122	1298	ICAM1	SMAD2	0.020781
1254	GCA	GNAS2	-0.037891	1299	CSPG	GTPBP4	-0.020641
1255	TGFb1	SMAD3	-0.037211	1300	GTPBP4	AQP1	-0.019944
1256	RAMP3	FGF1	-0.036553	1301	CSPG	GNAS2	-0.019624
1257	Endothelin1	GNAS2	-0.036484	1302	SMAD3	SMAD2	-0.019514
1258	SMAD2	TGFb1	0.03644	1303	CXCL12	CFH	-0.019394
1259	FGF1	GNAS2	0.036397	1304	RAMP3	ATP6V0D1	0.019166
1260	CSPG	KLF6	-0.036301	1305	GAPDH	CDYL12	-0.018925
1261	PHGDH	CASP3	-0.036258	1306	PRSS23	FZD4	0.018764
1262	FGF1	TGFb1	0.035926	1307	RHOJ	RAMP3	0.018729
1263	CFH	GTPBP4	-0.035682	1308	CALM2	CDYL12	0.018216
1264	SMAD3	ATP6V0D1	0.035381	1309	CSPG	Endothelin1	0.0181
1265	SMAD2	ICAM1	0.034694	1310	CSPG	CYR61	0.017712
1266	KLF6	TGFb1	0.033117	1311	ICAM1	GAPDH	-0.017039
1267	GTPBP4	SMAD3	-0.032841	1312	GCA	Endothelin1	0.016283
1268	TGFb1	GNAS2	-0.032829	1313	c-Jun	GTPBP4	-0.016115
1269	c-Jun	ATP6V0D1	0.032591	1314	UGDH	TGFb-R2	0.015939
1270	CDYL12	CFH	0.032497	1315	CYR61	GTPBP4	-0.015793
1271	TGFb1	FZD4	-0.032205	1316	**HOXA3**	PRG	-0.015214
1272	AQP1	CDYL12	0.031851	1317	FGF1	TGFb-R2	-0.014054
1273	Endothelin1	GTPBP4	-0.031419	1318	CSPG	TGFb-R2	-0.013688
1274	CSPG	CDYL12	-0.030937	1319	CSPG	ICAM1	0.013586
1275	CXCL12	PRG	-0.030393	1320	GTPBP4	GNAS2	-0.012982
1276	GDI2	ATP6V0D1	0.030233	1321	PHGDH	GAPDH	-0.012926
1277	CXCL12	GTPBP4	0.029552	1322	GNAS2	RHOJ	-0.012764
1278	RAMP3	Endothelin1	0.0293	1323	FGF1	CALM2	0.012379
1279	CXCL12	NOS3	-0.02826	1324	AQP1	GTPBP4	-0.011851
1280	**HOXA3**	TGFb-R2	0.0281	1325	NOS3	**HOXA3**	-0.011407
1281	TGFb1	NOS3	0.028084	1326	PHGDH	SMAD3	-0.011334
1282	GDI2	GNAS2	0.027886	1327	GDI2	GTPBP4	-0.011329
1283	GAPDH	GTPBP4	0.027262	1328	RAMP3	TOR3A	0.011063
1284	TGFb1	CASP3	0.026022	1329	SMAD2	ATP6V0D1	0.010975
1285	GTPBP4	UGDH	-0.025925	1330	FGF1	UGDH	-0.010446
1286	RAMP3	NOS3	0.025804	1331	GCA	GTPBP4	-0.010385
1287	CXCL12	GNAS2	0.025759	1332	RAMP3	KLF6	-0.010189
1288	PHGDH	SMAD2	-0.02565	1333	SMAD2	TGFb-R2	-0.010061
1289	AQP1	CALM2	0.025582	1334	CFH	KLF6	-0.009063
1290	UGDH	ATP6V0D1	0.02521	1335	**HOXA3**	GNAS2	-0.008812
1291	NOS3	ATP6V0D1	0.025143	1336	FGF1	GAPDH	-0.00809
1292	TGFb-R2	SMAD3	0.024022	1337	GCA	TGFb1	0.00773
1293	CSPG	PLD	0.023137	1338	AQP1	ATP6V0D1	-0.007463
1294	AQP1	GDI2	-0.023122	1339	GAPDH	SMAD2	-0.007294
1295	CSPG	UGDH	0.022083	1340	c-Jun	SMAD2	-0.007251

Position	from	to	Strength of interaction	Position	from	to	Strength of interaction
1341	CSPG	c-Jun	0.007172	1356	CSPG	NOS3	0.003981
1342	FGF1	Endothelin1	0.006814	1357	GAPDH	GDI2	-0.003754
1343	FGF1	c-Jun	-0.006599	1358	FGF1	GTPBP4	0.003615
1344	RAMP3	CYR61	0.006419	1359	**HOXA3**	CALM2	-0.003165
1345	UGDH	c-Jun	-0.006185	1360	CSPG	FZD4	-0.003139
1346	TGFb1	GTPBP4	-0.005989	1361	GCA	TOR3A	-0.002917
1347	CSPG	TOR3A	-0.005917	1362	ICAM1	GTPBP4	0.002773
1348	Endothelin1	ICAM1	0.005312	1363	CSPG	ATP6V0D1	-0.002376
1349	CYR61	CYR61	-0.005309	1364	AQP1	GNAS2	-0.002362
1350	AQP1	TGFb1	-0.005141	1365	GDI2	SMAD2	0.00147
1351	UGDH	GTPBP4	-0.004599	1366	c-Jun	NOS3	-0.001442
1352	CFL1	GTPBP4	0.004236	1367	CFH	RAMP3	-0.000653
1353	CSPG	SMAD2	-0.004167	1368	CSPG	RAMP3	-0.000426
1354	CSPG	TGFb1	0.004105	1369	AQP1	RHOJ	-0.000233
1355	FGF1	CFH	0.004089				

Interactions between transiently expressed candidate genes were ranked according to their strength, starting from the strongest value of interaction. Certain threshold values for both, activating and inhibitory effects were set in order to incorporate only the most significant interactions into the gene network relevant to diabetic microangiopathy. Positive values representing activating effects had to be greater than a certain threshold of 1.334 , whereas negative values indicating inhibitory effects had to be smaller than -1.130. Three interactions involving HOXA3 were found to be significant for the gene network of relevance for diabetic microangiopathy. These were the activating and the inhibitory effect of CFL1 and CASP3 respectively on HOXA3 as well as a positive effect of HOXA3 on its own expression.

Abbreviations

7-AAD	…7-amino-actinomycin D
80K-H	…80 kDa protein substrate for protein kinase C
ABL	…Abelson tyrosine kinase
ADF	…Actin depolymerising factor
AGE	…Advanced glycation end product
ATPase	…Adenosine triphosphatase
ATP6VOD1	…D1 subunit of the transmembrane VO domain of ATPase
BCR	…B cell receptor
BECs	…Blood vessel endothelial cells
BSA	…Bovine serum albumin
CASP3	…Caspase 3
cDNA	…Complementary deoxyribonucleic acid
CFL1	…Cofilin1
CMV	…Cytomegalovirus
C1s	…serine protease (subunit of the multimeric C1 protein complex)
Ct	…Cycle threshold
CXCL12	…Chemokine (C-X-C motif) ligand 12
CXCR4	…Chemokine (C-X-C motif) receptor 4
DAG	…Diacylglycerol
DAPI	...4´6-diamidino-2-phenylindole dihydrochloride
DKA	…Diabetic ketoacidosis
DMA	…Diabetic microangiopathy
DNA	…Deoxyribonucleic acid
dNTP	…Deoxynucleotide triphosphate
ddNTP	…Dideoxynucleotide triphosphate
EBF	…Early B-cell factor
ECL	…Enhanced chemiluminescence
ECM	…Extracellular matrix
ECMV	…Encephalomyocarditis virus
EGFP	…Enhanced green fluorescent protein
eNOS	…Endothelial nitric oxide synthase
EPHA4	…Ephrin type A receptor 4

ET-1	…Endothelin-1
FBXO	…F-box proteins
FBS	…Fetal bovine serum
FC	…Fold change
FZD4	…Frizzled homolog 4
GAD	…Glutamic acid decarboxylase
GAPDH	…Glyceraldehyde-3-phosphate dehydrogenase
GCA	…Grancalcin
GFAT	…Glutamine:fructose-6-phosphate amidotransferase
GDM	…Gestational diabetes mellitus
GJA1	…Gap junction protein alpha 1
GSH	…Reduced glutathione
HMEC-1	…Human microvascular endothelial cell line-1
HOX genes	…Homeobox genes
HOXA3	…Homeobox A3
HOXD3	…Homeobox D3
hTERT	…Human telomerase reverse transcriptase
ICAM1	…Intercellular adhesion molecule 1
iHUVECs	…Immortalized human umbilical vein endothelial cells
IL-1	…Interleukin-1
IL-8	…Interleukin-8
IPTG	…Isopropyl-beta-D-thiogalactopyranoside
IRES	…Internal ribosomal entry site
IRES2	…Internal ribosomal entry site 2
ITGA1	…Integrin alpha 1
KLF6	…Krüppel-like factor 6
LacZ	…Beta galactosidase
LB	…Luria Broth
MHC class II	…Major histocompatibility complex class II
MMP-14	…Matrix metalloproteinase-14
mRNA	…Messenger ribonucleic acid
$NADP^+$/NADPH	…Nicotinamide adenine dinucleotide phosphate
NARS	…Asparaginyl-tRNA synthetase
NF-κB	…Nuclear factor-kappa B

NOS3	…Nitric oxide synthase 3
OGT	…O-linked N-acetylglucosamine transferase
OptiMEM	...Optimized minimal essential medium
OST-48	…Oligosaccharyltransferase 48kD subunit
PAI-1	…Plasminogen activator inhibitor-1
PARK7	…Parkinson disease 7
PARP	…Poly (adenosine diphosphate-ribose) polymerase
PAX1	…Paired box gene 1
PBGD	…Porphobilinogen desaminase
PBS	…Phosphate buffered saline
PCR	…Polymerase chain reaction
PFA	…Para-formaldehyde
PHGDH	…3-phosphoglycerate dehydrogenase
PKC	…Protein kinase C
PLD	…Phospholipase D
PRSS23	…Protease serine 23
$p21^{Ras}$	…21 kDa protein encoded by the ras gene family
RAGE	…Receptor of advanced glycation end products
RHOJ	…Ras homolog gene family member J
RNA	…Ribonucleic acid
ROS	…Reactive oxygen species
RPIB1	…Ribose-5-phosphate isomerase 1
RPMI	…Roswell Park Memorial Institute (development of RPMI medium)
SDS	…Sequence detection software
SDS-PAGE	…Sodium dodecyl sulfate polyacrylamide gel electrophoresis
SERPINE1	…Serpin peptidase inhibitor, clade E, member 1
SMAD3	…Mothers against decapentaplegic homolog 3
SMAD4	…Mothers against decapentaplegic homolog 4
SORBS1	…Sorbin and SH3-domain-containing-1
TARDBP	…TAR DNA binding protein
TBS	…Tris-buffered saline
TBST	…Tris-buffered saline Tween
TCA	…Trichlor acetic acid
TCA-cycle	…Tricarboxylic acid cycle

TNF-α	…Tumor necrosis factor-alpha
TGF-β	…Transforming growth factor-beta
UDP	…Uridine diphosphate
UGDH	…Uridine diphosphate -glucose dehydrogenase
UDPGlcNAc	…Uridine diphosphate -N-acetylglucosamine
uPA	…Urokinase-type plasminogen activator
uPAR	…Urokinase-type plasminogen activator receptor
VCAM-1	…Vascular cell adhesion molecule-1
VEGF	…Vascular endothelial growth factor
X-gal	…5-bromo-4-chloro-3-indolyl-β-D-galactopyranoside

Curriculum Vitae

Personal information

Name:	**Andreas Thader**
Date of birth:	December 11th, 1978
Place of birth:	Vienna, Austria
Address:	Peter-Jordanstrasse 81/8/5
	A-1180 Vienna
E-mail:	andi.thader@chello.at

Education

2006 – 2008	Diploma thesis at the Institute of Clinical Pathology, AKH, Vienna, supervised by Nikolaus Wick, MD
Since 1999	University of Vienna
	Study of Biology (Microbiology and Genetics)
1998 – 1999	Vienna University of Technology (TU Wien)
	Study of Technical Physics
1997	High school diploma (Matura)
1989 – 1997	High school (Gymnasium und Realgymnasium)
	GWIKU Haizingergasse
	A-1180 Vienna
1985 – 1989	Elementary school (Volksschule)
	Bischof Faberplatz 1
	A-1180 Vienna

Additional activities

1999 – 2006	Marginal employement (Billa supermarket)
1997 – 1998	Military Service for 8 months, Vienna